Numerical modelling in laboratory scale estuaries.

X-Beach versus The Metronome

02-02-2024

Master Thesis

M.L.C. Wagenaar – 6688306

Supervisors:

Prof. dr. Maarten Kleinhans
Dr. Timothy Price

Utrecht University

Department of Physical Geography
Earth Surface and Water

| Abstract

In this study, the X-Beach model was used to model the hydrodynamics in laboratory-scale estuaries simulated in the metronome. The metronome is a tilting flume in which estuaries are simulated and studied. This estuarine research is performed as these highly dynamic areas are important for both nature and humans because they provide a place where species can thrive and cities and harbours can flourish. To protect estuaries from changes in the system, their processes are studied both with laboratory experiments and numerical models. By combining these two, a more complete spatial and temporal data set of the experiments can be gathered as well as providing possibilities for upscaling of the laboratory experiments in the model. Initially, the modelled metronome experiments showed large floods. Numerous model test runs were conducted which can be grouped in five categories: 1) Runs with adaptations to the bed level, 2) Runs with different bed roughness, 3) Runs with different tidal inputs, 4) Runs with an additional seaside discharge and 5) Runs with adaptations to the source code. Most tests showed similar floods to the initial runs. However, by implementing a new boundary condition the floods were solved. This new boundary condition forces the tidal inputs to the whole seaside instead of only the corners of the modelled domain. The model was then validated using water level and flow velocity measurements from the metronome experiments by using different bed roughness values. The X-Beach results are quite close to the measured values with errors of a few millimetres for the water levels and a few centimetres per second for the flow velocity. These errors are in the same range as errors found when modelling the metronome using the Nays2D model. Expressed as a Brier Skill Score the X-Beach model performs reasonable to excellent with values in the same range as other X-Beach studies of normal scale coasts. Besides these promising results, some improvements can still be made concerning the new boundary condition and flow velocity measurements. In future studies, waves and morphology can be added to the model which makes the model a valuable addition to the metronome experiments and estuarine research.

| Contents

1. | Introduction

Estuaries can be found all over the world. They form in places where rivers flow into the sea under the influence of tides and waves. In the highly dynamic estuaries many different habitats can be found, which all have their own characteristics such as inundation duration or salinity. This makes estuaries, which are sheltered from the hydrodynamic energy form the sea, essential coastal ecosystems for many different species (Potter, 2001; US EPA, 2023). The high biodiversity of estuaries shows that they are one of the most productive ecosystems on earth (NOAA, 2023). Next to the significance for nature, estuaries are also very important to human society. Over 1.2 billion people inhabit cities in the coastal zone, many of which are built near estuaries like Hong Kong, Buenos Aires and London (Day et al., 2012; Small & Nicholls, 2003). Estuaries are a preferred location for cities, because of marine food availability, fertile soils for agriculture and because of their access to both river and sea. This makes them economically important, because transport of people and goods over water can start and end here (Wetz & Yoskowitz, 2013). These are just a few things showing why estuaries are such important areas for both nature and humans. However, estuaries are facing a lot of challenges as well, most of them directly or indirectly caused by human actions. An example of this is dredging in estuaries to improve the navigability for large ships in the estuaries. This can destroy habitats and may result in unwanted morphological changes to the estuary (Cox et al., 2022). Another example of challenges for estuaries is the rising sea level. Because of global warming, sea level is rising with a rate of 3.2 mm/year globally since the end of the twentieth century (Mimura & Horikawa, 2013; Oppenheimer et al., 2019), while sediment supply decreases because of changing precipitation patterns and the construction of dams (Lu et al., 2013; Ranasinghe et al., 2019). When there is less sediment available, sediment accumulation is not enough to keep up with the rising sea level. To prevent losing these estuarine environments, it is important to study them. When we understand the processes happening in estuaries, we may be able to predict the consequences when changes to the system occur.

Estuarine studies are often performed using numerical models. These models can be used to simulate all kind of estuarine processes including estuarine hydrodynamics and morphodynamics (Ganju et al., 2015; Hibma et al., 2004). Based on these simulations, the processes in estuaries and effects of changes in them can be studied. A large benefit of the use of models is the fact that data can be gathered continuously and much quicker. In real life estuaries, measurements are often only made on specific locations in space and time through the years, rather than considering the system as a whole. Small-scale laboratory sized estuaries are another way to study the dynamics of their real-size versions. Because of their smaller scale, data can be gathered much more quickly than in real size estuaries (Kleinhans et al., 2017). Studies using laboratory-scale estuaries can also benefit from this continuous data gathering using models (Weisscher et al., 2022). Nevertheless, the modelling of laboratory estuaries is not commonly used, if only because laboratory experiments of estuaries are rare. There are only few examples where processes in flumes are modelled such as water levels (Namin et al., 2004) and particle transport (Henniger et al., 2010).

The aim of this study is to validate the coastal X-Beach model for the metronome flume. The numerical computer model X-Beach, which simulates coastal hydro-morphodynamics, will be compared to laboratory experiments conducted in the tilting metronome flume. This flume is used to study laboratory scale estuaries which can benefit from a well working model. With a well working model more data of hydrodynamics and morphological processes can be modelled for longer experiment times. Compared with the previously used 1D Speer-Aubrey model and Nays2D model (Kleinhans et al., 2017; Weisscher et al., 2022), X-Beach is especially made to deal with more complex coastal processes. This is important when trying to upscale the metronome experiments in future studies to real size estuaries. To make X-Beach work with the metronome, flow velocity and water level data from previous and new laboratory experiments will be used to validate the hydrodynamic part of the X-Beach model and to identify the most important factors which influence the model results.

The following chapters will first cover some background information on estuaries, the metronome and coastal models with in particular the X-Beach model (**Chapter 2**). After this the methods of the metronome experiments and data collection and analysis (**Chapter 3**) and the results (**Chapter 4**) are presented. Following this, the results are discussed (**Chapter 5**) after which the report concludes with a set of conclusions and recommendations (**Chapter 6**).

2. | Background

This chapter provides background to the X-Beach study. It first gives a brief overview of the processes taking place in estuaries (**Chapter 2.1**). This is followed by an introduction to the metronome flume and the various data collected in it (**Chapter 2.2**). Finally, attention is paid to the use of computer models in coastal research (**Chapter 2.3**) with a special focus on the X-Beach model used in this study (**Chapter 2.4**).

2.1 | Estuarine processes

Due to the many forms of estuaries it is difficult to give an all-encompassing definition of an estuary. Pritchard (1967) defines an estuary as "*(…) a semi-enclosed coastal body of water which has a free connection with the open sea and within which sea water is measurably diluted with freshwater derived from land drainage.*". This definition shows the unique combination of marine and terrestrial influences acting on the same area. These influences include waves, tides, currents and storms from the seaside, and river sediment and fresh water supply from the riverside (**Figure 1a**). Both river and sea provide energy to the estuary system with these processes. The part of the estuary closer to the sea is dominated by marine influences. Closer to the mouth of the river, this balance of energy is river dominated. In the middle we find a mixed energy zone (Dalrymple et al., 1992). This balance between marine and river forces makes every estuary a unique system. Because these forces are different in every estuary, a division can be made based on the most important force acting on the estuary: tides, waves or the river (**Figure 1b**). These three forces drive the processes in an estuary and therefore also determine its shape (Cooper, 1993; Friedrichs, 2011).

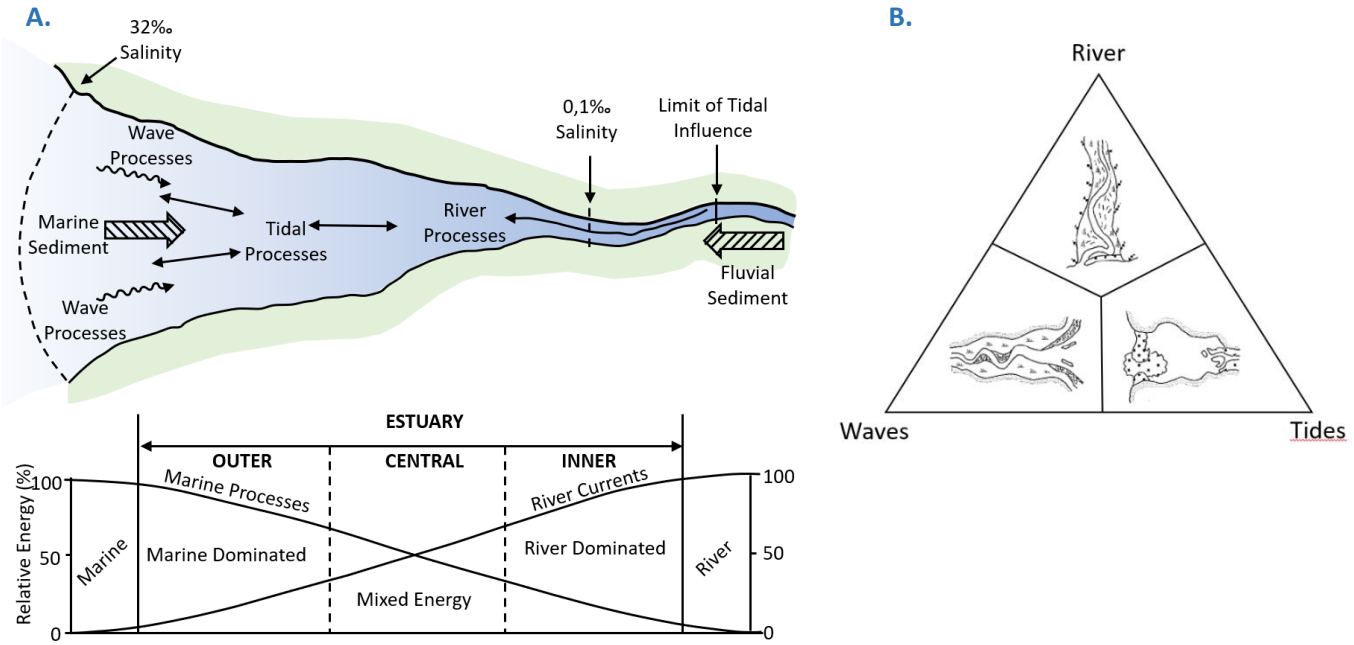

***Figure 1**: (a) Some of the processes in an estuary. These processes control the energy distribution over the estuary causing erosion and sedimentation. According to Pritchard (1967), the estuary borders are defined by the salinity of the water. Adapted from (Dalrymple et al., 1992). (b) River, wave and tide dominated estuaries. The shape of the estuary is determined by the most important force acting on it. Adapted from (Friedrichs, 2011).*

The complex interaction of marine and terrestrial drivers results in a highly dynamic environment. In an estuary, we often find large patterns of channels and shoals in the centre of the estuary, while the banks are characterised by areas with mudflats and marshes.

The deeper subtidal channels experience higher flow velocities from the tidal currents going in and out the estuary. This makes high amounts of sediment transport possible here, forming bedforms like dunes at the bottom of the channel. Some channels are more active during ebb or flood. These are more open to one of

the two currents because of their orientation relative to the current. These channels are often located at a shoal where the channel ends (**Figure 2**) (Kleinhans et al., 2015; Van Veen, 1950). When these shoals are surrounded by ebb and flood channels, a circulation pattern can occur in which sediment is transported around a shoal. This has been observed in both experiments and real estuaries such as the Western Scheldt (Leuven et al., 2018).

In contrast to the channels, the intertidal shoals are much more shallow and therefore not continuously inundated. Currents are less strong here causing less sediment transport and therefore smaller bedforms like ripples may develop. Although the channels and shoals differ from each other, there is still a lot of interaction between them in the form of sediment exchange. Driven by the currents, sediment from shoals is brought back into the channels and the other way around, shaping the morphology of the estuary (Schramkowski et al., 2004; Schuttelaars & De Swart, 1999). The dimensions of the shoals are related to the rest of the estuary. Bar height is for example correlated to the local water depth and bar length and width are related to the width of the estuary (Leuven et al., 2016).

Lastly, on the sides of the estuary we find the mudflats and marches. These areas are characterised by finer sediment and even less or no inundation time compared to the shoals. This makes it possible for vegetation to grow here making different ecomorpholocial feedbacks possible.

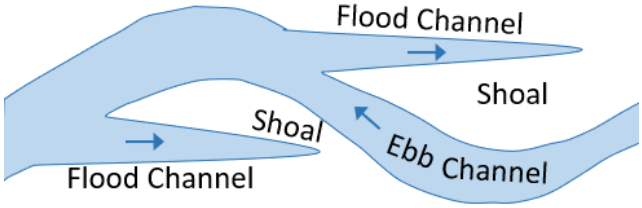

***Figure 2**: Ebb and flood dominated channels in estuaries ending at shoals. Adapted from (Van Veen, 1950).*

2.2 | The Metronome flume for scale experiments of estuaries

Estuaries can be studied in three ways: either by using data from a real estuary, recreate an estuary at laboratory scale, or model the estuary and the processes in it using a computer. The benefit of looking at a real estuary is that the actual processes can be studied. However, because estuaries have a large spatial scale, changes may take a lot of time. Therefore, it takes a lot of time to collect a representative dataset. To solve this, estuaries are recreated both in computer models and in small scale laboratory experiments. The benefit of these two methods is that data can be gathered more quickly, as the processes are happening in a computer (for the model) or on a much smaller spatial scale (for the laboratory experiments).

These laboratory experiments are often performed in flumes. Usually, water flows in at one side of such a flume, and out the other. In the area between the in- and outlet, the hydrodynamics and morphodynamics of the system can be studied. One of the flumes in which estuary experiments are being performed, is 'the metronome'. The metronome was built between 2014 and 2015 at Utrecht University. In this flume, currently located in the Earth Simulation Laboratory (ESL), small scale estuaries can be created and studied. The flume itself consists of a steel basin, which is 20 metres long, 3 metres wide and 0.4 metres deep on the inside (**Figure 3a**) (Kleinhans et al., 2017). Both ends of the metronome are equipped with a small tank. Water is being pumped in here from the 12 m^3 reservoir next to the metronome. In the current set-up, the riverside tank is closed off from the estuary so water can only infiltrate in the sand but not flow freely in and out the estuary from this side.

The unique ability of this flume is that the whole flume can tilt over its central, short axis in the middle of the 20 metre length. The name of the flume, metronome, is based on this periodic tilting of the flume. The tilting is done by four actuators, two on each side. When the riverside is above the horizontal, the river pumps are turned on, giving a small discharge at the river inflow. When the seaside is above the horizontal, a wave maker

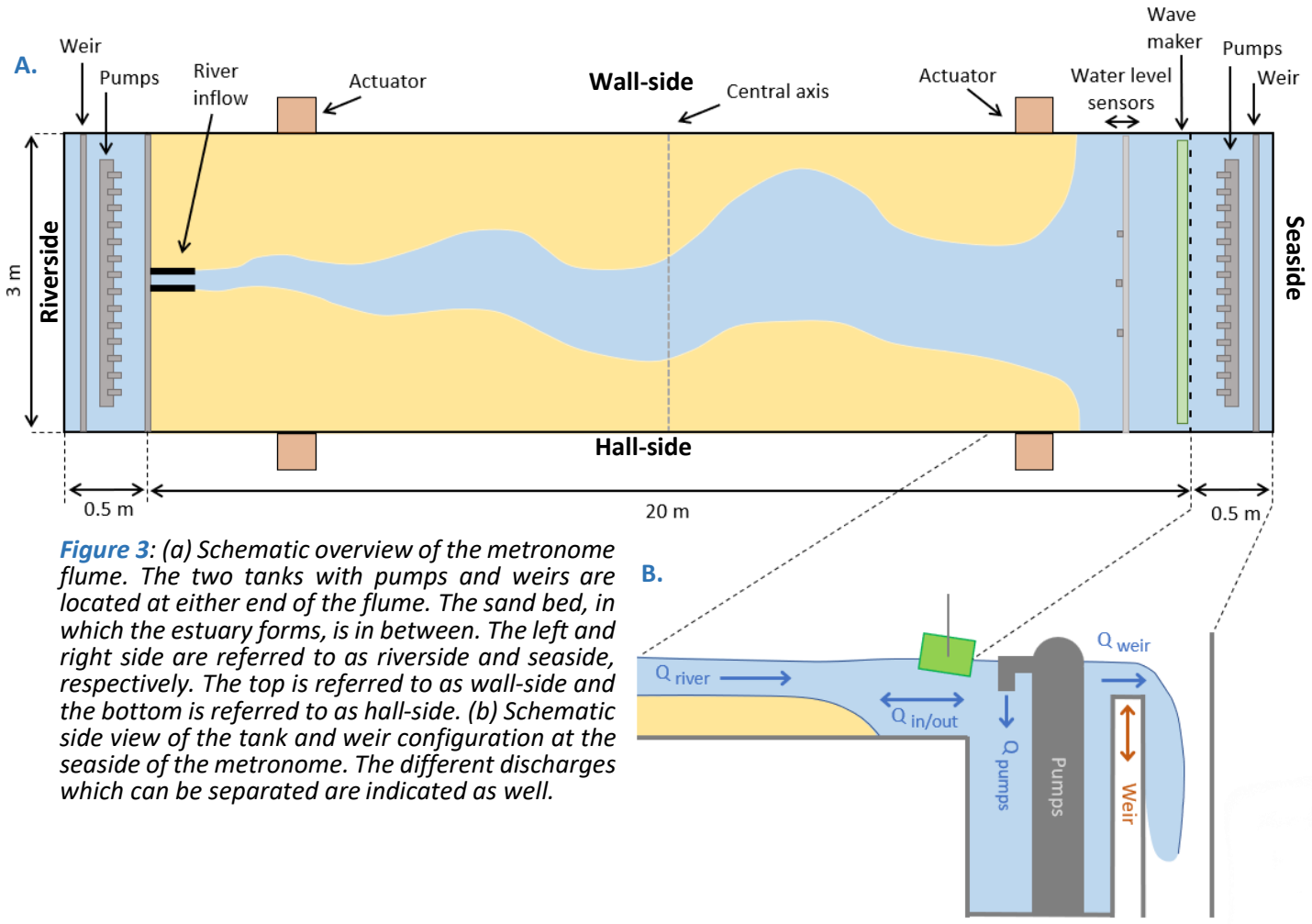

Figure 3: (a) Schematic overview of the metronome flume. The two tanks with pumps and weirs are located at either end of the flume. The sand bed, in which the estuary forms, is in between. The left and right side are referred to as riverside and seaside, respectively. The top is referred to as wall-side and the bottom is referred to as hall-side. (b) Schematic side view of the tank and weir configuration at the seaside of the metronome. The different discharges which can be separated are indicated as well.

is turned on. By asymmetrical movements of a foam beam, small waves are created. To control the water level in the two end tanks, there is a weir at the end of each tank, behind the pumps (**Figure 3b**). These weirs can move up and down to prevent too much water from flowing out while the metronome is tilting. Water flowing over the weir has a critical flow and is returned to the main reservoir (Kleinhans et al., 2017). Because the riverside tank is closed off from the rest of the system in the current setup, only the seaside weir is used.
To avoid confusion over locations in the metronome, the two ends of the flume are referred to as the sea- and riverside, right and left in **Figure 3a**. Because the metronome is positioned along a wall in the laboratory, the two long sides are referred to as wall-side and hall-side, top and bottom in **Figure 3a** respectively. The coordinate system of the metronome has its origin at the point where the hall-side meets the riverside tank. From there the positive x-axis goes towards the seaside where the bed ends at x = 20 m. The positive y-axis goes towards the wall-side to the other edge of the flume at y = 3 m.

The tilting of the flume makes it possible to study long laboratory scale estuaries. Previous experiments tried to recreate these estuaries in a flume by sea level fluctuations to simulate the tide (Reynolds, 1887, 1889; Tambroni et al., 2005). However, in these experiments no large-scale estuaries formed because of the low sediment mobility and an ebb dominated transport (Kleinhans et al., 2014). In natural systems, this sediment mobility is much higher, causing more sediment transport. A higher sediment mobility can be acquired in a laboratory setting by using a larger bed gradient. The gradient has to be even larger than the gradient of natural systems, because the water depth in the laboratory is much less than in nature (Leuven et al., 2018). The larger gradient increases the shear stress, resulting in an increase in transportation of the sand grains. To acquire this larger bed gradient, the metronome was constructed. Due to the possibility to tilt the whole flume, the flow velocity and shear stress are higher, causing an increase in sediment mobility and transport, resulting in longer, naturalistic estuaries. Since the construction of the metronome, 62 experiments and several pilot

runs have been conducted. These include experiments studying estuary forms (Leuven et al., 2018), the influence of vegetation and mud (Weisscher et al., 2022),the effects of dredging (Cox et al., 2022) and ongoing research on the effects of dikes.

In the current study, data from the 54th and 59th metronome experiment were used. Both experiments were designed to study the effect of different dike setups on the estuary channel network. In both experiments, sandpaper dikes were placed in the bed of the metronome to restrict the water flow. The sandpaper was used as dikes because the coarse surface has a higher friction. In experiment 54, the dikes were set up in a wavy line from river to sea, based on the morphology attained after 2000 metronome cycles in a previous experiment (**Figure 4a**). In experiment 59, the dikes were set up in a straight line from the river to the sea (**Figure 4b**). To gather data from the experiments, seven overhead cameras, a SLR (Single Lens Reflex) camera and a laser scanner, all mounted above the metronome, and three water level sensors, hanging above the bed, were used. In the current study, data from the overhead cameras, the laser scanner and the water sensors was used, both from the 54th and 59th experiment. With this, flow velocities, bed levels and water levels can be obtained.

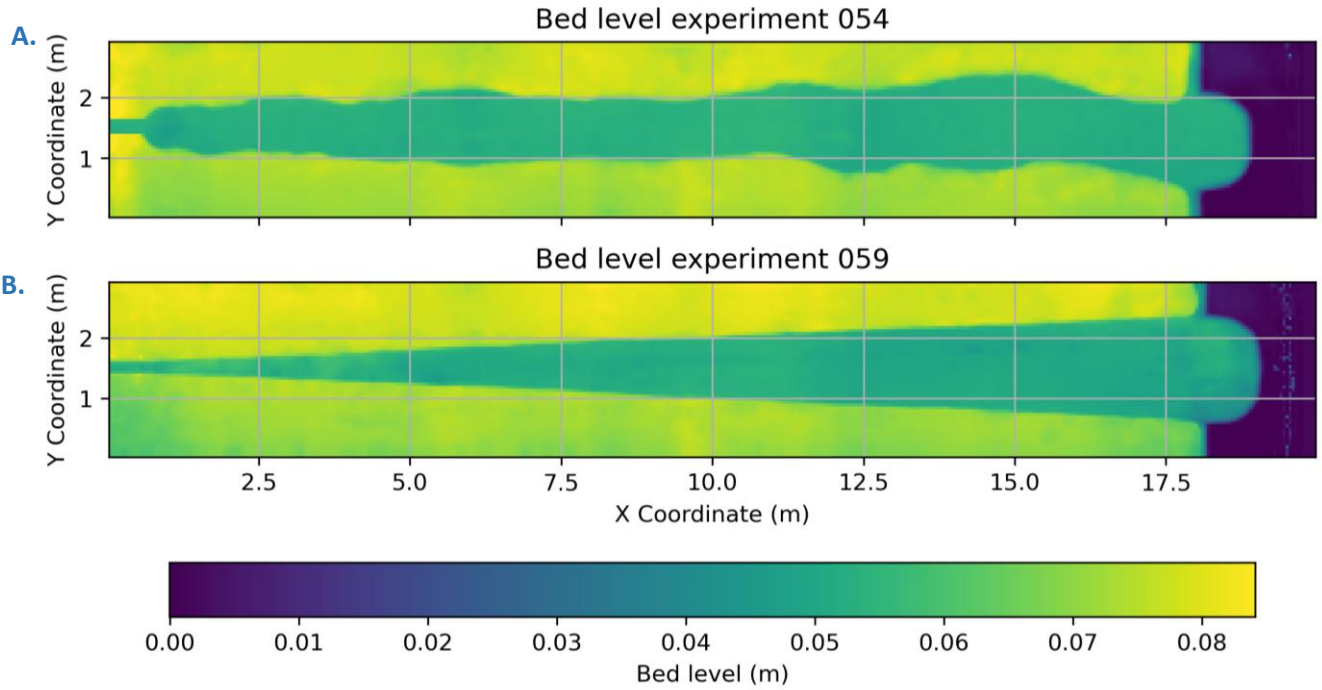

Figure 4: Bed levels of experiment 54 (a) and experiment 59 (b). The dike setup is well visible. For experiment 54 the dikes were placed based on a 2000 cycle morphology. In experiment 59 the dikes were placed at the begin of the experiment and made as straight as possible from river to sea instead of the more wave pattern of experiment 54.

2.2.1 | Flow velocity measurements

Flow velocity in the metronome is measured using a technique called Particle Image Velocimetry (PIV). The PIV technique is based on tracking objects in a moving medium. These can be dust particles in the air, but also floating particles in water (Thielicke & Stamhuis, 2014). Based on the movement of the particles, velocities can be calculated. PIV can be used both in laboratory experiments and in-situ studies. When PIV is used in large scale studies, it is called Large Scale Particle Image Velocimetry (LSPIV). Natural or artificial particles are followed as they are transported by the flow of a river or other body of water. Natural particles which can be used are for example leaves, foam patches or ice floes (Leenman & Eaton, 2023). These particles are then followed with cameras mounted to helicopters (Legleiter & Kinzel, 2020), drones (Bandini et al., 2021) or with stationary cameras (Hauet et al., 2008). From the imagery, the distances travelled by the particles are calculated and from that the speed of the particles and hence the flow speed of the current. A very similar

process is done at the metronome, but at a much smaller scale. The collection of flow velocity data is important because the flow velocity is a key factor for the sediment transport in the metronome.

The velocity data gathered using this PIV technique is the surface velocity of the water because it is measured based on the floating particles in the flow. However, the X-Beach model, used in this study, calculates depth averaged flow velocities. Flow velocities near the bottom of a channel experience more friction and are therefore lower than flow velocities higher up in the water column. It is therefore necessary to convert the surface velocities into depth average flow velocities to compare the measured and modelled values. The conversion done using the logarithmic velocity profile equation which describes the change in velocity from bottom to surface (**eq. 2.1**).

$$\frac{u}{u_*} = \frac{1}{k}\ln\left(\frac{z}{z_0}\right) \qquad \textbf{eq. 2.1}$$

In this equation u is the flow velocity at depth z. u_* represents the shear velocity, k is the Von Kármán constant which has a value of 0.4 and lasty z_0 represents the roughness length. Using this equation factor α can be calculated. This is the ratio between depth averaged velocity U and surface velocity u_s. By using the logarithmic velocity profile equation for both velocities and substituting them, the following equation is obtained (**eq. 2.2**) (Biggs et al., 2023):

$$\alpha = \frac{U}{u_s} = \frac{1}{1 - e^{-\left(\frac{u_s k}{\sqrt{gHS}}\right)}} - \frac{\sqrt{gHS}}{u_s k} \qquad \textbf{eq. 2.2}$$

In here g is the gravitational acceleration, H is the water depth and S the bed slope. For this equation the assumption is made that a shallow flow with relative high roughness is used (Biggs et al., 2023), something which is the case for the metronome flume. With this equation the factor α can be calculated. By multiplying α with the measured surface velocity, the depth averaged flow velocity can be found, which then can be compared to the X-Beach model results.

2.2.2 | The bed of the metronome

The bed of the metronome consists of a layer of sand. The sand used in the bed has a median grain size of 0.52 millimetres with a D_{10} (10% is finer) and D_{90} (10% is coarser) of 0.33 and 1.2 millimetres (Leuven et al., 2018). In the area behind the dikes, the sand layer is approximately 8 centimetres thick. In the channel, the layer is around 5 centimetres thick. In the sea part of the metronome there is no sand. Here a layer of artificial grass, which continues under the sand, makes up the bottom. This artificial grass is placed to ensure there are no large roughness gradients at places in the channel where all the sand has been eroded.

The metronome is equipped with a line laser scanner on a gantry to make Digital Elevation Models (DEMs) of the bed. This is done by making laser scans of the dry bed. This results in DEMs with a vertical resolution up to 0.2 millimetre and a horizontal resolution of 3 millimetre (Weisscher et al., 2022). The development of the morphology of the bed is tracked with seven overhead CMOS MAKO color cameras which are triggered once every cycle (Leuven et al., 2018).

2.2.3 | Water level monitoring

Water levels are obtained from three water level sensors, which can be moved along the metronome. The water level sensors are so-called Single Beam Echo Sounders (SBES's). These sensors send out an acoustic signal, which reflects on the water surface. By measuring the time between the outgoing and incoming signal, the distance between the sensor and the water can be calculated, and from this the water level. In the metronome setup, there are 3 Massa M320/150 loggers (Onselen, 2017). The sensors are at fixed y-locations of y = 1.03, 1.48 and 1.96 m (**Figure 3a**), but the beam to which the sensors are mounted can be moved along the flume to take measurements at different x-positions. The sensors have an accuracy of 0.1% of the target

range. The data of these sensors will be used to compare the water levels in the metronome with the modelled ones of the X-Beach model.

2.3 | Numerical modelling of estuaries

Next to laboratory experiments, computer models are often to study coastal morphodynamics, because they are an easy way to change only one condition to see the effects it has on the system as a whole. This way, processes in an estuary can be studied and the effects of, for example, vegetation or dredging on the estuary morphology may be predicted. Furthermore, it is possible to study these effects in the future. This can evidently not be done using a real-life estuary, making this one of the many advantages of using a model. An additional advantage of models is that continuous data is available for the whole estuary. Accurate measurements for flow velocity and water depth can often not be taken continuously in real estuaries, so data is only available at certain (biased) moments in time. The same data acquisition problem also applies for experimental estuaries, so these small scale estuaries also benefit from the possibilities of numerical models (Weisscher et al., 2022).

When modelling estuaries, there is a wide choice of (numerical) models available. In previous studies, models like Delft3D, TELEMAC, FINEL2d WAQUA, unTRIM, MIKE3, ROMS and SWAN, have been applied to estuaries all over the world (Dam et al., 2016; George et al., 2012; He et al., 2022; Talke & de Swart, 2006; Warner et al., 2005). In these cases, the models were used on real life estuaries. However, laboratory estuaries can also be modelled, although this approach is not frequently used. In one study, a numerical model was used in a flume with a small tidal basin experiment to model flow velocity (Stefanon et al., 2010). In the metronome, two models have previously been used. The first one is the Speer-Aubrey one-dimensional numerical model. This model was built to study the influences of friction and geometry on the tidal distortion in an estuary (Friedrichs & Aubrey, 1988). The model was adapted for the metronome and good results were obtained with it (Kleinhans et al., 2017). Because this model works only in one dimension, an additional study using a two-dimensional model has been performed at the metronome. In this study, the numerical Nays2D model has been used for the metronome flume. This model, which is often used in river research (Bahremand et al., 2020; Hun et al., 2015; Schuurman et al., 2016), predicts hydrodynamics and sediment transport. Because the model is compatible with a very shallow flow of only a few centimetres deep, it is especially suited to laboratory experiments (Weisscher et al., 2020). During the experiment in the metronome, only hydrodynamics and the sediment transport were considered, while morphological changes were not (Weisscher et al., 2020). A major disadvantage of this model is the limited possibilities for the morphology, as well as the fact that it is a Japanese model with Japanese documentation, making it difficult to use. Therefore, in this study the X-Beach model will be used. This model is expected to perform better when looking at morphology, as it was developed to model this for near shore environments (Deltares, n.d.). Furthermore, all documentation is available in English making the model easier to use.

To assess how well a model is performing, the results from the model can be evaluated based on the bias, the accuracy and a skill score. The bias refers to the difference between the modelled results and observations. This shows if the model is over- or underpredicting. The bias can be shown by calculating the difference between the mean (**eq. 2.3**) or median (**eq. 2.4**) of both the model prediction values and observations.

$$Bias_{mean} = \frac{1}{n}\sum_{n=1}^{n}\left(x_{n,prediction} - x_{n,observation}\right) = \overline{X_{prediction}} - \overline{X_{observation}} \qquad \textbf{eq. 2.3}$$

$$Bias_{median} = X_{M,prediction} - X_{M,observation} \qquad \textbf{eq. 2.4}$$

In here $x_{n,prediction}$ and $x_{n,observation}$ are a value at the same place and time out of the data sets with n model predictions ($X_{prediction}$) and n observations ($X_{observation}$). $X_{M,prediction}$ and $X_{M,observation}$ are the median values out of these two data sets. The lower the bias, the better the model is performing. This gives an indication about the model's reliability (Sutherland et al., 2004).

However, a reliable model may still be wrong. This is why the accuracy of a model should also be considered. The accuracy measures the error of the modelled results. The error is roughly equivalent to the difference between the two datasets and can be calculated with the mean absolute error (MAE) (eq. 2.5), the mean square error (MSE) (eq. 2.6) or the more commonly used root mean square error (RMSE) (eq. 2.7).

$$MAE = \frac{1}{n}\sum_{n=1}^{n}\left|x_{n,prediction} - x_{n,observation}\right| = \overline{\left|X_{prediction} - X_{observation}\right|} \quad \text{eq. 2.5}$$

$$MSE = \frac{1}{n}\sum_{n=1}^{n}\left(x_{n,prediction} - x_{n,observation}\right)^2 = \overline{\left(X_{prediction} - X_{observation}\right)^2} \quad \text{eq. 2.6}$$

$$RMSE = \sqrt{\frac{1}{n}\sum_{n=1}^{n}\left(x_{n,prediction} - x_{n,observation}\right)^2} = \sqrt{\overline{\left(X_{prediction} - X_{observation}\right)^2}} \quad \text{eq. 2.7}$$

Based on these errors, it may be quantified how close the modelled predictions are to the measured observations to see how well the model is performing (Sutherland et al., 2004).

The accuracy was calculated based on the modelled and measured values during the experiment at the same location and at the same time. However, it is possible to relate the model predictions to, for example, the initial bed level. Such a comparison to a baseline predictor is the skill score of a model. This skill assesses how well the model's predictions match observed values compared to a scenario where no predictions are made. It measures whether the model represents real-world conditions better than a situation with no modelled changes, helping to evaluate the model's accuracy. An often-used skill score in coastal modelling is the Brier skill score (BSS) (eq. 2.8) (Davidson et al., 2010; Sutherland, 2016; L. C. Van Rijn et al., 2003; L. C. V. Van Rijn et al., 2002).

$$BSS = 1 - \frac{MSE(X_{prediction}, X_{observation})}{MSE(X_{baseline\ predictor}, X_{observation})} \quad \text{eq. 2.8}$$

The skill score will be a number ranging from negative to 1, where a negative score indicates a bad result and 1 indicates an excellent result (Table 1) (Sutherland et al., 2004; L. C. Van Rijn et al., 2003).

Table 1: *Classification table Brier Skill score. Adapted from* (Sutherland et al., 2004)

	BSS
Excellent	1.0-0.5
Good	0.5-0.2
Reasonable	0.2-0.1
Poor	0.1-0.0
Bad	<0.0

2.4 | Coastal modelling with the X-Beach model

2.4.1 | Original development of the model

The model used to model processes in the metronome in the current study, is the X-Beach model. After the enormous damage left by hurricanes in the USA during the hurricane seasons of 2004 and 2005, a project was started to assess the vulnerability of coastal areas. This resulted in the Morphos-3D project of the US Army Corps of Engineers. Part of this project was a new model, named X-Beach (eXtreme Beach), which predicts near shore hydrodynamics and morphology including waves, currents and erosion. The development of this model was led by Prof. Dano Roelvink and involved experts from UNESCO-IHE, Deltares, Delft University of Technology and the University of Miami (Deltares, n.d.). With this open source model, coastal vulnerability could be assessed to improve coastal safety for future hurricane events. Using 2D horizontal equations, the model solves waves and flow. This includes both long and short waves, also taking wave groups with their 'surf

beat' into account. Sediment transport is then modelled using these hydrodynamics. From this, morphologic changes to the seabed, beach and dunes can be predicted, including possible overwash and breaching of the dunes to assess the coastal safety.

2.4.2 | Functioning of the X-Beach model

The X-Beach model is an extensive model with many options which can be used. All possibilities are described in the X-Beach manual and different papers about the model (Deltares, 2023; Roelvink, 2015; Roelvink et al., 2009; Smit et al., 2010). The sort version of this is presented in the flowchart in **figure 5**.
The model starts with reading the user defined inputs. This are variables such as bed friction and sediment sizes but also information about the coordinate system and bed levels. Next to this time series for tides and discharges can be specified and the boundary conditions and start and end times are entered.
All calculations are made based on a cartesian coordinate grid. In this grid, the orientation of the x-axis is always towards the coast from the seaside with an alongshore y-axis. Most values are calculated for the cell centres. However, some, like velocities, sediment transport and radiation stress gradients, are calculated for the cell interfaces and then interpolated for the cell centres (Roelvink et al., 2009).

2.4.3 | Boundary conditions in X-Beach

After reading the inputs, the time step is determined. In each time step a series of model sections is executed. At the end and the time step the outputs are saved and if the end time is not reached, the series of model parts starts over again. The first step is to check whether the boundary conditions are met. There are three sets of boundary conditions one for the wave computations, one for the shallow water equations and one for the sediment transport. Because this study focusses on the hydrodynamics, the shallow water equation boundary conditions are the most important. This set of boundary conditions consist of 4 parts. First of all we

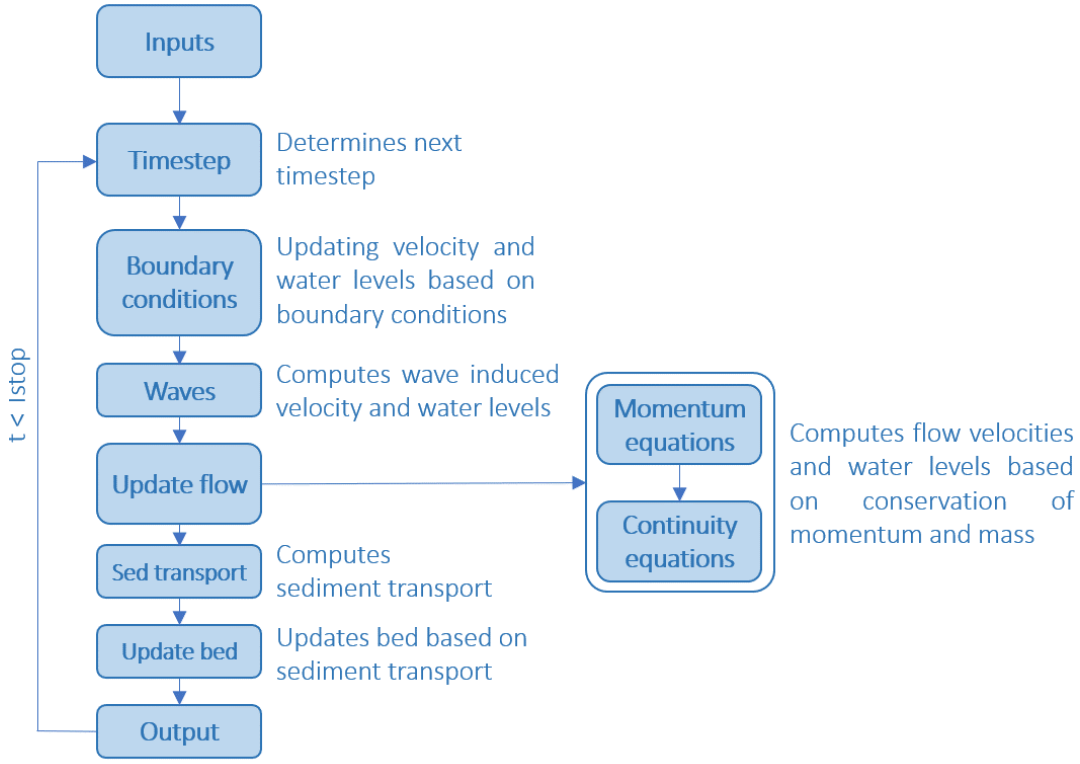

***Figure 5**: Simplified flow chart of the X-Beach model. The model starts by reading all input parameters. After this, the time step is determined and the boundary conditions are checked. Then, wave motion and its velocities are calculated. Next, the flow and water levels in the modelled domain are computed. This is done based on the conservation of momentum and mass using a continuity equation (**eq. 2.13**). When flow velocities and water levels are calculated, they are used to compute the sediment transport. This transport is then used to update the bed based for the places where sedimentation or erosion takes place. Lastly, the outcomes are stored in the output file. When the end time is not reached yet, another cycle of calculations is performed for the next timestep. Adapted from* (Smit et al., n.d.).

have the offshore boundary. This boundary condition describes how the water at the offshore edge of the modelled domain is behaving. There are several options but in this study most of the time the 'wall' or 'absorbing-generating' boundary condition was used. The 'wall' boundary condition is a no flux boundary where no flow is possible through the boundary. This causes waves to reflect back at the boundary. The 'absorbing-generating' condition describes the boundary using a formulation in which waves and flow will be absorbed by instead of being reflected at the boundary. This can be either in a one-dimensional or a two-dimensional way. The second boundary condition is for the lateral boundaries. This one also has a no flux 'wall' boundary. Another used option for this boundary condition is the Neumann boundary condition which states that along these lateral boundaries there is no change in water level and flow velocity. This to prevent large gradients at the sides. The third shallow water equation boundary condition has to do with the tides. The model forces a certain water level or water level series to the corners of the modelled domain. These forced water levels are then used in the model calculations for that timestep. The last boundary condition describes the position and discharge of river inputs. These rivers can enter the modelled domain from the sides if their location and discharge is specified in the input file.

2.4.4 | Hydrodynamic calcualtions in X-Beach

When the boundary conditions are accounted for, X-Beach starts with calculating the wave action (**Figure 5**). The first versions of X-Beach were made to resolve short waves on the scale of wave groups. Hence, long waves connected to the wave groups are also included in X-Beach. Based on the wave action balance wave induced water levels and flow velocities can be calculated. In the metronome, the waves have a vastly different scale compared to those in real coastal zones. However, the 1 cm small waves in the metronome behave like normal size gravity waves, and therefore normal wave equations can be used (Onselen, 2017). The wave motions are not the main driver for the sediment transport in the metronome. Therefore, the wave part is not used in this study to validate X-Beach for the metronome hydrodynamics.

More important for the metronome hydrodynamics are the mean flows and their velocities as they induce most of the sediment transport in the flume. These currents are calculated in the next step of the X-Beach model (**Figure 5**). The currents are defined together with the low-frequency waves by the non-linear shallow water equations in the X-Beach model. To account for mass fluxes and return flows the shallow water equations are formulated using the Generalized Lagrangian Mean (GLM) (Andrews & Mcintyre, 1978; Walstra et al., 2000). With this method, velocities are split up in an Eulerian part and a Stokes drift part (**eq. 2.9**). The Lagrangian velocity (u^L) is calculated as the distance covered by a water particle in a single wave period divided by the duration of that period. This velocity can be seen as the velocity 'felt' by the water particles. The Lagrangian velocity is the sum of the Eulerian velocity (u^E) and the Stokes drift (u^S). The Eulerian velocity is described as the velocity of a particle when looking from a fixed location. This can be used as an estimation of the velocity as 'felt' by the bottom of the basin. Therefore, it can be used for sediment interactions. The Stokes drift (**eq. 2.10**) is the net motion of a water particle in a wave which results in the transport of water. This GLM formulation attempts to get the vertical dimension in the 2D horizontal model.

$$u^L = u^E + u^S \text{ and } v^L = v^E + v^S \qquad \textbf{eq. 2.9}$$

$$u^S = \frac{E_w cos\theta}{\rho hc} \text{ and } v^S = \frac{E_w sin\theta}{\rho hc} \qquad \textbf{eq. 2.10}$$

In these two equations, for the x and y directed velocities, E_w is the short wave energy which varies between wave groups. To obtain the Stokes drift, the energy is divided by water density ρ, water depth h and wave celerity.

Using both the Lagrangian and Eulerian flow velocities, GLM momentum equations are formulated for both x and y directed velocities (**eq. 2.11, 2.12**).

$$\frac{\partial u^L}{\partial t} + u^L \frac{\partial u^L}{\partial x} + v^L \frac{\partial u^L}{\partial y} - f v^L - \nu_h \left(\frac{\partial^2 u^L}{\partial x^2} + \frac{\partial^2 u^L}{\partial y^2} \right) = \frac{\tau_{sx}}{\rho h} - \frac{\tau_{bx}^E}{\rho h} - g \frac{\partial \eta}{\partial x} + \frac{F_x}{\rho h} + \frac{F_{v,x}}{\rho h} \quad \text{eq. 2.11}$$

$$\frac{\partial v^L}{\partial t} + u^L \frac{\partial v^L}{\partial x} + v^L \frac{\partial v^L}{\partial y} - f u^L - \nu_h \left(\frac{\partial^2 v^L}{\partial x^2} + \frac{\partial^2 v^L}{\partial y^2} \right) = \frac{\tau_{sy}}{\rho h} - \frac{\tau_{by}^E}{\rho h} - g \frac{\partial \eta}{\partial y} + \frac{F_y}{\rho h} + \frac{F_{v,y}}{\rho h} \quad \text{eq. 2.12}$$

In the two momentum equations, we have the velocity terms using the Lagrangian velocities, a Coriolis term with the Coriolis coefficient f and a viscosity term with the horizontal viscosity ν_h on the left hand side. On the right hand side we find a wind shear stress term (τ_{sx}), a bed shear stress term (τ_{bx}^E), wave (F_y) and vegetation ($F_{v,y}$) induced stresses and the water level η. Based on the conservation of momentum and mass, these momentum equations are then used in the continuity equation (**eq. 2.13**) which gives the relationship between the elevation of the depth averaged flow velocity and the water surface.

$$\frac{\partial \eta}{\partial t} + \frac{\partial h u^L}{\partial x} + \frac{\partial h v^L}{\partial y} = 0 \quad \text{eq. 2.13}$$

In this equation, the first term $\frac{\partial \eta}{\partial t}$ represents the water level change over time. The other two terms represent the x and y direction velocity change over time. An important thing to note here is that the X-Beach velocities are depth averaged velocities and not the flow velocity at the water surface.

2.4.5 | X-Beach morphodynamics

When calculations for the waves and flow are finished, sediment transport is calculated (**Figure 5**). Based on an advection-diffusion equation, sediment concentrations are calculated. This includes both bed load and suspended load. The last step is to update the bed level based on the calculated sediment transport. This is done based on the gradients of this sediment transport which indicate if erosion or sedimentation takes place at a certain location. In this step, there is also accounted for too steep slopes. When ridges are steeper than the maximum critical bed slope, sediment will be moved down to make the slope less steep. This avalanching can be seen as a trick to solve the problem that arises in many models, which is that the depth of channels is overestimated (Baar et al., 2019).

After the morphodynamics are calculated, all results of the current timestep are stored in the output file. When the end time is not yet reached, the loop starts over again for the next timestep.

3. | Methods

This chapter will discuss the used methods. To validate X-Beach for the metronome measurements of the metronome experiments are needed. Therefore, the workflow of the metronome and the collection of data in the metronome will be discussed first (**Chapter 3.1**). After this, the use of X-Beach is further explained and the different tests runs are clarified using 5 main categories of parameters that were tested within the X-Beach model (**Chapter 3.2**).

3.1 | Data collection in the metronome

3.1.1 | Normal workflow metronome

A metronome experiment consists of a repetition of a certain number of cycles in which the metronome tilts periodically. Measurements are conducted after the preparations before a new experiment, in between cycles and at the end of the experiment to collect the wanted data. All proceedings concerning the experiment are noted in the experiment log. The logs of experiment 54 and 59, from which data are used in this study, can be found in **appendix A**. At the start of an experiment, the bed has to be prepared. This preparation depends on the kind of experiment to be performed, but will always include some reworking of the sand and the levelling of the bed. As the metronome simulates a flood dominant system, more sand will be transported upstream than downstream during an experiment. When starting a new experiment, this sand has to be moved back to the seaside. After roughly distributing the sand evenly, the bed is levelled, further distributing the sand. In the experiments used in this study, sandpaper dikes were placed in the sand bed. Therefore, the area outside of the dikes and the channel area inside of the dikes had to be levelled separately at different heights. The levelling is done by moving the bridge, which is mounted on the metronome, back and forth while moving sand which a horizontal lateral movable board attached to the bridge. Next to this, a semi-circular delta is made at the seaward side. At this point, photos and scans of the initial dry bed are taken using the SLR camera and laser setup mounted in the gantry. When this is finished, the metronome is filled with water and another set of photos is made, this time of the initial wet bed. When the preparation is finished, the experiment can start.

The movement of the metronome and weir is controlled by a computer. The bed level of the seaside of the metronome (z_b) is described by a sinusoidal function (**Figure 6**, **eq. 3.1**). The variables for this function can be found in **table 2**. The weir uses **equation 3.1** as well but an offset of 67 mm is added. In the equation ω_1 and ω_2 are the angular velocities which are defined with $\omega = \frac{2\pi}{T}$.

$$z_b = z_{w0} + a_1\, cos(\omega_1 t - \varphi_1) + a_2\, cos(\omega_2 f t - \varphi_2) \qquad \textbf{eq. 3.1}$$

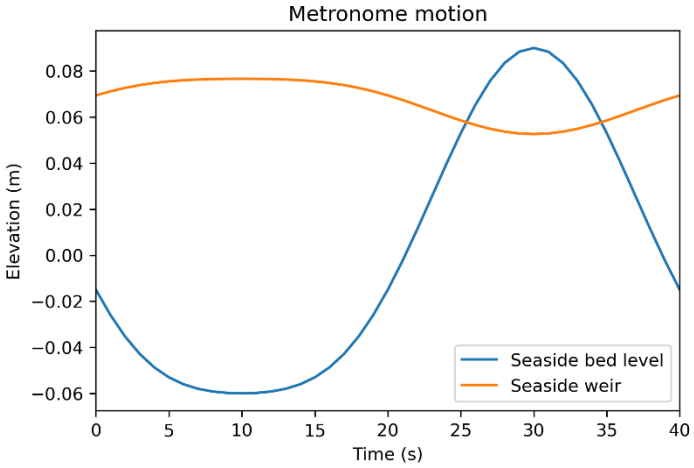

Figure 6: *Sinusoidal function of the metronome and weir movement. The metronome elevation is in respect to its horizontal position. The weir elevation is in respect to the bed level.*

Table 2: *Sinusoidal function variables of metronome tilt and seaside weir with symbol and X-Beach variable name.*

	Tilt	Weir	*Symbol (X-Beach)*
Period (s)	40.0	40.0	T, $metro\_period$
1st amplitude (mm)	75.0	12.0	a_1, $metro\_amp1$
2nd amplitude (mm)	15.0	2.4	a_2, $metro\_amp2$
Phase shift 1 (°)	90	90	φ_1, $metro\_phase1$
Phase shift 2 (°)	0	0	φ_2, $metro\_phase2$
Frequency multiple (-)	2	2	f, $metro\_period2$
Offset weir (mm)	0	67.0	z_{w0}

In addition to these parameters, the trigger time for the overhead cameras and the number of cycles are specified in the computer. Because changes to the bed tend to happen more quickly at the start of the experiment, smaller numbers of cycles (100, 200 or 500 cycles) are being done at the start of the experiment. This number is increased later, when the changes to the bed take more time (1000, 2000 or more cycles). While the metronome is turned on, the river gives a discharge of 500 l/h while the riverside is above the horizontal position of the flume. When the riverside is below the horizontal, there is no water coming from the river. While the metronome is moving, the overhead cameras are triggered once every cycle when the flume is horizontal. Using these images, the development of certain features in the bed can be tracked.

When the metronome has finished a set of cycles, the current state of the bed is captured. This is done by collecting imagery of the wet and dry bed. From the top, an image is taken every 50 centimetres by the SLR camera on the laser gantry of the wet bed. Furthermore, a handheld camera is used to take images from the sides of the metronome. These images can be used to zoom in on interesting features in the estuary. When this set of images is collected, the flume is drained by lowering the seaside weir and turning off the pumps. When the bed is dry, another set of images is taken with the SLR camera in the gantry. After this, a laser scan of the dry bed is made. To avoid scattering in the scan, the lights above the metronome are turned off. With all data collected the flume is filled again after which a new set of cycles can be started. This procedure, of running the experiment for a certain number of cycles and collection of imagery, is repeated until the channel reaches the sides of the flume (in the current experiments, the aforementioned dikes made this impossible) or when the delta reaches the wave maker at the end of the basin.

In addition to this normal workflow, sometimes additional data on flow velocities and water levels are gathered. This is not done in between each set of cycles, as it takes quite some time to do the measurements which would otherwise delay the experiment. When flow velocity and water level data are needed, they are measured at the start and the end of an experiment. This way, data are available for the initial situation and for the situation with a developed morphodynamic bed.

3.1.2 | PIV measurements

To validate X-Beach for the hydrodynamics in metronome flume, flow velocity measurements are used. Flow velocities in the metronome are measured using Particle Image Velocimetry (PIV). The velocity is determined by measuring the displacement of small particles on the water surface in repeated images.

During the PIV process the flume is seeded with small white plastic particles with a diameter of around 3 mm. The particles are scattered as evenly as possible, to achieve a well-distributed cover without large clumps of particles. While the metronome is tuned on, the particles flow back and forth with the water. Meanwhile, the overhead cameras are triggered multiple times in a row at a 25 Hz frequency. This way, the cameras take a sequence of ten images with 40 milliseconds between them. These image sequences are later analysed to determine the flow velocity. Usually the PIV measurements take ten cycles. During the first four cycles, image sequences are made at 22.5 seconds into the cycle. At this point, the metronome is in between ebb and flood phase and is in a horizontal position. During the remaining cycles, when the water is moving more freely, image

sequences are made every fifteen seconds. Because the metronome tilts with a 40 second period during the experiments used in this research, this resulted in data at 0-15-30-5-20-35-10-25-0-15-…etc. seconds. With all the images collected, the PIV particles are removed from the flume, taking care not to disturb the bed.

The next step is to analyse the collected data. For each time the cameras were triggered, there is a set of 70 images (ten sets of seven images along the flume). The sets of seven images are stitched together so they form one large image. Because there are only seven images with limited overlap, the stitching is not perfect. The current stitching technique is based on camera locations and overlap percentages of the images. However, these stitched photographs are still preferred over an analysis using each camera separately, as this takes much more time, and errors are more likely, because seven coordinate systems of the different images have to be matched.

The stitched images are analysed with the PIVlab toolbox (version 2.62) (Thielicke, 2023). PIVlab is developed by Dr. William Thielicke as an add-on for MATLAB (The MathWorks Inc., 2023). The analysis in PIVlab consists of three major steps: pre-processing, image evaluation and post-processing. The pre-processing consists of defining a Region Of Interest (ROI) and enhancing the images. The Region Of Interest is defined by masking the areas behind the dikes and outside of the metronome. This way, only particles in the channel are taken into account, and particles which have fallen outside of the channel are ignored. This mask is applied to all 10 images. The second step of pre-processing is optimizing the contrast by applying a Contrast Limited Adaptive Histogram Equalization (CLAHE) filter on the images. This filter optimizes regions with both low and high exposure independently, by distributing the most common intensities throughout the entire data range in the image (Thielicke & Stamhuis, 2014). Different image enhancement options are available in PIVlab in addition to the CLAHE filter: high pass, denoise and low pass, intensity capping and subtract mean intensity. The subtract mean intensity option gives a lot of noise. The other options give very similar results to the CLAHE option. Because the CLAHE filter was recommended by the option information in PIVlab, this filter was used in the current study.

The image evaluation takes place after the pre-processing. In this next step, the frames are analysed. The images are paired in sets of two, so [A+B], [B+C], [C+D] etc. For 10 images this results in 9 image pairs. Each image pair has a timestep of 40 ms between them. For the actual analysis, a Fast Fourier Transform (FFT) Window Deformation algorithm is used. In this algorithm, a Discrete Fourier Transform (DFT) is used to find the displacement between two images based on a certain interrogation area. In the first pass, a normal DFT analysis is performed. The corresponding interrogation areas from the first and second image are compared and the displacement is calculated. Because there is an overlap for the interrogation areas, the displacement information is available for the middle and corners of the areas (**Figure 7a**). Based on this displacement, the interrogation area of the second image is deformed (**Figure 7b**). This deformed area is then used in the next pass, and compared again with the DFT method to the first image (Thielicke & Stamhuis, 2014). This is repeated

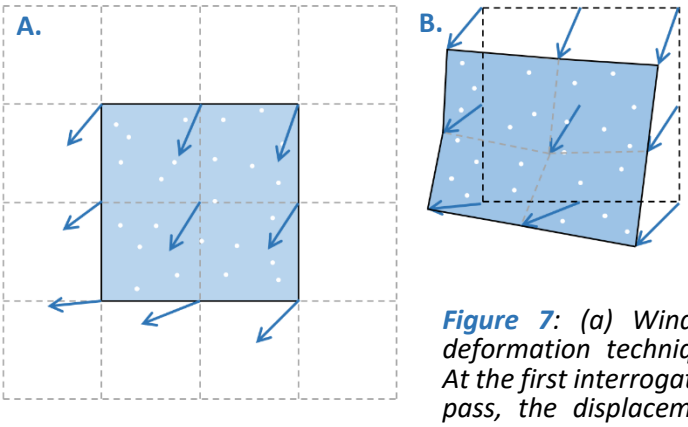

***Figure 7**: (a) Window deformation technique. At the first interrogation pass, the displacement of the cell centres is calculated for each pixel. (b) Then the area is deformed based on the displacement. This is done with several step sizes to obtain accurate data. Adapted from (Thielike, & Stamhuis, 2014).*

4 times, each pass with a smaller interrogation area going from a square with a side of 128 pixels in the first pass to a square with 16 pixel sides in the last pass. The found displacements are added together to form a total displacement. This results for each image pair in a displacement of a certain number of pixels for each cell within the image.

These obtained displacement data are then calibrated. This is done by determining a reference distance in a reference image. Now the displacement data can be represented in the right spatial units, in this case m instead of px. Furthermore, the x and y offset are indicated by pinpointing the x = 0 and y = 0 locations. Unfortunately, it is not possible to zoom in to make the placement of reference length and the x and y offset locations more accurate. In combination with the 40 ms timestep in between images, velocities can now be displayed in m/s. After this calibration, a validation step is performed as part of the post-processing. The outliers are removed by defining velocity limits. This is done in the program by plotting the u and v velocities (velocities in x and y direction) for all data points (**Figure 8**). This can result in a very dense cloud of points and some outlying points which are further excluded by drawing a selection box over the dense cloud. When the outliers are removed, the missing data are interpolated using an interpolation method based on sparse linear algebra (D'Errico John, 2023). The last step is to average the nine image pairs after which the velocity data is stored. These data will later be used to compare the measured velocities of the metronome with the results of the X-Beach model. To improve the comparison with the model, the data is rescaled to the same 5 cm cell size of the X-Beach model by taking an average for each cell, as well as interpolated over the missing timesteps in the 40 second metronome cycle. The surface velocities obtained with this are then converted to depth average velocities with **equation 2.2**.

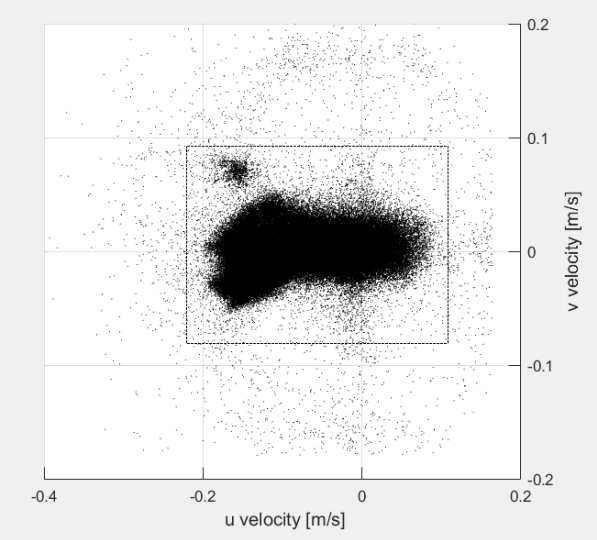

Figure 8: *Vector validation. Velocity limits are defined to exclude outliers.*

3.1.3 | Water level measurements

Just like the PIV measurements, water level measurements are not performed regularly either, because they take quite some time. Furthermore, the overhead imagery is partly blocked while the water sensors are being moved over the flume. The metronome has three water sensors mounted to a beam crossing the 3 metres width of the metronome. When the water level measurements are taken, first some measurements of the stationary water are made, when the metronome is not moving. For these measurements the sensors are turned on for 1 minute. Additionally, the height between the sensor and the bed is measured to calibrate the output of the sensors. This measurement is usually done at x = 19.5 metres as the beam with the sensors is positioned here when not in use. When the still measurements are finished, the metronome is turned on to collect water level data of the flowing water. During the first 6 cycles, nothing is measured, because the water needs some time to get in motion. After this, at every 50 centimetres along the flume, the water levels are

measured. At each location, the sensors are measuring for three cycles. After this, there is 1 cycle to move the sensors to the next location. Next to the water level measurements, tilt data is also collected by a fourth sensor. The tilt data are used to process the water level data later. While processing the data, the water levels are filtered for outliers, averaged over the three measured cycles, normalized to the tilt, smoothed and saved. This results in a dataset containing the water levels for every measurement location along the flume over one metronome cycle period. These data will also be used for the validation of the X-Beach results.

3.2 | Running X-Beach

To run the X-Beach model, all used variables need to be specified. All files with variables for a run are stored in a dedicated folder for that run. The most important file in this folder is the so called params file. The model uses this file to read all variables specified in it. This may either be single values, or paths to the location where a time series or grid is stored in another file. Some important parameters in the params file are the grid and bed level file, bed friction, river discharge, the tide file and boundary conditions (**Table 3**). Additionally, parts of the model, like the sediment transport and morphology change or the waves, can be turned on or off in the params file. Because this study is focussed on getting the hydrodynamics to work, the aforementioned options are turned off (**Figure 9**). The params file also specifies which variables need to be saved in the output file and what kind of output file this should be. In this case a netCDF file was used to store the data.

Table 3: *Most used X-Beach variables and boundary conditions with the different range/options which have been used during the study.*

	Description	Tested range/options
depfile	Specifies the initial bed level of the X-Beach run.	Bed exp 54, Bed exp 59
front/back	Flow boundary condition at sea- and riverside.	wall (no flux), abs_1d (absorbing 1d), abs_2d (absorbing 2d)
left/right	Lateral side flow boundary condition.	wall (no flux), Neumann (no gradient)
bedfriccoef	The bed friction coefficient (Chézy).	15 - 55 $m^{1/2}/s$
tideloc	Tidal boundary condition. Tidal time series specified in *zs0file*.	0 (constant sea level), 1 (tides forced at seaside corners), 2 (tides forced at all four corners)
zs0file	Tidal time series.	Seaside weir elevation, measured water levels at x = 19.76 m
disch_time series_file	Discharge time series at river inlet.	Only river discharge, river and seaside discharge

The X-Beach model is made to model real life, non-tilting coastal areas, in which waves and currents cause sediment transport. However, in the metronome, the tilting is the most important driver for the hydrodynamics and sediment transport. Therefore, the tilting of the metronome was implemented in the X-Beach code (**Figure 9**). In this adjusted model version, some new variables were introduced related to the tilting of the metronome (**Table 2**). They describe the motion of the bed level in the modelled area, which is updated each time step based on the tilt of the metronome. The X-Beach bed level at the seaside is given by the same sinusoidal function which is used for the metronome tilt (**eq. 3.1, Figure 6**). To calculate the bed levels for the whole metronome the length of the basin is necessary as well. This basin length is specified in X-Beach with variable l. These new parameters are all specified in the params file when a X-Beach run is executed.

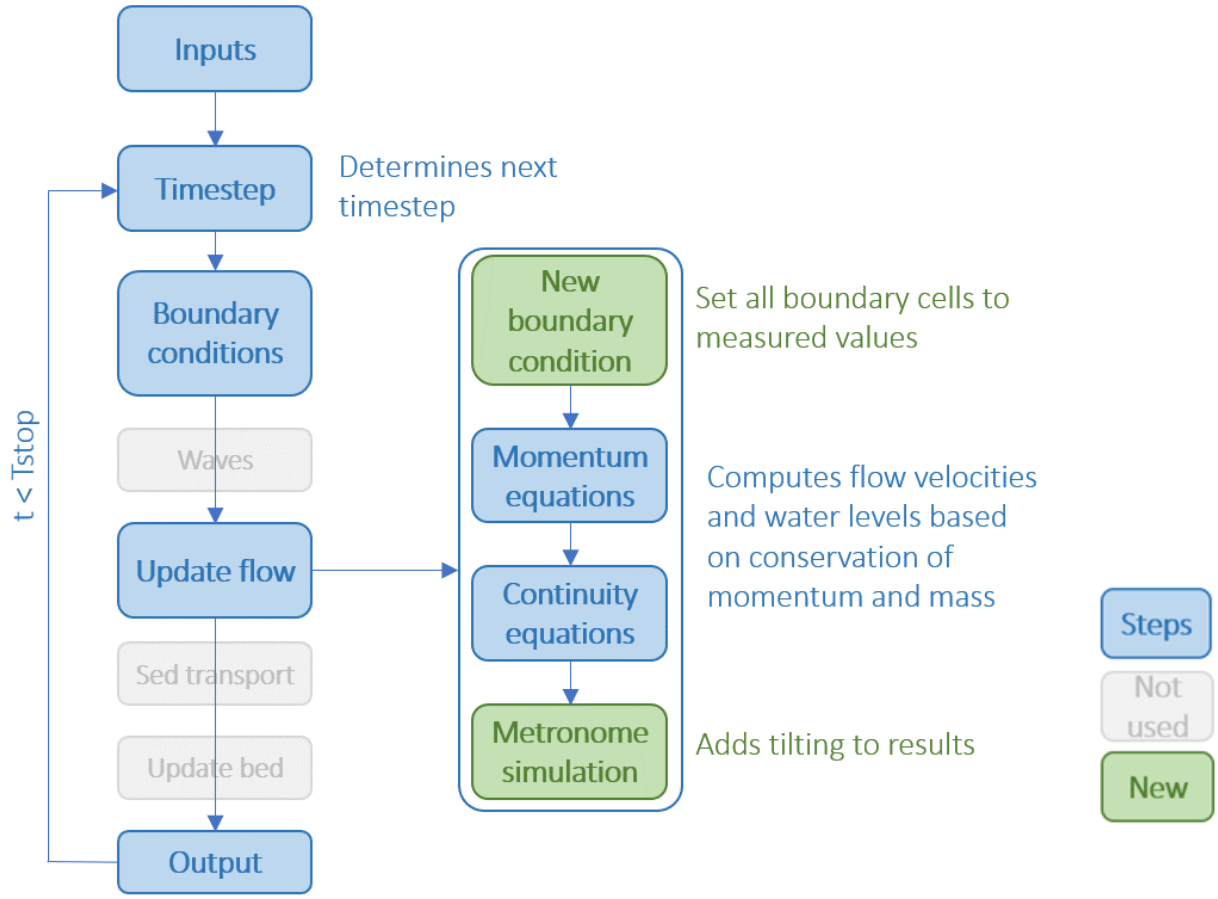

Figure 9: Simplified flow chart of the adapted X-Beach model used in this study. The model starts as normal with the inputs timestep determination and the boundary conditions. After this the wave part is skipped. In the flow calculation part, the new boundary condition is accounted for. Also the metronome movement are added to the results here. After this, sediment transport and bed updating are ignored and the results are stored in the output file. Adapted from (Smit et al., n.d.).

Because X-Beach calculates everything from the seaside to the riverside, the grid of the metronome had to be changed. Instead of the x = 0 to x = 20 from riverside to seaside, now x = -20 to x = 0 from seaside to riverside is used. For the width of the metronome in X-Beach y = 0 to y = -3 is used, for the hall-side to the wall-side. This is specified in the grid file. Cells of 5 by 5 centimetres were used, which results in a grid of 59 by 400 cells for the area of the metronome. For each cell, a bed level is calculated from the laser scans. The data from the laser scan is resized to the 5 centimetre cell size and the river input and seaside are adapted to remove the elements which do not belong to the metronome bed, such as the river inlet and wave maker setups at both ends. This bed level data is stored as a separate file in the run folder.

From the initial tests it became clear that the model was flooding much more than expected. Many of the 95 runs were devoted to solving this persistent problem. All runs can be found in **appendix B**, including a short description of which variables were changed in each run and which results came out. The runs can be classified in a few main categories based on the changed inputs, including initial conditions, boundary conditions and model parameters (**Table 4**). The first category contains runs in which changes to the bed level were made. The second group includes runs in which different bed frictions have been used. The third and fourth category deal with water inputs: tides and discharge, respectively. The fifth group includes runs which tested changes to the source code. An overview of these five categories can be found in **table 4**. Further explanations of the methods for each category can be found in the following sections.

Table 4: *The main changes made in the five run categories with their expected results to solve the floods.*

	Changes	Expected results	Section
Bed level adaptations	• Raising flood plains. • Building a dike in the channel mouth.	• The sides will not flood any more. • Inflow from the seaside is blocked preventing floods.	3.2.1, 4.3.2
Bed friction tests	• Different Chézy values were tested.	• A lower friction causes higher flow velocities with lower water levels.	3.2.2, 4.3.3
Tidal input tests	• Different tidal boundary conditions were tested (tideloc = 0, 1, 2). • The tidal time series based on weir movement was replaced by a measured water level time series.	• By forcing tides on more locations, more forced values are used by the model decreasing the floods. • Tides based on the measured metronome water levels should be more accurate than the weir elevations.	3.2.3, 4.3.4
Seaside discharge tests	• A seaside discharge was added.	• With a seaside discharge water levels can be controlled with the amount of water coming in the domain.	3.2.4, 4.3.5
Source code changes	• Added bed level changes in the continuity equation • Introduced a new tidal boundary condition	• Bed level changes are not neglectable for the metronome because of its tilt • By forcing the tidal time series to the whole sea side, the incoming water is limited.	3.2.5, 4.3.6

3.2.1 | Initial bed level adaptations

The bed levels are specified for the model in the bed level grid. The values are derived from the laser scans made during the metronome experiments. In several runs, these bed levels have been adapted in an attempt to get rid of the floods in the model. These adaptations include making a new dike at the entrance of the sea or in the estuary mouth to prevent water from entering the basin (**Figure 10a**) and raising the area behind the dikes (**Figure 10b**). Both the new dike and the areas behind the dikes have been raised to two metres in the bed level grid file, to ensure no water would flow over it.

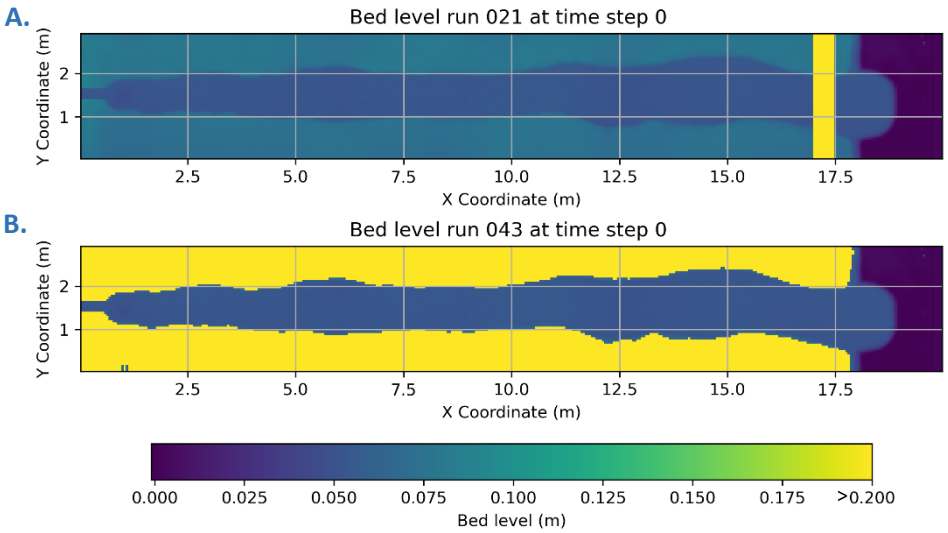

Figure 10: *Bed levels adjustment attempts to solve the flooding problem. All yellow areas are 2 m high. (a) A wall was built in the channel mouth, to keep water from entering the channel. (b) The area behind the dikes was raised to keep all water in the channel.*

3.2.2 | Bed friction changes

Similar to the bed levels, the bed friction can also be defined in a grid. However, most of the time, a single value for the whole domain is used. Several runs have been done with different bed frictions to test its effects. The bed friction is an important factor for the hydrodynamics, as it partially controls how fast the water near the bottom can flow and hence it also is important for the sediment transport. For most runs, a constant bed friction with a Chézy of 15 $m^{1/2}/s$ was used. This is an estimate for the roughness of the metronome bed, as the actual roughness is unknown. The roughness is higher in the metronome than in real life situations as we have a much lower water depth, but normal sized sand. This scale problem results in a roughness which is much higher compared to a real life estuary. A Chézy of 15 $m^{1/2}/s$ is comparable with a mountainous rocky stream (Warmink et al., 2007). It is also possible to use a spatially varying bed friction. This was also tried by making a grid defining a bed friction for each cell. When the model was performing better after several runs, the friction was adjusted to get the modelled flow velocities closer to the measured ones.

3.2.3 | Different tidal inputs

The third variable, much used in the different runs, is the tidal input. In the model the tides can be specified using the tideloc variable. Three different options for this variable were tested. The first option is a run with tideloc = 0. This means that only a constant water level is specified (zs0) as an initial condition. Alternatively, a time series of water levels can be forced to the corners of the domain. For this, there are two options: tideloc = 1 and tideloc = 2. With tideloc = 1, a water level time series is forced to the two sea side corner cells of the grid. These two get the same value representing an alongshore uniform water level. With tideloc = 2, a second time series with water levels is used. This second water level time series is forced to the two corners cells on the riverside. With this option, all corners have a forced water level. The used water levels are specified in a text file which has a column for the time and a column for the water level time series. Several different time series have been used in the different runs. In the first runs, the water level time series was based on the movement of the seaside weir. Because the weir is below the water surface, this was changed to measured water levels from the metronome. For the riverside these are the values from x = 1 metre. This is the closest location to the river where measurements are possible. For the seaside, water level measurements were taken at x = 19.76 metres. This is the most seaward location where measurements can be taken as the last part of the sea until x = 20 metres is occupied by the wave maker. The wave maker was turned off while the water levels were measured at this location. A third water level time series which was used in just a few runs is based on both the weir and the measured seaside values. The function which describes the motion of the weir (**eq. 3.1**) was fitted to match with the measured values. This function was then shifted down 1 cm and the amplitude was decreased by 1 centimetre. With the use of this shifted function was tried to lower the high water levels during the flood stage.

3.2.4 | Addition of a seaside discharge

Instead of forcing a certain water level to the boundaries of the basin with the tide options, the water levels should also be controllable by limiting the discharge going in to the estuary. Some runs were used to look further into this idea. 4 different discharges are distinguished in the metronome (**Figure 3b**). These four are the river discharge, pump discharge, weir discharge and the discharge going in and out the channel. The river discharge is specified in the params file. A simple text file with the coordinates of two points between which the river flows is sufficient. In addition to this, a time series is needed which specifies the river discharge per time step which flows out of the river inlet (**Figure 3a**). This time series is based on the river discharge of the metronome. The river discharge during the metronome experiments is 500 l/h for the moments when the riverside is up. When the seaside is up, the discharge from the river is 0 l/h. From this we get a time series with 22.5 seconds of 0.000138 m^3/s followed by 17.5 seconds of 0 m^3/s. For most runs, only this river discharge is used. However, several tests have been done in which the rest of the discharges were also taken into account (**Figure 3b**). From these discharge the amount of water going in and out the channel and sea was calculated

using **equation 3.2**. This discharge was then used as a new 'river' discharge at the seaside of the modelled domain by adding the time series in a new column in the file with the river discharge.

$$Q_{in/Out} = Q_{Pumps} + Q_{river} - Q_{weir} \quad \textbf{eq. 3.2}$$

To calculate this In/Out discharge, additional measurements in the metronome were necessary. First of all the discharge of the pumps (Q_{Pumps}) was measured by filling the metronome flume while measuring the water levels. The volume of water which entered the metronome was calculated, based on the metronome's area and the water level change while filling. This volume is then divided by the time the pumps were turned on. The seaside pumps and the known river discharge (Q_{river}) are supplying water to the system. All the excess water flows over the seaside weir out of the system (Q_{weir}). The discharge over this weir was determined by additional water level measurements above the weir.

3.2.5 | Source code changes

With the previous mentioned changes to the different inputs there were no decent results obtained. Therefore, some changes were made to the X-Beach source code by Dr. Saeb Faraji Gargari. The first change was to test another way of updating the water levels in the model. In the original model, the water levels are calculated with a continuity equation (**eq. 2.13**). Because the model is built for real life systems, the term correcting the water levels for bed level changes in a single timestep is neglected as they are very small. However, in the metronome these bed level changes are significant as the whole bed is tilting. Therefore, the water levels are updated based on the change in bed level. This is done after the part with the continuity equations. To test if this was the right way of incorporating the bed level changes, the continuity equation was extended with the bed level change term which is neglected in the original model (**eq. 3.3**).

$$\frac{\partial \eta}{\partial t} - \frac{\partial d}{\partial t} + \frac{\partial hu^L}{\partial x} + \frac{\partial hv^L}{\partial y} = 0 \quad \textbf{(eq. 3.3)}$$

The $\frac{\partial d}{\partial t}$ term represents the bed level change over time. In a few runs this new approach was used instead of the water level updating afterwards. With this term added, the bed level is taken into account directly in the continuity equations.

Next to this change to the water level updating, a new boundary condition was introduced into the model (**Figure 9**). During the testing, it became clear that the current boundary conditions in X-Beach are not applicable to the metronome. The boundary conditions are mainly focussing on the flow at the boundary leaving the water levels, set by the tidal input. To incorporate the water levels more, a new boundary condition was introduced which forces a certain water level, or a water level time series, to the whole seaside or riverside boundary. With the previous approach, a certain water level or water level time series was only forced to the corner cells by the tidal input regardless of the boundary conditions. This makes it possible for the model to model higher water levels than intended at the seaside in between the corner points, causing more water to flow into the domain.

This new boundary condition was updated later because of the discretization of X-Beach. To calculate all variables for a cell, X-Beach uses the values of the surrounding cells as well. However, at the boundaries, these values of surrounding cells are not all available, because it is a cell at the boundary. Therefore, the calculations for these boundary cells are approached in a different way by the model. For the new boundary condition this means that the forced water levels are not making their way into the rest of the model resulting in a strange water level jump. Therefore, the forced water levels were extended by adding an extra column. In this way, the forced water levels are now making their way into the rest of the model.

After testing with the aforementioned changes, a decent working model was obtained in which no large scale floods appeared anymore. This model was further finetuned to match the measured water levels and velocities better by changing the bed friction. A range of Chézy values from the initial 15 $m^{1/2}/s$ to 50 $m^{1/2}/s$

was tested with steps of 5 $m^{1/2}/s$. For these runs, the bias, mean absolute error and Brier skill score were calculated to compare the runs with different bed frictions. As baseline predictors for the skill score, the situation of a non-tilting metronome was used with a water level baseline predictor of 6 cm and a velocity baseline predictor of 0 m/s.

4. | Results

The results are divided into 3 parts. First, the results of measured flow velocities and water levels will be presented (**Chapter 4.1**). This will be followed by the results of the X-Beach runs. These are divided into two parts: the flooding model (**Chapter 4.2**) and the non-flooding model (**Chapter 4.3**). Here, qr codes can be seen alongside the figures. These can be scanned or clicked for a view of the corresponding figure changing over time to get a better understanding of the results through time.

4.1 | PIV measurements

The PIV measurements were performed at the start and halfway of experiment 54 and at the start and end of experiment 59. There is data available for every 5 seconds during the 40 second period of one cycle with the exception of t = 0 / t = 40 as the trigger which makes the overhead images cannot be triggered at t = 0 seconds. The difference between the start and end of the experiments is the bed. At the start of the experiment, the bed is still flat. At the end of the experiment, morphological features such as shoals and channels have developed, causing the water to flow through certain channels in which velocities are higher. This is clearly visible in the PIV results of experiment 059 (**Figure 11, appendix C**). For the initial conditions, there is a simple flow pattern. At the beginning of the cycle, the water is flowing straight to the right, towards the sea (**Figure 11a**). At the end of the cycle, when the seaside comes down towards the horizontal position again and the riverside goes up to the horizontal position, a similar pattern appears but in the other direction, towards the left. There are no shoals and channels which guide the water flow. Therefore, the velocity vectors are all pointing in the same direction. Only at the transition between estuary and sea, the flow is going slightly more to the sides. The flow velocities go up to around 0.4 m/s in both directions. In **figure 11b** the flow velocities

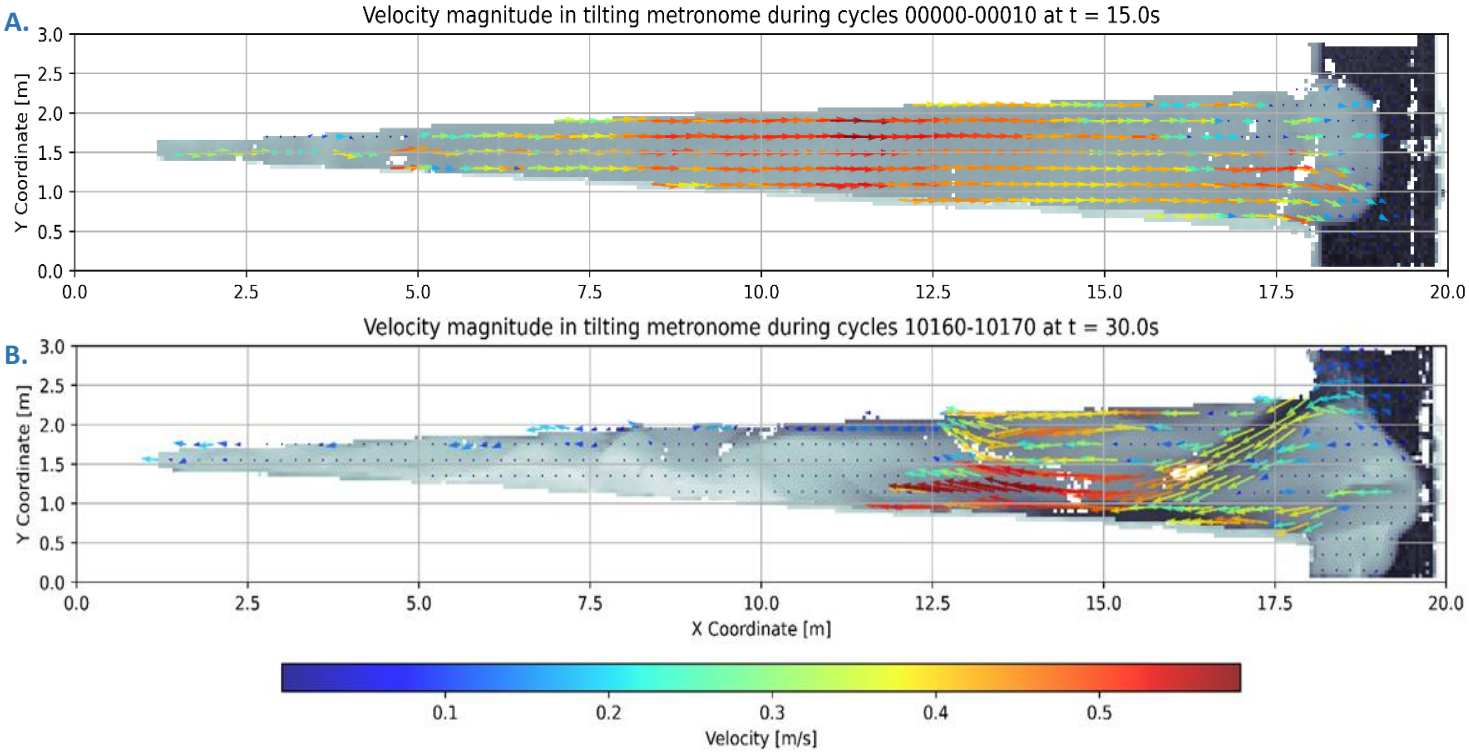

Figure 11: *Measured surface flow velocity vectors, colour-coded by magnitude of (a) the start of experiment 059 at 15 seconds and (b) the end of experiment 059 at 30 seconds. At t = 15 s, the water flows towards the sea side. At t = 30 s, the water flows to the river side. At the start of the experiment there is no morphology yet causing a simple divergent flow pattern. At the end of the experiment there is a developed morphology causing the water to flow predominantly through the channels.*

during the flood phase are plotted for the end of the experiment. After 10.160 cycles, the bed is much more developed, with channels and shoals. At the hall-side, a few large shoals developed making the water to flow through the wall-side channel. As it is deeper here, the flow velocities are higher than the velocities with the initial conditions. At the sea there are also two channels visible where water is flowing around the shoals in and out the estuary. The flow velocities are now slightly higher than at the start of the experiment, when there was no developed morphology yet. The water levels now range up to 0.6 m/s in both directions.

For the comparison with X-Beach the PIV surface velocities have to be converted to depth averaged velocities. This was done by calculating α (**eq. 2.2**). For the whole metronome this gave a mean value of α = 0.58. This α is used in the X-Beach runs to convert the measured surface velocity to depth average velocity to be able to compare the modelled and measured velocities.

4.2 | Water level measurements

At the start and middle of experiment 54 and start and end of experiment 59, the water levels were measured. At the start of both experiments the bed of the channel was still flat, while at the end, there is a developed bed with shoals and channels. The water level data of multiple cycles was processed resulting in the water levels for one 40 second metronome period at multiple locations. For the data gathered at the middle of experiment 54, and at the start and end of experiment 59 this was done every 0.5 m along the flume from x = 1 to x = 19.5 metre. For the start of experiment 54 this was only done at 5 locations: x = 5.6 m, x = 9.7 m, x = 14.5 m, x = 18.4 m and x = 19.5 m. This gives big gaps in the data making it unusable for comparisons with X-Beach along the whole flume. Therefore, in the comparison with X-Beach, only data from experiment 59 will be used, as this data set is more complete. Although experiment 54 and 59 have different dike setups (**Figure 4**), the water levels are very close to each other which justifies the use of the measured values of experiment 59 for the channel of experiment 54. The five measured locations of experiment 54 were compared with the water level of experiment 59 (**Figure 12**). This resulted in a mean difference of 1.77 millimetre for all three sensors during the 40 second metronome cycle. This is around 10% of the water depth. Measurement locations were the sensors were above the sand behind the dikes in one experiment but above the channel in the other experiment were excluded.

In **figure 13** the water levels during the first cycle(s) of experiment 59 are plotted for 10 x-locations. In **figure 14**, the water levels at the same locations are plotted, but for the end of experiment 59. In each subplot, data from all three sensors are shown. There are some small deviations between the three sensors caused by small differences in water levels at the different y-locations they are positioned at. At the lower x-values, closer to

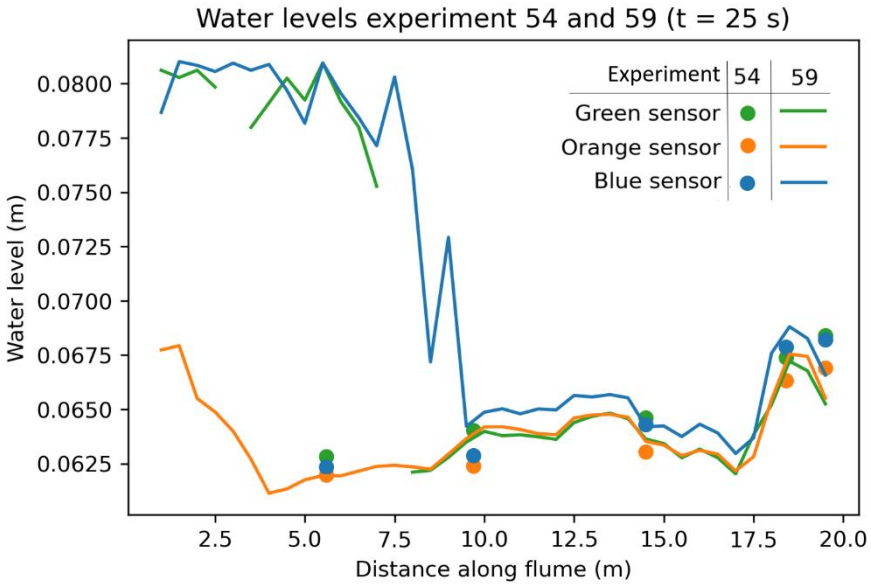

Figure 12: *Measured water levels of experiment 54 and 59. The water levels of both experiments are close to each other. Only for the most left measure location of experiment 54, both experiments are far from each other for the blue and green sensor. This is because the channel was wider here in experiment 54 than in experiment 59. This caused the sensors to be above the higher sand instead of above the water.*

the riverside, the deviations between the orange sensor and green and blue sensors are slightly bigger. This is because the green and blue sensor are above the area behind the dikes at these x-locations, and not above the water in the channel. Hence, they are measuring the constant sand level and not the changing water level. Therefore, in the comparison with X-Beach, the data from the orange sensor are mostly used as this data set covers the whole length of the flume.

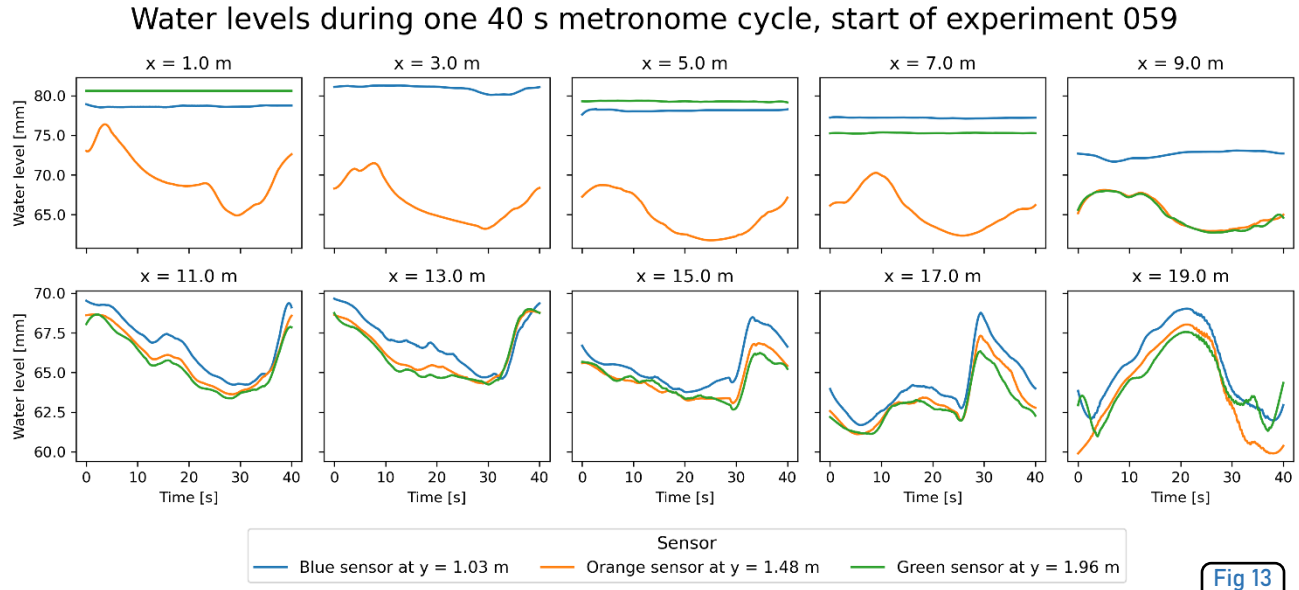

Figure 13: *Water level measurements at the start of experiment 059. The water levels were measured every metre along the metronome flume for one 40 second cycle. The three lines show the water levels at each sensor location.*

Fig 13

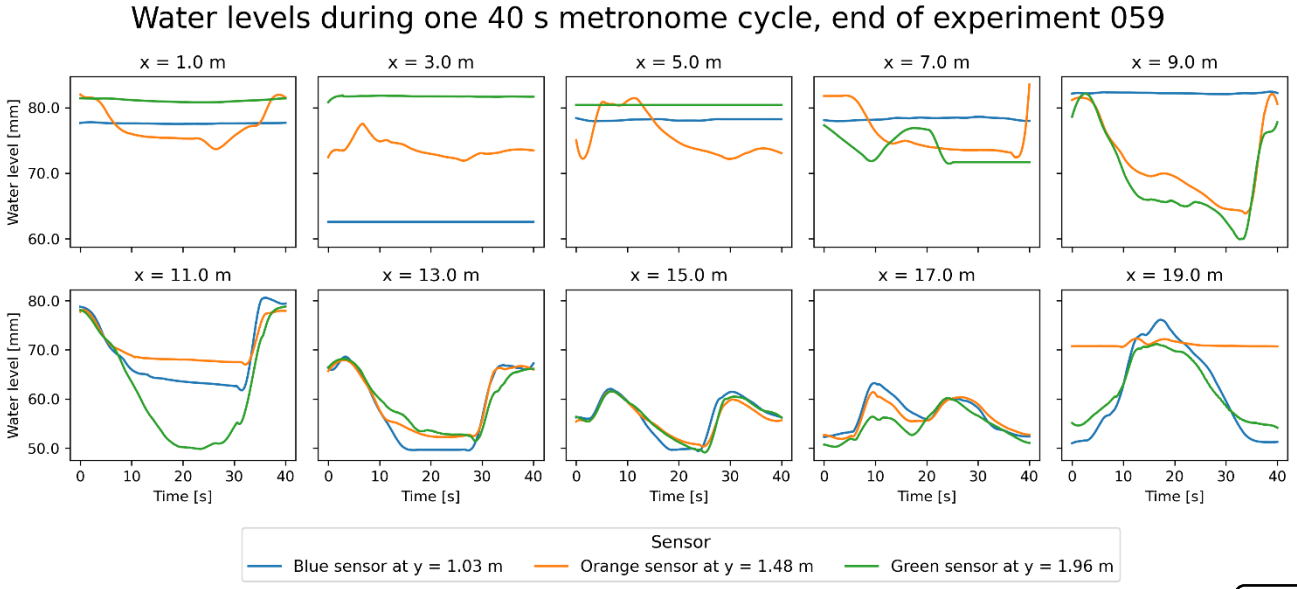

Figure 14: *Water level measurements at the end of experiment 059. The water levels were measured every metre along the metronome flume for one 40 second cycle. The three lines show the water levels at each sensor location.*

Fig 14

At the start of experiment 59 the asymmetric tide of the metronome can be seen. The period from low water to high water is much shorter than from high water to low water (**Figure 13**). Furthermore, the high water peak does not seem to reach each location at the same time. At the seaside at x = 19 m, the highest water levels can be seen just after 20 seconds. Going from the seaside to the riverside, we see the high water peak shift to the right, later in the cycle, or even at the beginning of the next cycle for the riverside half of the

****Chapter 4 will present the results of the measurements and model runs. Not all results can be properly shown in figures as there are too many timesteps. Therefore, at some figures a qr-code is available which leads to an animation of additional timesteps of that particular run. The codes can be scanned as well as clicked on when reading this digitally.****

metronome. At the end of the experiment, the water levels look very different from the start (**Figure 14**). This is again caused by channels and shoals which have developed after 10.160 cycles. This morphology causes some places to be under water for only a shorter period of the 40 second cycle. This is clearly visible at x = 11 where the orange and blue sensor show a sort of plateau at t = 20 s. Here we see the top of a shoal which falls dry during the ebb stage.

4.3 | Solving the floods in the X-Beach model

In sections 4.3 and 4.4 the results of the model runs will be presented. Almost 100 runs have been conducted. A selection of runs will be presented here showing the results of different changes to start conditions, parameters and boundary conditions (**Table 5**). A description of all other runs can be found in **appendix B**.

4.3.1 | Floods during initial runs

In the first tries with the adapted X-Beach model, in which the bed tilting was added, it had become clear that the modelled metronome basin was flooding (**Figure 15c**). During the first 20 seconds the modelled values look promising. When the riverside tilts up, water starts flowing towards the sea without any floods. However, after these first 20 seconds, the floods start from the sea side and spreads at the sides of the channel, until the whole domain is flooded. When the river side comes down again at t = 30, the floods become less at the areas behind the dikes. At t = 40, when the second cycle starts, the river side comes up again. The water which is still on the flood plains near the river, starts to flow over the sides towards the sea. However, at t = 60 a new flood starts from the sea side which meets this returning water in the middle and creates a new flood like the first one. This process repeats itself each cycle. In the first cycles, the water depths of the floods increase gradually. After six cycles, the modelled water depths stabilize and remain constant the rest of the modelled cycles.

The floods are the biggest at the riverside where the water collides with the wall at the end of the metronome. At the seaside, the water levels are actually much closer to the measured values. At the riverside, the floods reach water depths over 20 centimetres during high water (**Figure 15a**). The maximum measured water depths are just a few centimetres high at this same moment. In addition to the water depths, the flow velocities do not seem to correspond to measured values either (**Figure 15b**). The modelled peak velocities in the u direction are much higher than those of the measured ones. The modelled velocities peak around -0.4 m/s and 0.4 m/s,

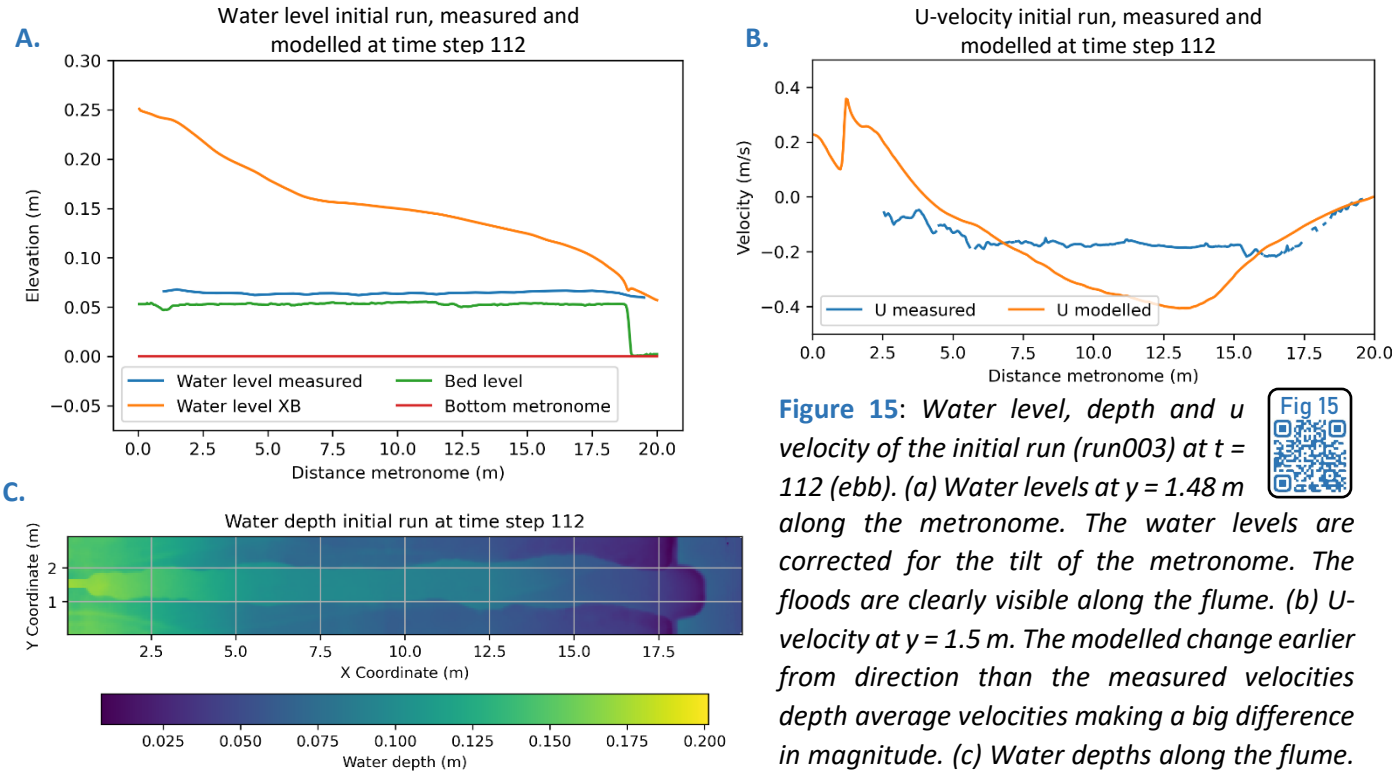

Figure 15: *Water level, depth and u velocity of the initial run (run003) at t = 112 (ebb). (a) Water levels at y = 1.48 m along the metronome. The water levels are corrected for the tilt of the metronome. The floods are clearly visible along the flume. (b) U-velocity at y = 1.5 m. The modelled change earlier from direction than the measured velocities depth average velocities making a big difference in magnitude. (c) Water depths along the flume. The high water levels are also flooding the floodplains behind the diked channel.*

Table 5 : Model runs presented in the results with their most important differences. These runs and all other runs can be found in **Appendix B**.

	Run	Name	Chézy ($m^{1/2}/s$)	Tides (Boundary condition, time series)	Other
Initial run	003	Initial run	15	Tideloc = 1, weir movement	
Bed level changes	021	Seaside dike	15	Tideloc = 1, weir movement	Dike in channel mouth
	043	Raised sides	15	Tideloc = 1, measured water levels	Raised floodplains
Bed friction	027	Varying friction	0.01 – 15	Tideloc = 1, measured water levels	First 5 columns at sea side 0.01, rest 15 $m^{1/2}/s$
	035	Normal friction	15	Tideloc = 1, measured water levels	
	036	Low friction	55	Tideloc = 1, measured water levels	
	037	High friction	0.001	Tideloc = 1, measured water levels	
Tidal input	025	Measured wl tide	15	Tideloc = 1, measured water levels	
	032	Constant wl	15	Tideloc = 0, zw0 = 0.0652	
	034	Tideloc = 2	15	Tideloc = 2, measured water levels	
	046	Shifted function wl	15	Tideloc = 1, Shifted function	
Discharge	056	Seaside discharge	15	Tideloc = 1, measured water levels	Additional seaside discharge
Source code	050	Original continuity	15	Tideloc = 1, measured water levels	
	053	New continuity	15	Tideloc = 1, measured water levels	Bed level update included in continuity eq.
	069	New BC constant tide	15	New BC, zw0 = 0.06	
New boundary condition	072	New BC standard friction	15	New BC, measured water levels	
	081	New BC best friction	20	New BC, measured water levels	
Updated boundary condition	078	Updated BC standard friction	15	Updated BC, measured water levels	

where the measured velocities just reach -0.2 and 0.2 m/s. Also the phase of modelled and measured velocities is not matching. In the modelled results, the ebb flow reaches its peak velocity almost 10 seconds earlier than the measured values at the riverside. Furthermore, the ebb flow continues longer at the seaside. Here the flood flow is almost 10 seconds behind on the measured values (**Figure 15b**). This is the result of the large amounts of water which are causing the floods and then going back and forth trough the flume.

4.3.2 | Effect of the initial bed on the floods

In the first category of runs an attempt was made to solve the flooding problem by adapting the bed level file which is used by X-Beach as an input. The two main adaptations were raising the area behind the dikes and creating a dike in the estuary mouth. The first of the two resulted in similar conditions to the original runs for the flow in the channel. As the area behind the dikes was raised now, this area was not flooding anymore. However, because this area stayed dry now, even more water came in to the channel, resulting in water levels which are higher than in the original runs (**Figure 16a**). For the flow velocity, the adaptation to the bed level meant that the modelled and measured velocities became even more out of phase, to the point where the modelled flow is completely contrary to the measured flow direction at some time steps (**Figure 16c**). For the other case, where a dike was built in the channel mouth, other things happen to the hydrodynamics. The water levels in the channel are much better (**Figure 16b**). They are, at some time steps, slightly higher than the measured ones, but the areas behind the original dikes are not flooding. In the sea, however, the water levels are way too high. This confirms the idea that the excess water, causing the floods, is coming from the sea side.

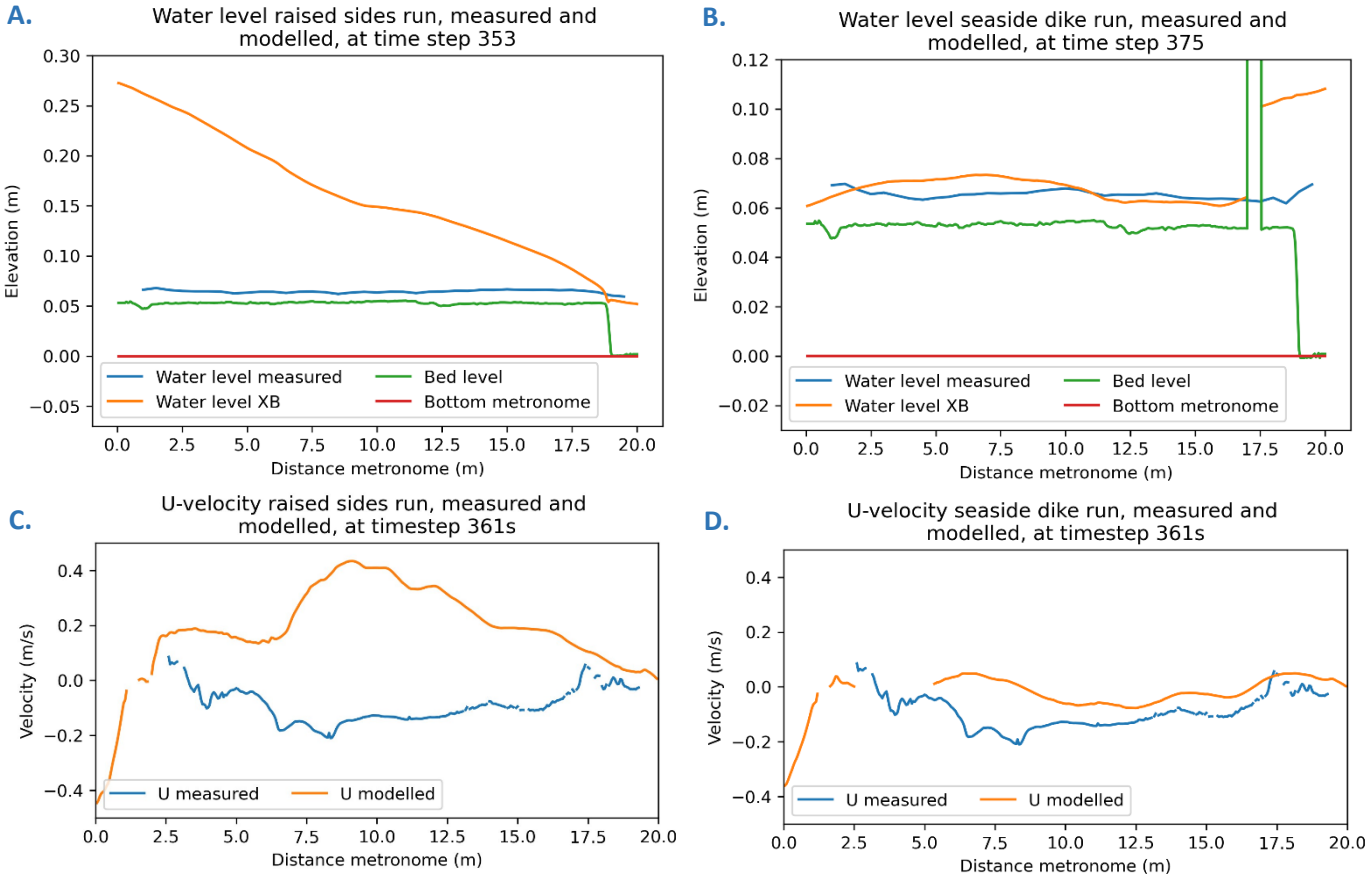

Figure 16: *Water level and u velocity for runs with bed level adaptations: raised floodplains (left), and an additional dike in the channel mouth (right). (a) By raising the areas behind the dikes, all water is concentrated in the channel resulting in no floods on the sides but higher water levels in the channel. (c) The flow velocities deviate more. At some timesteps, the flow in the modelled results is still flowing one way while the measured velocities already show that the flow has turned around. (b) By building a dike in the channel mouth, the water levels in the channel are much lower, resulting in no floods. (d) However, the flow velocities are too low compared to the measured values.*

Fig 16

While the water levels in the channel are performing quite well, the flow velocity is not. Because the open access with the sea is lost, the water has a lower flow velocity than the measured velocities (**Figure 16d**).

4.3.3 | Effect of bed friction on the floods

In addition to the bed level adaptations, test runs with the bed friction were done. Both spatially constant and spatially varying bed frictions were tested. By decreasing the Chézy number, and therefore increasing the roughness, the flow velocities will decrease. This is clearly visible in **figure 17a,b,c** where different flooding patterns are present for the different roughness values. With a lower bed friction, the water can flow back and forth with a higher flow velocity than for a bed with a high bed friction. This causes larger areas to dry up, as the water flows away more quickly in the runs with a lower bed friction. With the higher bed frictions, the

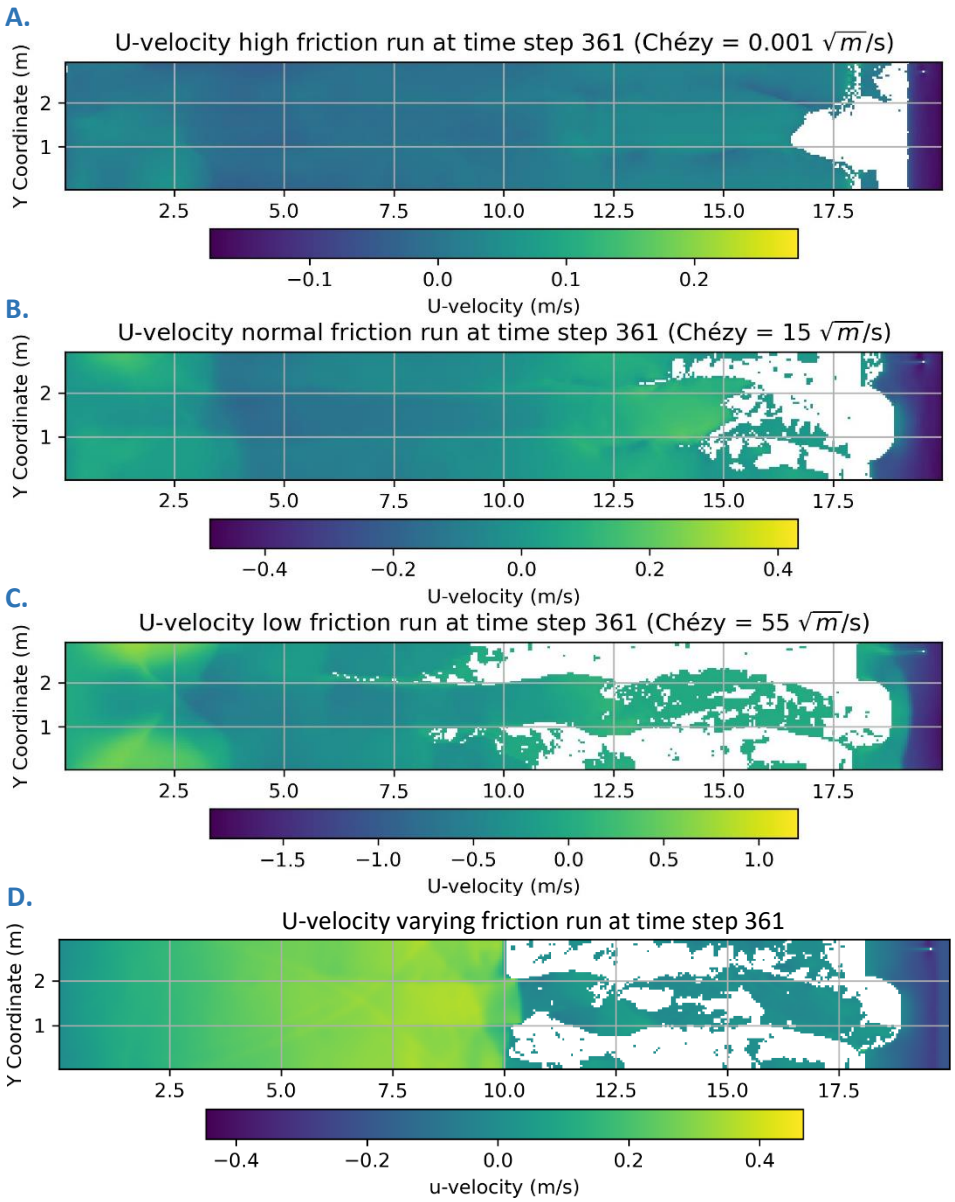

Fig 17

Figure 17: *Flow velocity in u direction for several runs with different bed frictions. In the top three plots (a, b and c), a uniform bed friction was used resulting in higher flow velocities for higher Chézy values. These higher flow velocities result in more dry areas as the water flows away quicker. In the bottom plot (d), a spatially varying bed friction was used with a lower friction in the channel than at the right part of the sea. The boundary between the two can be seen in the difference in flow velocities at the right side of the sea (a more darker blue next to a more green line). The area right to the darker blue, has a higher friction resulting in lower flow velocities.*

opposite is visible. The water flows much slower, leaving larger areas inundated. For the run with a high bed friction, flow velocities are ranging from -0.28 m/s to 0.17 m/s. For the run with the lowest bed friction, the flow velocities are ranging from -1.20 m/s to 1.88 m/s, which is much higher.

An attempt was made to keep water from entering the basin by increasing the bed friction at the sea side. When the water is flowing slower there, less water will enter. At the five most seaside columns the friction was changed from Chézy = 15 $m^{1/2}/s$ to 0.01 $m^{1/2}/s$. The u velocity results are shown in **figure 17d**. The transition between the two different frictions can be seen. On the left side of the area with the higher friction, there are suddenly higher flow velocities. Compared to **figure 17b**, where the bed friction has a Chézy of 15 $m^{1/2}/s$ everywhere, the range of velocities is very similar. A result of the varying friction is that there are fewer flooded areas compared to when a spatial uniform friction is applied (**Figure 17b**).

4.3.4 | Effect of tidal input on the floods

From all runs it became clear that the key to solving the flooding problem lies at the seaside boundary. The surplus of water which floods everything, is entering from here. Therefore, the water levels on this side and options for the tidal input were investigated further. As said before, the main three options for the tidal input, controlled with tideloc, are a constant water level, a water level time series forced to the two sea side corner cells or two water level time series, one forced to the seaside corner cells and the other one to the riverside corner cells. To test this tidal input and its influence on the floods, different time series have been used in the different attempts to solve the flooding problem.

In the initial runs, the tideloc = 1 option was used. The height of the seaside weir was used as water level time series (Initial run, run 003). Later, measured values from the water level sensors were used, in their original form (Measured wl tide, run 025) and also as a shifted function (Shifted function wl, run 046) in which a function was fitted to the measured values from which the amplitude was decreased. In **figure 18** the water levels at the sea- and riverside can be seen. For the seaside, the water levels of both the initial run, with the time series based on the weir height, and the run with measured water levels as tides are too high. This is probably the surplus of water flooding the metronome. The water levels based on the shifted function in run shifted function wl are performing much better, but still not matching perfectly with the measured values.

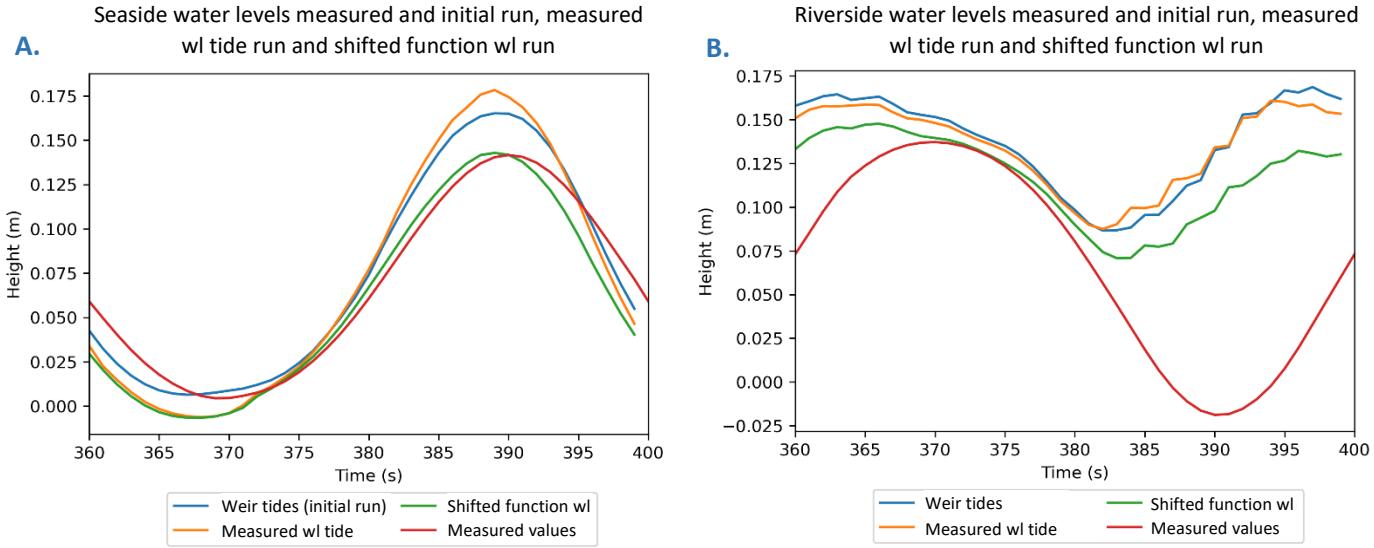

Figure 18: *Water levels on the seaside (a) and riverside (b) for the initial run (run 003, tide based on weir), run measured wl tide (run 025, tide based on measured values) and run shifted function wl (run 046, tide based on the shifted function). The water levels of the initial measured wl tide run are several centimetres higher than the measured values during high water. The shifted function run, performs better during high water. During low water, all runs are quite off. However, the riverside shows even larger deviations from the measured values. Also on this side, shifted function run is the 'best' one of the three.*

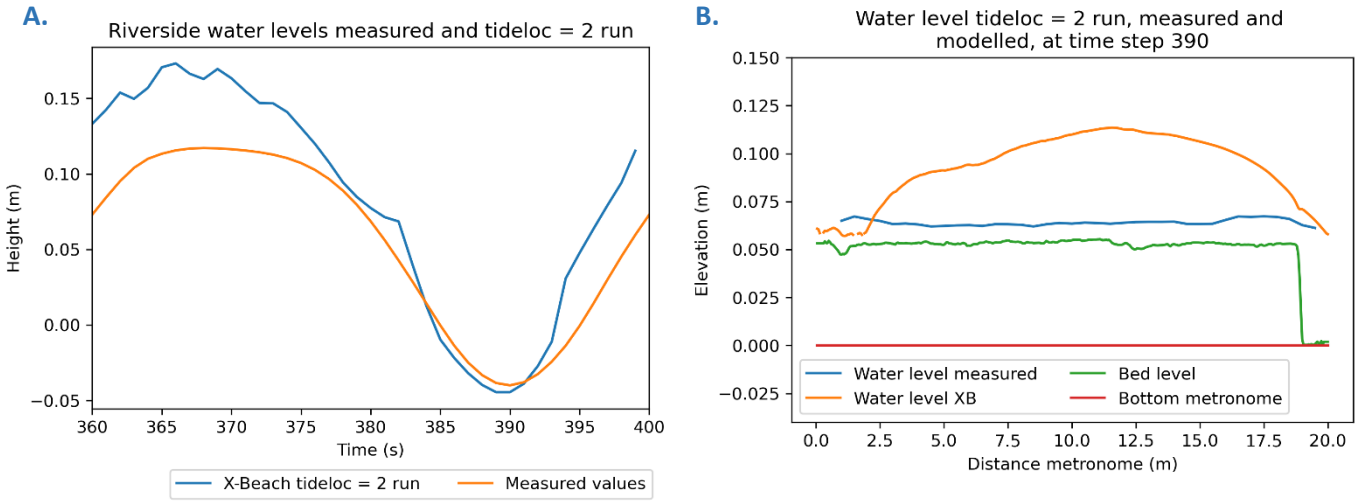

Figure 19: *(a) Water levels at the riverside for tideloc = 2 run. Tideloc = 2 forces a water level time series to the two corner cells on the seaside as well as to the riverside. This made the water levels follow the measured values better, but improvement is still possible. (b) With the water levels forced on two sides, a water bulge formed in the middle of the estuary.*

Fig 19b

Especially during ebb, the water levels are too low. For the river side, all three variants are deviating considerably (**Figure 18b**). On this side of the metronome, the floods are the biggest, which is clearly visible. The tides of the shifted function in run 046 are again the closest to the measured values although still rather different.

The tideloc = 2 option was tested with the measured water level values. For the seaside, the same values were used as in the measured wl tide run, giving similar results (**Figure 18a**). However, the riverside improves a lot compared to the measured wl tide run (**Figure 18b**). With the forced corner cells, on the riverside, the water levels follow the measured values better compared to the tideloc = 1 runs (**Figure 19a**). This is only not true for the middle part of the estuary. As the water levels on both ends are now forced, a water bulge forms in the middle of the channel (**Figure 19b**). This is rather different to the measured water level values.

When a constant water level is used, the water levels are lower compared to the runs with tideloc = 1 and tideloc = 2 (**Figure 20**). However, the floods on the areas behind the dikes are still present. This is probably because the constant water level is not corrected for the tilt of the metronome, like the time series used with the other tideloc options. Therefore, the water depths are almost 0 in the sea at some moments in time. This

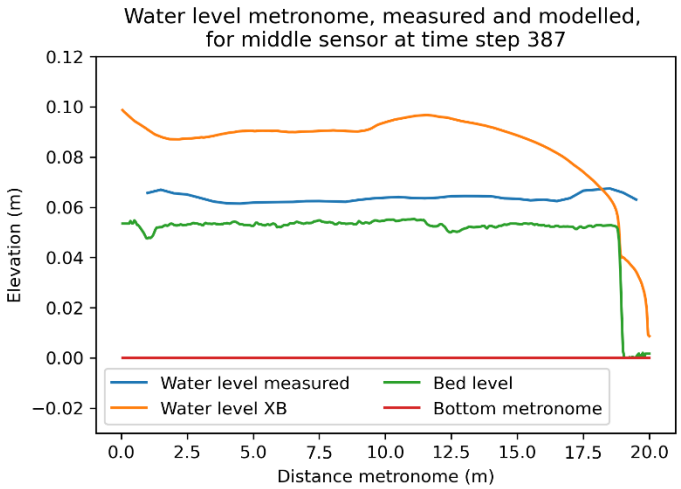

Figure 20: *Water levels in the constant wl run with constant water level at the seaside. Floods are still present but the water depth is lower than with other tidal inputs.*

Fig 20

could be solved by making a time series out of it, but that would result in a similar approach to tideloc = 1, which is not giving the wanted results either.

4.3.5 | Effect of a seaside discharge on the floods

Instead of only using a tidal input to control the amount of water, there have been some runs in which a seaside discharge input was used as well. Three of the four discharges in the metronome are known or measured. With this data, the discharge going in and out the channel and sea, and the raising or lowering of the water level there, could be determined. All discharges over 1 metronome cycle are shown in **figure 21**. The discharge going in and out of the channel is used as a river discharge in the X-Beach model. With this approach, the water levels are both controlled by the forced water levels as well as by a certain amount of water which is able to go in and out of the domain. In the model this situation is harder to achieve. With the new hydro file, in which the new discharges are specified, the familiar floods are still present (**Figure 22**). Water levels up to almost 30 cm are reached again at the riverside. To check if the double river set up is working, the original river at the riverside and the new river at the seaside, higher discharges than the measured ones where used. This showed that there is indeed water flowing in from the inflow coordinates when there is a positive discharge and water is flowing out with negative discharges.

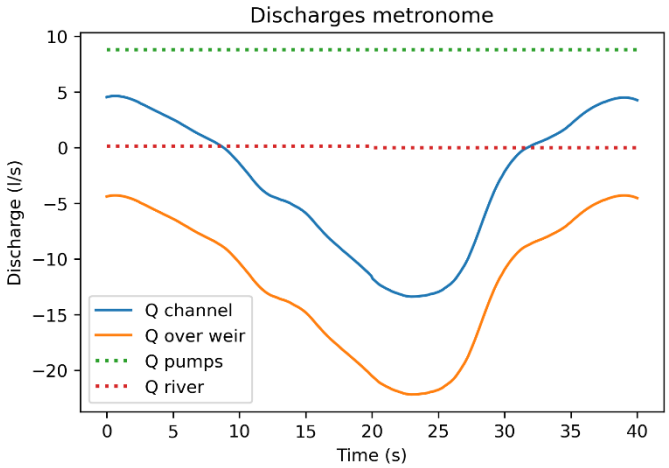

Figure 21: *Discharges in the metronome. The discharge of the pumps plus the river discharges minus the discharge over the weir results in the discharge going in or out the channel and sea.*

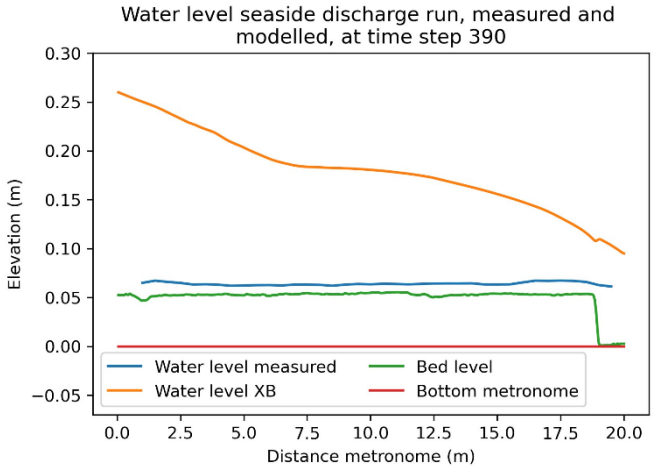

Figure 22: *Water levels of the seaside discharge run which has an additional discharge point at the seaside following a discharge time series with measured discharges from the metronome.*

Fig 22

4.3.6 | Source code changes to solve the floods

Next to the implementation of the tilt of the metronome, there have been two major new elements to the X-Beach code. These are the addition of a bed level change term in the continuity equations and a new way to force the water levels to the boundaries. The first change resulted in a new interesting flooding pattern in which the water is flowing back and forth and leaving the river- or sea side almost completely dry (**Figure 23c,d**). This while the other half is inundated by some floods. When looking at the water levels at the sea- and riverside, the new continuity approach is giving better results at the seaside (**Figure 23a**). The water levels are even lower than the measured ones during high water. However, on the riverside the water levels are nowhere near the measured values (**Figure 23b**). Over half of the period, the river side falls dry. On top of that, the water levels are totally out of phase compared to the measured values. There is only water when the lowest water levels should be reached (**Figure 23c,d**). Therefore, this change was abandoned, as it does not solve the floods and makes the flooding pattern worse.

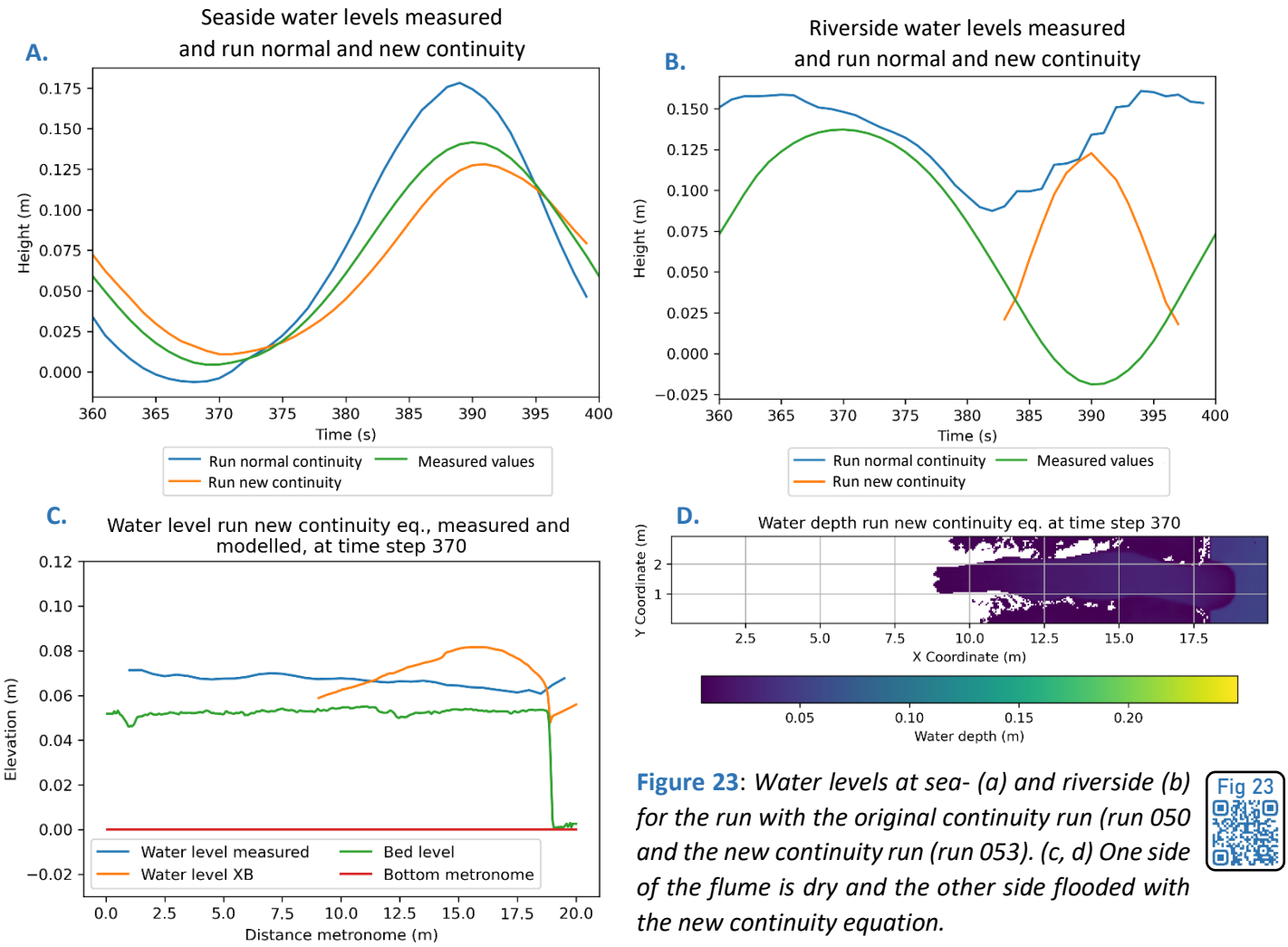

Figure 23: *Water levels at sea- (a) and riverside (b) for the run with the original continuity run (run 050 and the new continuity run (run 053). (c, d) One side of the flume is dry and the other side flooded with the new continuity equation.*

Fig 23

The other big change to the source code has to do with the forced water levels at the sea- and riverside. Instead of forcing these to only the corner cells, they were now forced to the whole sea side or riverside boundary. In the first runs with this new option, a water depth of 0.06 m was used at the seaside and a water depth of 0.01 m at the river side. This yielded much better results, as can be seen in **figure 24**. The water levels at both the seaside and riverside are much more closely following the measured values (**Figure 24a,b**). However, the differences are still 1 to 2 cm on some timesteps. Because the modelled values are now much closer to the measured ones, the water levels in the estuary stay a lot lower (**Figure 24c**). The biggest differences can be found just next to the forced values at both the river- and seaside. Here, next to the forced values, the modelled water levels are lower (or higher at other timesteps) compared to the measured water levels. However, these differences are not big enough to cause floods like we saw in earlier runs. There is still some water on the areas behind the dikes, but this is very shallow water moving back and forth. At the start of the 10 modelled cycles, there is more water on the sides but it slowly gets less after a few cycles. These results show a large improvement compared to the earlier runs showing that the modelling of the metronome in X-Beach clearly has some potential.

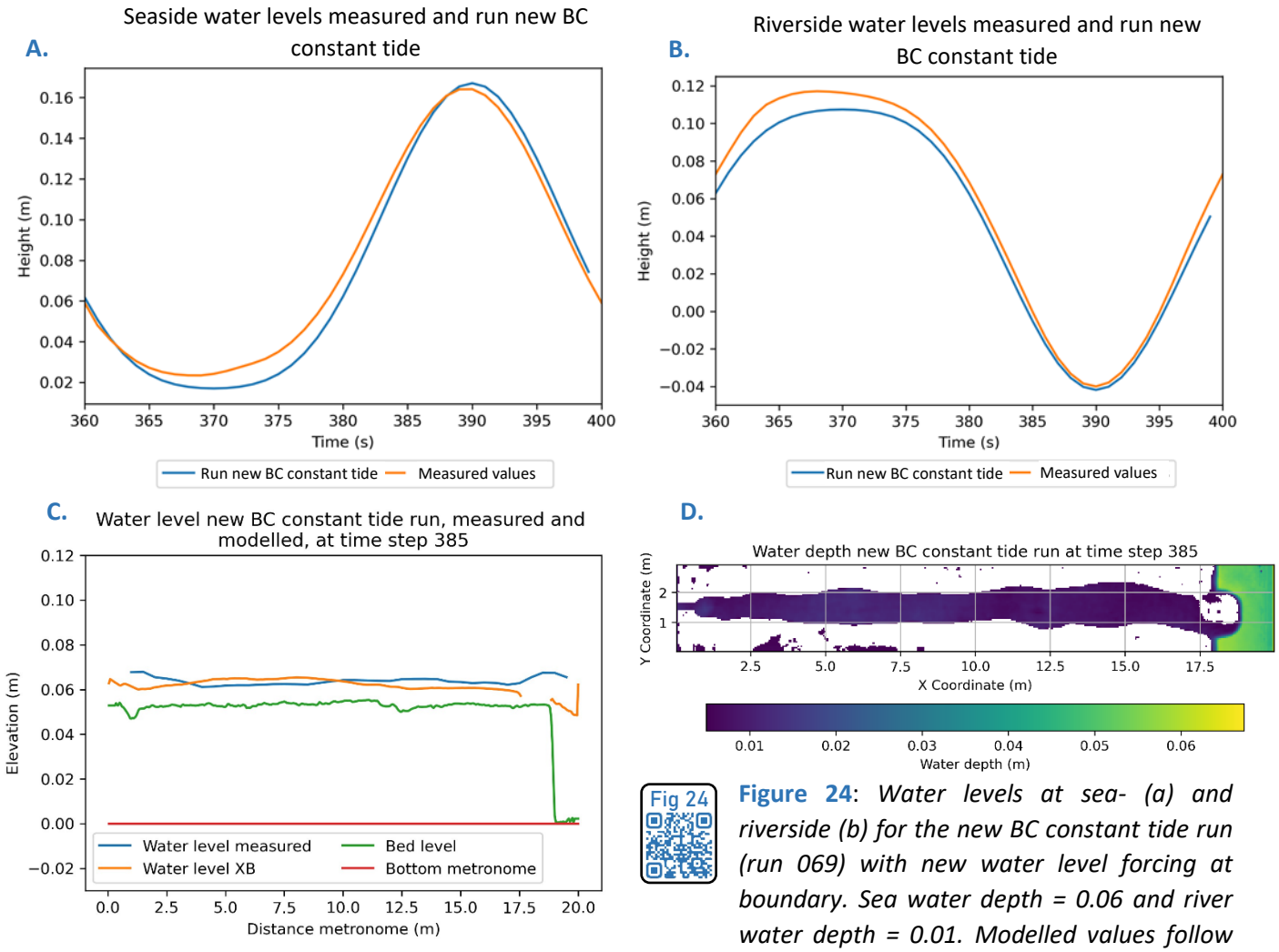

Fig 24

Figure 24: *Water levels at sea- (a) and riverside (b) for the new BC constant tide run (run 069) with new water level forcing at boundary. Sea water depth = 0.06 and river water depth = 0.01. Modelled values follow the measured values much better. Also in the rest of the estuary, the water levels are close to the measured values (c). With the water levels performing better, there are no large scale floods anymore (d).*

4.4 | The non-flooding model

4.4.1 | Model improvements with the new tidal boundary condition

Based on the results of all runs it seemed feasible to include a new boundary condition. With this new boundary condition, a single water level or water level time series can be forced to a range of coordinates, in our case the river inlet and the seaside boundary. With this new option, similar results as in run new BC constant tide (**Figure 24**) are obtained. However, the modelled and measured water levels are now perfectly matching for the new BC standard friction run (**Figure 25a,b**). Just like in the new BC constant tide run (run 069), at the seaside and riverside, next to the forced values, there are some strange deviations in water levels between the measured and modelled values (**Figure 25c**). However, all in all, the water levels along the flume are looking quite decent, especially when compared to the runs in which the whole flume flooded. Additionally, the modelled velocities are still slightly lower compared to the measured values, just like in the previous runs (**Figure 25d**).

These lower velocities can be seen when the modelled and measured velocities are plotted against each other together with a 1:1 line. It becomes visible that X-Beach is slightly underpredicting the flow velocities (**Figure 27e**). The water levels are predicted a bit worse: the values are all spread around the 1:1 line. Compared to the initial run, in which there were still large floods, the improvement of both the modelled water levels and velocities is visible (**Figure 27a,d**). This is also visible in the bias, mean absolute error (MAE) and Brier Skill

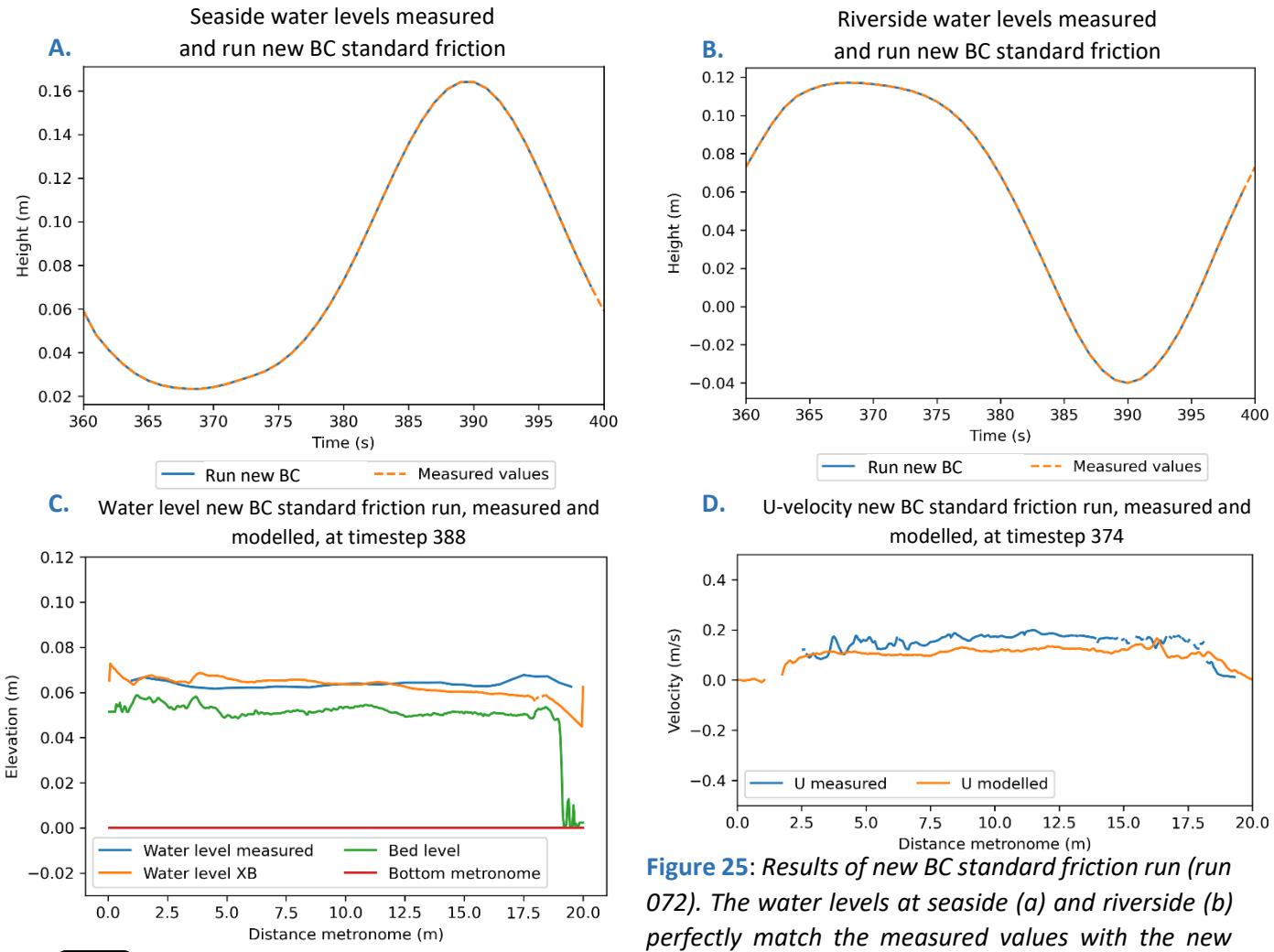

Figure 25: *Results of new BC standard friction run (run 072). The water levels at seaside (a) and riverside (b) perfectly match the measured values with the new boundary condition. Immediately next to these forced values, there are some parts in which the values are a bit off (c). However, the water levels are looking quite well overall. This is different for the modelled velocities (d). These are much lower than the measured ones.*

Fig 25c

Table 6: *Bias, MAE and BSS of the modelled water levels (m) in run 003 (Initial run), run 072 (New BC standard friction and run 081 (New BC best friction.*

	Run 003	Run 072	Run 081
Bias	0.0512	-0.0018	-0.0016
MAE	0.0530	0.0034	0.0037
BSS	-109.8695	0.4453	0.3528

Table 7: *Bias, MAE and BSS of the modelled flow velocities (m/s) in run 003 (Initial run), run 072 (New BC standard friction and run 081 (New BC best friction.*

	Run 003	Run 072	Run 081
Bias	0.0973	0.0014	0.0006
MAE	0.1529	0.0591	0.0533
BSS	-1.2205	0.6974	0.7311

Score (BSS) of both runs. The MAE of the water levels goes from 5.3 centimetres to 3.4 millimetres and also the skill score is improving considerably (**Table 6**). A similar trend is visible for the flow velocities which are improving even more between the initial run and the new BC standard friction run (**Table 7**).

This new BC standard friction run was further improved by changing the bed roughness. To get the flow velocities higher, as X-Beach is underpredicting them, the bed roughness was decreased by making the Chézy value higher, in steps of 5 Chézy. For the velocity, the best results were obtained in the new BC best friction run (run 081) with a Chézy of 20 $m^{1/2}/s$ (**Figure 26**). This run had the smallest MAE and the highest BSS for the velocities (**Table 7**). With this decrease of friction, the modelled values become higher, making the right top of the cloud shift to the right, closer to the 1:1 line and the left bottom peak shift to the left, also closer to the

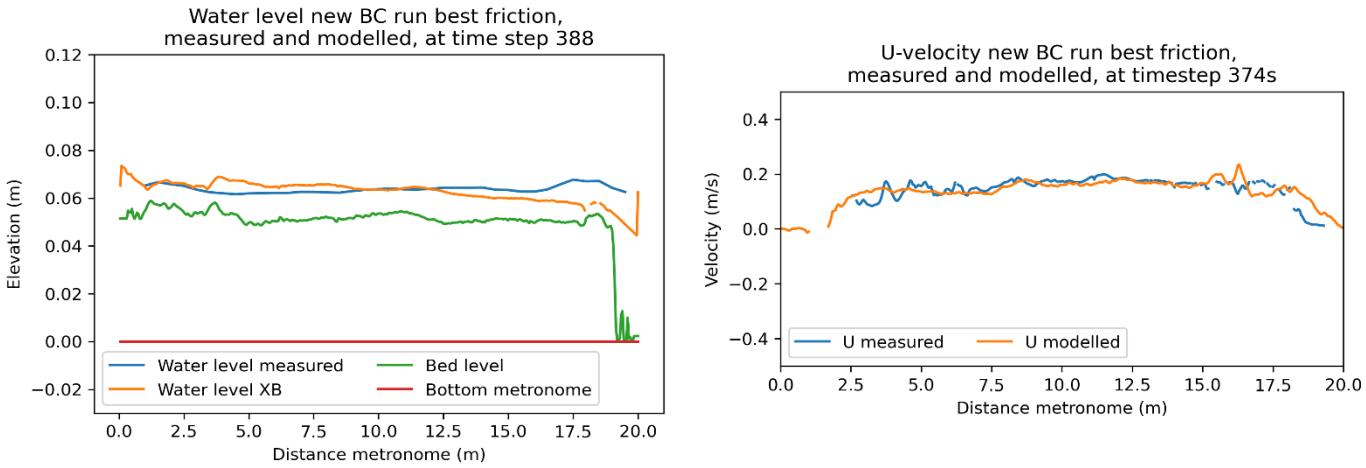

Fig 26

Figure 26: *Water level and velocity plots for the initial new BC best friction run (run 081) in which the bed friction of Chézy = 15 $^{m1/2}$/s was changed to Chézy 20 $m^{1/2}$/s. The water levels are very similar to the water levels of the standard friction run. The water levels are now performing better and are matching quite well with the measured values.*

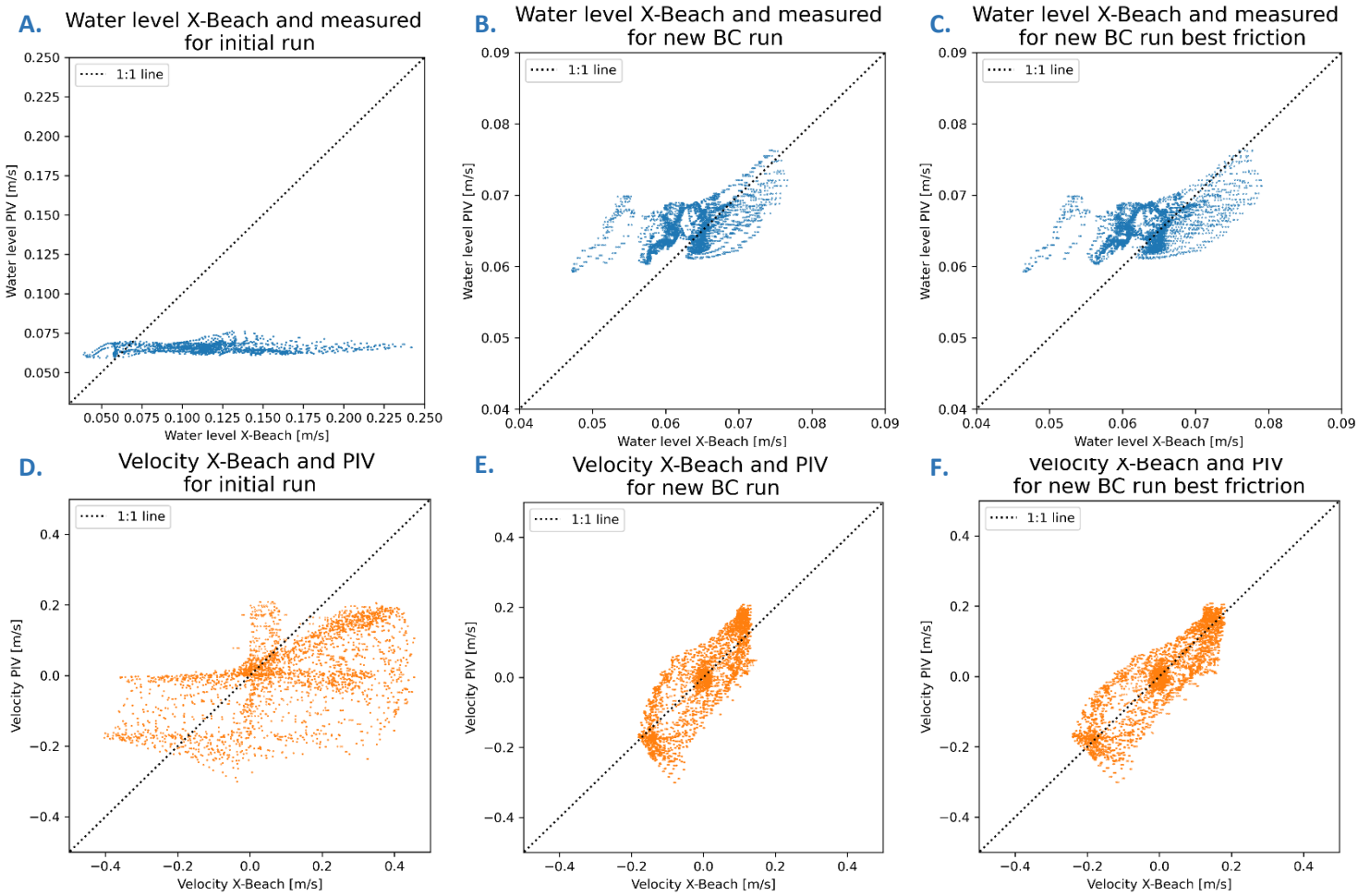

Figure 27: *Water level and velocity plots for the initial run (22a,d), in which the model is still flooding, the new BC standard friction run (22b,e), first run with updated boundary conditions, and new BC best friction run (22,f), in which the bed friction of Chézy = 15 $^{m1/2}$/s was changed to Chézy 20 $m^{1/2}$/s. For the initial run there is a large range for both the water levels and velocities, compared to the two runs where the channel is not flooding. When lowering the bed friction, the modelled velocities match the measured velocities better even though the scatterplot becomes a bit more spread. This same widening happens to the points of the water levels, which is actually making the fit at the 1:1 line worse.*

1:1 line (**Figure 27f**). However, with the increasing Chézy values, the water levels results are getting worse. In the standard friction run the scattered points are roughly centred above the 1:1 line (**Figure 27b**). For the best friction run, the flow velocities are higher because of the decreased friction. For the water levels, this means that their range is increased, making overpredicted water levels more overpredicted and underpredicted water levels more underpredicted making the points to move a bit away from the 1:1 line (**Figure 27c**). This is also visible in the Mean Absolute Error and the Brier Skill Score of the modelled water levels. The standard friction run has a slightly smaller MAE and a higher BSS than those of the best friction run (**Table 6**).

4.4.2 | Updated new tidal boundary condition

Because of the way X-Beach handles the boundaries, the forced water levels at the seaside and riverside are not used for the computations of the rest of the basin. This is why there are two strange water level jumps at both the river- and seaside (**Figure 24c, 25c**). By expanding the column of forced water values of the new boundary condition to two rows, the forced values are making their way in the rest of the model. This then also solves the strange water level jump in run updated BC standard friction (**Figure 28a**). The water levels are now more smooth at the sides. Features like the flood wave going in to the estuary are therefore better visible

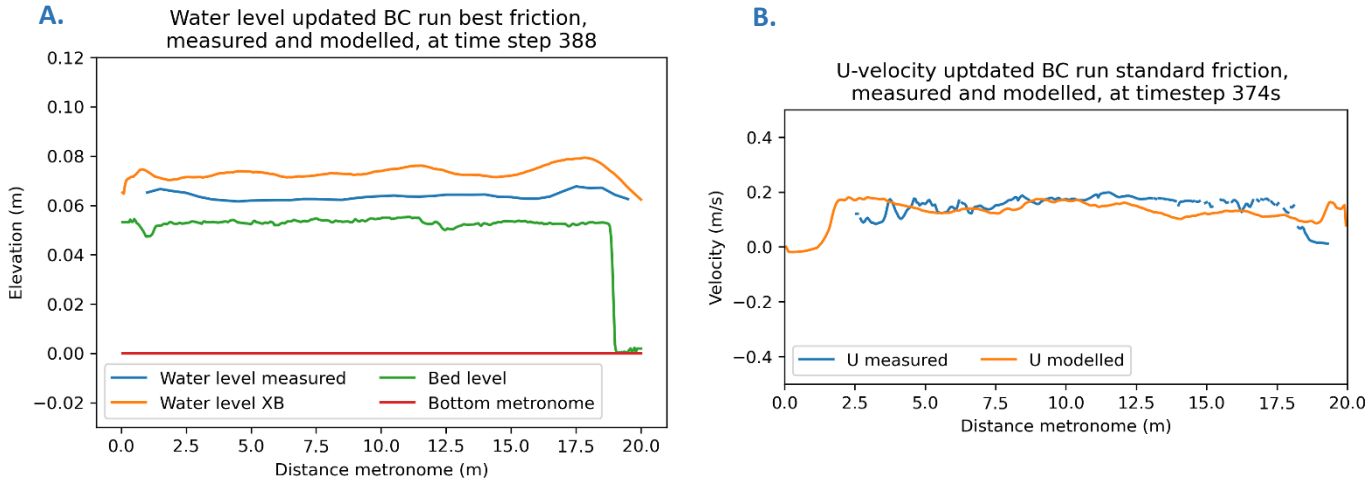

Fig 28

Figure 28: *Results of the update BC standard friction run (run 078). (a) The updated version of the new boundary condition solves the problem with the strange water level jump at the seaside and riverside. However, the water levels are a too high now. (b) The run was done with a Chézy of 15* $m^{1/2}/s$. *Flow velocities are again a too low.*

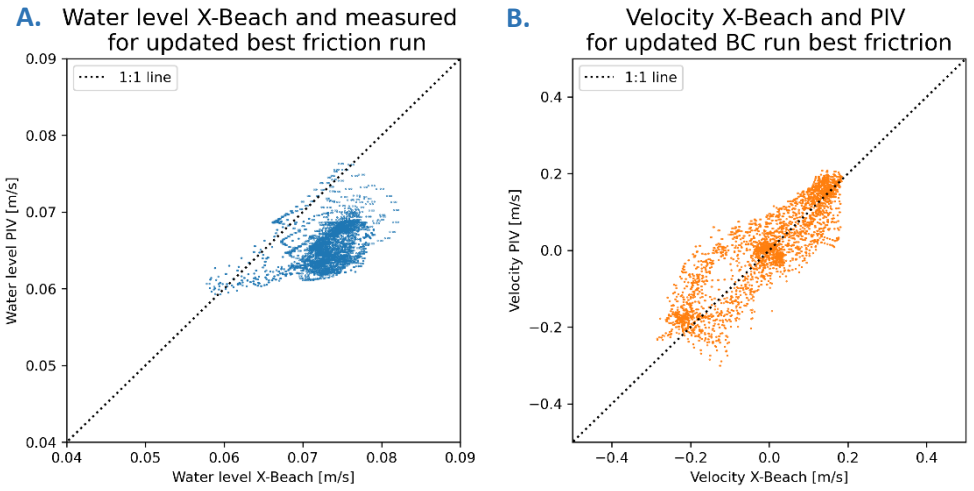

Figure 29: *Water level (a) and velocity (b) plots for the updated boundary condition standard friction run. The model is overpredicting the water levels as can be seen by the position under the 1:1 line. The velocity results are much more following the 1:1 line. The model is performing better for those.*

in the results as can be seen in **figure 28a**. The overall water levels are only too high now. The flow velocities are actually performing quite good **figure 28b**. In the run a Chézy of 15 $m^{1/2}/s$ was used. Compared to the new BC standard friction run, also with a Chézy of 15 $m^{1/2}/s$ (**Figure 25d**), the flow velocities are matching better with the measured values. Different bed friction were tested to see if more improvements were possible but best results were found for the initial Chézy of 15 $m^{1/2}/s$. **figure 29b**. However, the water levels still stayed too high because the model is overpredicting them. In **figure 29a** most points are scattered below the 1:1 line. When comparing the updated BC run to the new BC standard friction and best friction runs, we see a higher bias and MAE and a lower BSS for the water levels (**Table 8**). For the velocity, run 089 performs similar to run 083 with only a higher bias but almost the same MAE and BSS.

Table 8: *Bias, MAE and BSS of the modelled water levels (m) and velocities in the updated BC standard friction run.*

	Water level	**Velocity**
Bias	0.0075	-0.0110
MAE	0.0077	0.0517
BSS	-1.1600	0.7358

5. | Discussion

The results show the big improvements which have been accomplished for the modelling of the metronome using X-Beach. The floods of the initial model have been solved. This resulted in water levels with a MAE of 3.4 millimetres and flow velocities with a MAE of 5.2 cm/s when compared to the measured metronome values. Possible improvements to this comparison may be achieved by eliminating uncertainties in the measured values, which are discussed in the following section (**Chapter 5.1**). Furthermore, a comparison is made with other coastal X-Beach studies and the Nays2D model that was previously used to model the metronome using the Brier skill score (**Chapter 5.2**). Additionally, the limitations of the model are discussed (**Chapter 5.3**). Lastly, an outlook is given on the possibilities with the model when the morphology part is also included (**Chapter 5.4**).

5.1 | Uncertainties in the metronome measurements

To compare the X-Beach model to the metronome, measurements of the water levels and flow velocities were used. An attempt was made to get the X-Beach output as close as possible to these measured values by changing the input parameters and the model itself. However, considering the nature of lab measurements, there is always a range of error. For the water level sensors, the accuracy is 0,1% of the target range (MASSA, 2017). This range is around 140 mm depending on the sensor and the moment in the metronome cycle but this translates to an accuracy of roughly 0.14 mm. This is much less than the MAE's presented in **table 6**. So for the current best outcomes of the model, the error of the water level sensors is within the error of the modelled results. As the error is this much smaller, the measured water levels can safely be used as input for X-Beach.

For different experiments, small differences in the water levels will be present because of different morphologies between experiments but also during experiments. Therefore, it would be more useful to have a function as input for the tides instead of the experiment specific measured water levels. This would also be favourable because water level measurements are limited, especially for the riverside where the closest measurements are a whole metre away. In the process of solving the floods, function have been used as tidal time series. In the first few runs a tidal signal was used based on the movement of the weir. However, this function describes the weir elevation and not the water level elevation. During the metronome cycle, the water level above the weir is not constant. Therefore, this function cannot be used directly as tidal input. However, it should be possible to fit this weir function to the measured values by shifting it just like the function with decreased amplitudes used in this study. The shifted function was not matching the measured water levels perfectly so additional test with different water levels measurements should be conducted to find a good working function to describe the water levels similar to the metronome tilt and weir movement functions.

Errors in the PIV measurements arise from the imprecise stitching of the overhead images and the processing in PIVlab. The stitched images are in both horizontal and vertical direction somewhat off (**Figure 30**). This error is a few millimetre up to one centimetre for each stitch. In the comparison with X-Beach the u-velocities were used. In this x direction, the error of a few centimetres is of the full 20 metres of the flume. Therefore, the imperfect stitching should not be too big of a problem for the magnitude of the velocity measurements. Next to this, some particles are visible twice because of the imperfect stitching. However, because the double particles are still moving at the same speed as the rest of the flow. Furthermore, there is only 40 ms between two compared images which limits the number of particles crossing from one image to the neighbouring image. This should therefore not cause any strange values at the borders of the images. This is confirmed by the results. The borders between the images are hardly noticeable in the PIV data.

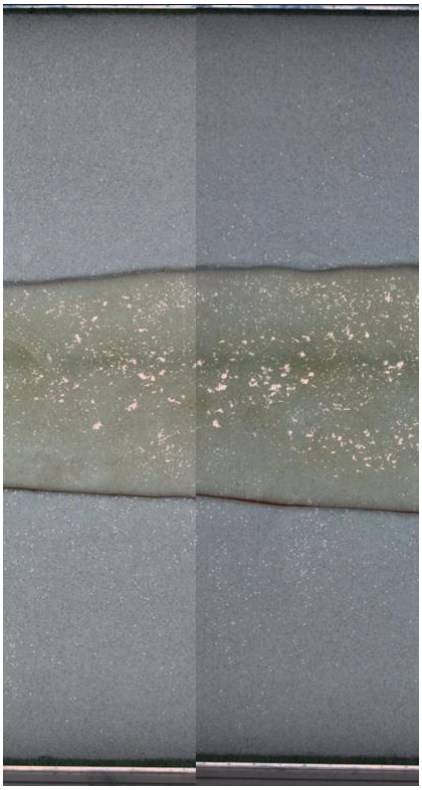

Figure 30: *Imperfect stitching. There is a bit of overlap between the two images and at the bottom at y = 0, the metronome side is not lining up well.*

Additional errors can arise while setting the reference length and x and y offsets. In PIVlab it is not possible to zoom in during this process making it hard to accurate pinpoint these locations. This error also influences the coordinate grid of the velocity measurements. Currently the velocity data is rescaled to 5 centimetre cells which makes inaccuracies in the coordinate grid less impactful. When in future model runs a smaller cell sizes is used, this may cause more problems. Work is currently being done on a method which co-aligns the images together with the images produced by the SLR gantry camera. The SLR camera has much more images of the flume and therefore more overlap in the images. This results in an almost seamless stitched images. With the co-alignment, both images sets and their camera positions are compared with each other to improve the stitching of the overhead imagery used for the PIV. Although, the co-alignment will increase computational times as 180 stitched images have to be created for one PIV data set of 10 cycles, it will improve the accuracy of both velocity and coordinates of the PIV data.

After the calibrating steps with the reference image, the outliers are removed in PIVlab by setting some velocity limits (**Figure 8**). This process is quite biased as it consists of manually drawing a box over a scatter plot. Because the flow velocities change over time, it is not possible to set a certain set of velocity limits for all time steps, as this still will contain a lot of outliers. Therefore, for every timestep, a new box has to be drawn roughly around the most dense part of the scatter plot. This method is definitely not perfect, as it is hard to decide whether a point is an outlier or not and therefore to decide where the border will be drawn. The rectangular shape of the box also results in outliers which are within the velocity limit box. It will probably be better to make use a separate script for the outlier detection outside of PIVlab.

5.2 | Model performance

To see how well the model performs, it was compared with the measured water levels and velocities. Based on this, the bias, mean absolute error and the Brier skill score were calculated (**Table 6,7,8**). The most successful runs, based on their BSS scores, are the new boundary condition normal friction and best friction run and the updated boundary condition standard friction runs. For the water levels, the bias is around half of

the MAE for the new BC normal and best friction runs and almost the same for the updated BC run. For the velocities, for all three runs, the bias is much smaller compared to their MAE.

In the past the Nays2D model has been used in the metronome to model meandering and braiding rivers, as well as estuaries (Weisscher et al., 2020). In the results of this study MAE errors were calculated for the water levels and flow velocities. The Nays2D was well working for the metronome, so a comparison of the MAEs of both models gives an indication of the performance of X-Beach. For the water levels, the errors were calculated for both maximum and minimum water depths. This resulted in an MAE of 1.96 mm with a bias of -0.07 mm during maximum water depth and an MAE of 2.64 mm with a bias of -1.62 mm for the minimum water depths (Weisscher et al., 2020). The new BC standard friction run performed the best here with an MAE of 3.4 mm with a bias of -1.8 mm. These X-Beach values are somewhat higher than the errors found for the Nays2D study. However, they are definitely in the same range as Nays2D. Weisscher et al. (2020) also looked into flow velocities: for the flow, an MAE of 6.45 cm/s was found. This value is actually a bit higher than the best values of X-Beach. The new BC best friction run has a MAE of 5.33 cm/s and the updated BC standard friction has a MAE of 5.17 cm/s. The major problem here is that the best water level results and the best velocity results are not achieved in the same X-Beach run. The best velocity results were achieved in the new BC best friction run and updated BC standard friction run. However, the error of the water levels was slightly higher again in this first run and much higher in the second. For the new BC best friction run, the error of 3.7 mm it is very close to the best X-Beach water level results in the new BC standard friction run and still only 1.1 mm different from the maximum water depth error of Nays2D. However, 3.7 mm is approaching 20% or more of the total water depth. So alterations should still be made here to improve the model.

For the X-Beach model runs, a skill score was calculated. This Brier Skill Score gives a valuation to the model. The BSS classification ranges from bad to excellent (Table 1) (Sutherland et al., 2004; L. C. Van Rijn et al., 2003). In previous studies, the X-Beach model was used to model real life coastal environments. In these studies, BSS values of 0.75 (McCall et al., 2015), 0.6 (Simmons et al., 2019) and 0.7 (Vousdoukas et al., 2011) were achieved. For all these different studies on different types of beaches, the model performed really well, showing the potential of X-Beach for modelling in coastal environments. For the new BC standard friction and best friction runs the water levels have a skill score which can be classified as good whereas the water levels of the updated BC standard friction run have to be classified as bad. All runs have better BSS's for the velocity values. These can all be considered as excellent making them fall in the same category as the aforementioned researches. However, these scores are rather arbitrary and heavily rely on the base line predictor which is used. Based on the results, a classification of excellent is perhaps slightly too ambitious.

From the three runs compared here, the new BC best friction run can be considered as the best run so far based on the MAE and BSS values, although it still used the original version of the new boundary condition without the correction at the sea- and riverside. Luckily, the river- and seaside are not the parts we are most interested about. That is the middle part of the estuary where most important processes and changes to the channel pattern happen. In that part the water levels are performing much better. When looking more visually, to how the water levels are behaving, the updated BC standard friction run is the best. In this runs elements such as the flood wave are much clearer present.

A point of attention is that the best results for the water levels and the best results for the flow velocity were not found with the same Chézy value. For the water levels a Chézy of 15 $m^{1/2}/s$ performed the best but for the flow velocities, a Chézy of 20 $m^{1/2}/s$ performed the best. While the flow velocities are improving for Chézy values closer to 20 $m^{1/2}/s$, the water depth accuracy became slightly worse. The MAE of the flow velocity went from 5.9 cm/s to 5.3 cm/s while the MAE of the water depths went from 3.4 mm to 3.7 mm. This may be a result of scaling problems in the metronome. The water depths in the metronome are just a few cm but the particle size of the sand is not scaled down with the same factor. When this would be done, the sediment will have cohesive characteristics influencing the experiment too much. X-Beach, on the other hand, is made for real life coastal environments without any scale problems. It is also possible that the conversion of surface

velocity to average depth velocity of the PIV measurements is not accurate enough. Currently, a mean value for the whole metronome is used but different water depths of course influence this conversion factor α as well.

5.3 | Limitations of the current model

In X-Beach, there are several flow boundary conditions available. However, in all cases, they are mostly focused on the flow velocity and fluxes going in and out of the domain. The water level is only based on the tidal input forced to the corner cells of the domain and the modelled flow. This makes it possible for the water in the model to 'freely' flow in and out of the model causing higher water levels than seen in the metronome flume. The new flow boundary condition solves this problem by forcing the whole seaside with a certain water level. The current best results are obtained using the original boundary condition in which only one column of cells has the forced measured values. However this way, we have the strange water level jump at sea- and riverside. This was solved with the update of the boundary condition which uses two rows of forced cells. This caused the riverside and seaside to perform much better, but the overall water levels are too high. With only changing the bed roughness, the better results of the water levels were not found. Therefore, testing of the model is necessary. Runs with a refined grid may help, as with the smaller cell sizes there will be smaller gradients between the cells. Next to this boundaries are further away from each other. This is especially important at the river side where the small channel only has 4 or 5 cells in between the boundaries. By having more cells with more data for the model to play with, this may to a better model performance.

A more practical model limitation has to do with running the model itself. In this study all runs were done on a simple laptop. For 400 time steps (10 metronome cycles of 40 seconds) this resulted in model runs which took around 5 to 10 minutes to compute everything. These small runs are perfectly feasible on a laptop. However, when the number of time steps was increased to, for example, 4000 time steps (100 metronome cycles), the model gets slower and slower when coming close to 1000 time steps and stops just after passing it. It is therefore not yet known if the model still performs well when a larger numbers of cycles is modelled. All results presented in this study are from runs of 10 cycles. When running cases with more cycles, it is recommended to not do this on a laptop but on a better equipped computer. When performing runs in which morphology is turned on, this also slows down the process. Also for these cases a better computer is recommended.

5.4 | Morphology and upscaling

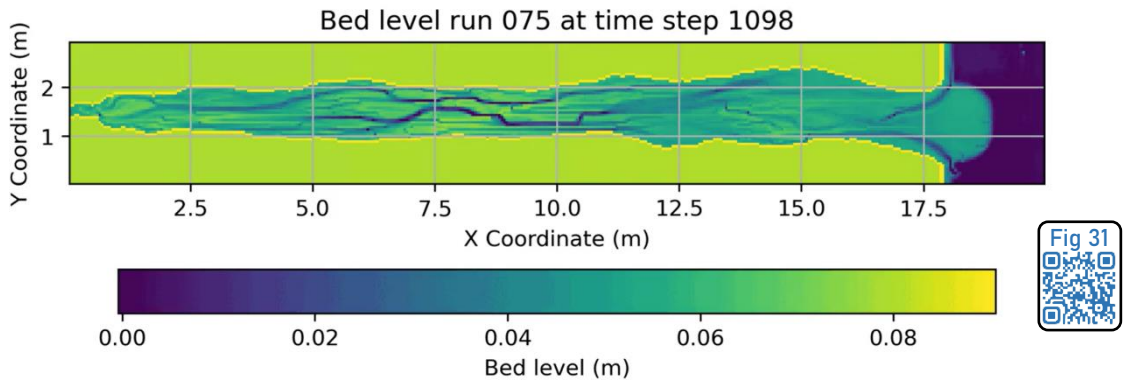

Figure 31: *Run 075 in which morphology is turned on. A bed develops extremely quickly with a morphology which is very similar to the metronome bed.*

This study was mainly focussed on the hydrodynamics of the metronome in the model. Although improvements are still possible, decent results were obtained in the end. In the performed model runs, waves and morphology were turned off in order to exclude variables influencing the hydrodynamics. However, for the best results, especially if longer model runs are done, the waves and morphology parts of X-Beach should

be included as well. This brings a new round of comparing modelled and measured values to validate the model for the morphology changes. There have been a few runs in which the morphology was turned on already. This worked quite nice already. The channels and shoals are comparable to the pattern which forms in the real metronome (**Figure 31**), especially the seaside half of the metronome. However, morphology changes appear much quicker than in the real metronome. In one cycle there is so much sediment transport that it is clearly visible in the bed levels. After 10 cycles, a similar pattern is visible as after 100 -200 real metronome cycles. This development is much too quick. The morph factor plays probably a large part in this. In future studies, this may be explored. Next to this, the modelled channels are much deeper than in the real metronome. This is a known problem of more present in more models in which gravity-driven sediment transport is too high (Baar et al., 2019).

Another subject for future studies is the upscaling of the metronome using a model. When X-Beach works properly for both the hydrodynamics and the morphology, the basin can be scaled up to larger sizes. It is possible to only scale the area of the metronome basin, but there are also possibilities to scale the whole three dimensional system to come closer to real-world systems. This will hopefully give better insights into the scale problems at the metronome. However, the system will be more complex as well as things like fresh and salt water mixing and vegetation should be taken into account. These parameters were not present in the current runs performed for the hydrodynamics in this study.

6. | Conclusions

The aim of this study was to investigate if X-Beach is suitable to model laboratory scale estuaries by validating the model for the metronome flume. This was done by comparing measured values from metronome experiments with the outputs of X-Beach runs. The measured values used are water levels, measured with echo sounders, and flow velocities measured using Particle Image Velocimetry. Initially, X-Beach modelled large floods in the metronome basin which are not present in the real flume. Therefore, several model adjustments were made to improve the results. This included a new boundary condition and the testing of different bed roughness values and tidal inputs. These attempts resulted in a model which gives decent results which are near the measured values. The best results for the water levels were found with a Chézy of 15 $m^{1/2}/s$, giving an error of 3.4 mm. For the flow velocities, the best results were found with a Chézy of 20 $m^{1/2}/s$, giving an error of 0.051 m/s. Expressed in the Brier Skill Score, this equates to a reasonable to excellent performing model. This score might be a bit too ambitious as there still is quite some room for improvement in the modelled results. To get these results, a new boundary condition for the tidal input was introduced, forcing the whole seaside instead of only the corners. This new boundary condition caused strange water level jumps. These were solved with an update to this new boundary condition. However, this caused water levels to be too high. To solve this further testing is needed. Next to this the measured data for the flow velocities can be improved as well with a better stitching method which should increase accuracy of the measurements. In conclusion, the X-Beach model is already performing quite well for the used laboratory scale experiments and has an even larger potential when the model is even further improved. When waves and morphology are included in the model in future studies, the model can really help with the research in the metronome to enlarge our knowledge about estuarine processes.

| Acknowledgements

A thesis is an individual project but impossible to write without the insights and help of others. Therefore I would like to thank my first supervisor Prof. dr. Maarten Kleinhans, second supervisor Dr. Timothy Price and Prof. Dano Roelvink for sharing their knowledge and feedback to bring this project to a successful end. Moreover, I want to thank Dr. Saeb Faraji Gargari for his valuable assistance and source code work with X-Beach to solve the floods in the model. My gratitude goes also to PhD candidate Eise Nota for his all-round support both substantive and practical. I also want to thank the technical staff at the Earth Simulation Laboratory. Ing. Marcel van Maarseveen, Ing. Bas van Dam, Ing. Henk Markies and Arjan van Eijk were always available for assistance if the metronome was not cooperating. Furthermore, I would like to thank Lotta Beyaard, Meryem Upson and Esmee van Amelsfort for working together at the metronome and sparring about our projects. Lastly my gratitude goes to those who read and provided feedback on this thesis.

| References

Andrews, D. G., & Mcintyre, M. E. (1978). An exact theory of nonlinear waves on a Lagrangian-mean flow. *Journal of Fluid Mechanics*, *89*(4), 609–646. https://doi.org/10.1017/S0022112078002773

Baar, A. W., Boechat Albernaz, M., van Dijk, W. M., & Kleinhans, M. G. (2019). Critical dependence of morphodynamic models of fluvial and tidal systems on empirical downslope sediment transport. *Nature Communications 2019 10:1*, *10*(1), 1–12. https://doi.org/10.1038/s41467-019-12753-x

Bahremand, A., Jamali, F., & Komaki, C. B. (2020). 2D Flood Simulation Using the Nays 2D Flood Model and Comparison with the Sentinel 2 Satellite Image (Case Study: Flood of March 2019 at the end of Arazkuse River, Golestan Province). *Journal of Water and Soil Conservation*, *27*(2), 223–236. https://doi.org/10.22069/JWSC.2020.17618.3325

Bandini, F., Lüthi, B., Peña-Haro, S., Borst, C., Liu, J., Karagkiolidou, S., Hu, X., Lemaire, G. G., Bjerg, P. L., & Bauer-Gottwein, P. (2021). A Drone-Borne Method to Jointly Estimate Discharge and Manning's Roughness of Natural Streams. *Water Resources Research*, *57*(2), e2020WR028266. https://doi.org/10.1029/2020WR028266

Biggs, H., Smart, G., Doyle, M., Eickelberg, N., Aberle, J., Randall, M., & Detert, M. (2023). Surface Velocity to Depth-Averaged Velocity—A Review of Methods to Estimate Alpha and Remaining Challenges. *Water 2023, Vol. 15, Page 3711*, *15*(21), 3711. https://doi.org/10.3390/W15213711

Cooper, J. A. G. (1993). Sedimentation in a river dominated estuary. *Sedimentology*, *40*(5), 979–1017. https://doi.org/10.1111/J.1365-3091.1993.TB01372.X

Cox, J. R., Lingbeek, J., Weisscher S A H, & Kleinhans M G. (2022). Effects of Sea-Level Rise on Dredging and Dredged Estuary Morphology. *Journal of Geophysical Research: Earth Surface*, 127. https://doi.org/10.1029/2022JF006790

Dalrymple, R. W., Zaitlin, B. A., & Boyd, R. (1992). *PERSPECTIVE ESTUARINE FACIES MODELS: CONCEPTUAL BASIS AND STRATIGRAPHIC IMPLICATIONS I*. http://pubs.geoscienceworld.org/sepm/jsedres/article-pdf/62/6/1130/2811129/1130.pdf

Dam, G., Van Der Wegen, M., Labeur, R. J., & Roelvink, D. (2016). Modeling centuries of estuarine morphodynamics in the Western Scheldt estuary. *Geophysical Research Letters*, *43*(8), 3839–3847. https://doi.org/10.1002/2015GL066725

Davidson, M. A., Lewis, R. P., & Turner, I. L. (2010). Forecasting seasonal to multi-year shoreline change. *Coastal Engineering*, *57*(6), 620–629. https://doi.org/10.1016/J.COASTALENG.2010.02.001

Day, J. W., Crump, B. C., Kemp, W. M., & Yáñez-Arancibia, A. (2012). Estuarine Ecology. *Estuarine Ecology*. https://doi.org/10.1002/9781118412787

Deltares. (n.d.). *About - XBeach - oss.deltares.nl*. Retrieved October 20, 2023, from https://oss.deltares.nl/web/xbeach/about

Deltares. (2023). *Welcome to XBeach manual's documentation! — XBeach manual 0.1 documentation*. https://xbeach.readthedocs.io/en/latest/index.html

D'Errico John. (2023). *inpaint_nans*. MATLAB Central File Exchange. https://nl.mathworks.com/matlabcentral/fileexchange/4551-inpaint_nans

Friedrichs, C. T. (2011). *Deltas and estuaries*. https://scholarworks.wm.edu/presentations

Friedrichs, C. T., & Aubrey, D. G. (1988). *Non-linear Tidal Distortion in Shallow Well-mixed Estuaries: a Synthesisa*.

Ganju, N. K., Brush, M. J., Rashleigh, B., Aretxabaleta, A. L., del Barrio, P., Grear, J. S., Harris, L. A., Lake, S. J., McCardell, G., O'Donnell, J., Ralston, D. K., Signell, R. P., Testa, J. M., & Vaudrey, J. M. P. (2015). Progress and Challenges in Coupled Hydrodynamic-Ecological Estuarine Modeling. *Estuaries and Coasts 2015 39:2*, *39*(2), 311–332. https://doi.org/10.1007/S12237-015-0011-Y

George, D. A., Gelfenbaum, G., & Stevens, A. W. (2012). Modeling the Hydrodynamic and Morphologic Response of an Estuary Restoration. *Estuaries and Coasts 2012 35:6*, *35*(6), 1510–1529. https://doi.org/10.1007/S12237-012-9541-8

Hauet, A., Kruger, A., Krajewski, W. F., Bradley, A., Muste, M., Creutin, J.-D., & Wilson, M. (2008). Experimental System for Real-Time Discharge Estimation Using an Image-Based Method. *Journal of Hydrologic Engineering*, *13*(2), 105–110. https://doi.org/10.1061/(ASCE)1084-0699(2008)13:2(105)

He, Z., Liang, M., Jia, L., Dong, H., Chen, K., Liu, J., Lin, Y., & Ou, J. (2022). Long-term morphological modeling and implication for estuarine regulation of the Modaomen Estuary, Pearl River Delta, China. *Applied Ocean Research*, *123*, 103184. https://doi.org/10.1016/J.APOR.2022.103184

Henniger, R., Kleiser, L., & Meiburg, E. (2010). Direct numerical simulations of particle transport in a model estuary. *Journal of Turbulence*, *11*(39), 1–31. https://doi.org/10.1080/14685248.2010.516257

Hibma, A., Stive, M. J. F., & Wang, Z. B. (2004). Estuarine morphodynamics. *Coastal Engineering*, *51*(8–9), 765–778. https://doi.org/10.1016/J.COASTALENG.2004.07.008

Hun, Y., Geun, C., & Do, Y. (2015). A Study on the Field Application of Nays2D Model for Evaluation of Riverfront Facility Flood Risk. *KSCE Journal of Civil and Environmental Engineering Research*, *35*(3), 579–588. https://doi.org/10.12652/KSCE.2015.35.3.0579

Kleinhans, M. G., van der Vegt, M., Leuven, J., Braat, L., Markies, H., Simmelink, A., Roosendaal, C., van Eijk, A., Vrijbergen, P., & van Maarseveen, M. (2017). Turning the tide: comparison of tidal flow by periodic sea level fluctuation and by periodic bed tilting in scaled landscape experiments of estuaries. *Earth Surface Dynamics*, *5*(4), 731–756. https://doi.org/10.5194/esurf-5-731-2017

Kleinhans, M. G., Van Rosmalen, T. M., Roosendaal, C., & Van Der Vegt, M. (2014). Turning the tide: Mutually evasive ebb-and

flood-dominant channels and bars in an experimental estuary. *Advances in Geosciences*, *39*, 21–26. https://doi.org/10.5194/ADGEO-39-21-2014

Kleinhans, M. G., van Scheltinga, R. T., van der Vegt, M., & Markies, H. (2015). Turning the tide: Growth and dynamics of a tidal basin and inlet in experiments. *Journal of Geophysical Research: Earth Surface*, *120*(1), 95–119. https://doi.org/10.1002/2014JF003127

Leenman, A. S., & Eaton, B. C. (2023). Remote sensing of laboratory rivers. *Earth Surface Processes and Landforms*. https://doi.org/10.1002/ESP.5577

Legleiter, C. J., & Kinzel, P. J. (2020). Inferring Surface Flow Velocities in Sediment-Laden Alaskan Rivers from Optical Image Sequences Acquired from a Helicopter. *Remote Sensing 2020, Vol. 12, Page 1282*, *12*(8), 1282. https://doi.org/10.3390/RS12081282

Leuven, J. R. F. W., Braat, L., van Dijk, W. M., de Haas, T., van Onselen, E. P., Ruessink, B. G., & Kleinhans, M. G. (2018). Growing Forced Bars Determine Nonideal Estuary Planform. *Journal of Geophysical Research: Earth Surface*, *123*(11), 2971–2992. https://doi.org/10.1029/2018JF004718

Leuven, J. R. F. W., Kleinhans, M. G., Weisscher, S. A. H., & van der Vegt, M. (2016). Tidal sand bar dimensions and shapes in estuaries. *Earth-Science Reviews*, *161*, 204–223. https://doi.org/10.1016/J.EARSCIREV.2016.08.004

Lu, X. X., Ran, L. S., Liu, S., Jiang, T., Zhang, S. R., & Wang, J. J. (2013). Sediment loads response to climate change: A preliminary study of eight large Chinese rivers. *International Journal of Sediment Research*, *28*(1), 1–14. https://doi.org/10.1016/S1001-6279(13)60013-X

MASSA. (2017). *Model M-320/150 Low Cost Sensor Data sheet* (pp. 1–3). MASSA PRODUCTS CORPORATION. https://www.massa.com/wp-content/uploads/2017/08/M-320-150-Datasheet-160229.pdf

McCall, R. T., Masselink, G., Poate, T. G., Roelvink, J. A., & Almeida, L. P. (2015). Modelling the morphodynamics of gravel beaches during storms with XBeach-G. *Coastal Engineering*, *103*, 52–66. https://doi.org/10.1016/J.COASTALENG.2015.06.002

Mimura, N., & Horikawa, K. (2013). Review Sea-level rise caused by climate change and its implications for society. *Proceedings of the Japan Academy*, *89*(7), 281–301. https://doi.org/10.2183/pjab.89.281

Namin, M., Lin, B., & Falconer, R. A. (2004). Modelling estuarine and coastal flows using an unstructured triangular finite volume algorithm. *Advances in Water Resources*, *27*(12), 1179–1197. https://doi.org/10.1016/J.ADVWATRES.2004.08.012

NOAA. (2023). *The Estuary—where fresh and saltwater mix*. National Oceanic and Atmospheric Administration. https://oceanservice.noaa.gov/facts/estuary.html

Onselen, E. P. van. (2017). *Scale effects on waves and sediment mobility in the Metronome tidal facility* [Msc Thesis, Utrecht University]. https://studenttheses.uu.nl/handle/20.500.12932/29828

Oppenheimer, M., Glavovic, B. C., Hinkel, J., Van de Wal, R., Magnan, A. K., Abd-Elgawad, A., Cai, R., Cifuentes-Jara, M., DeConto, R. M., Ghosh, T., Haym J, Isla, F., Marzeion, B., Meyssignac, B., & Sebesvari, Z. (2019). Sea Level Rise and Implications for Low-Lying Islands, Coasts and Communities. In *IPCC Special Report on the Ocean and Cryosphere in a Changing Climate* (pp. 321–445). Cambridge University Press. https://doi.org/10.1017/9781009157964.006

Potter, B. (2001). *Estuaries - National Institute of Water and Atmospheric Research*. https://niwa.co.nz/education-and-training/schools/students/estuaries

Ranasinghe, R., Wu, C. S., Conallin, J., Duong, T. M., & Anthony, E. J. (2019). Disentangling the relative impacts of climate change and human activities on fluvial sediment supply to the coast by the world's large rivers: Pearl River Basin, China. *Scientific Reports 2019 9:1*, *9*(1), 1–10. https://doi.org/10.1038/s41598-019-45442-2

Reynolds, O. (1887). On certain laws relating to the regime of rivers and estuaries and on the possibility of experiments on a small scale. *Br. Assoc. Rep., London*, 555–562.

Reynolds, O. (1889). Report of the committee appointed to investigate the action of waves and currents on the beds and foreshores of estuaries by means of working models. In *Papers on mechanical and physical subjects* (Vol. 2, pp. 1881–1900). Cambridge Univ. Press.

Roelvink, D. (2015). *XBeach Technical Reference: Kingsday Release*. https://doi.org/10.13140/RG.2.1.4025.6244

Roelvink, D., Reniers, A., Van Dongeren, A., Van Thiel De Vries, J., Mccall, R., & Lescinski, J. (2009). Modelling storm impacts on beaches, dunes and barrier islands. *Coastal Engineering*, *56*, 1133–1152. https://doi.org/10.1016/j.coastaleng.2009.08.006

Schramkowski, G. P., Schuttelaars, H. M., & De Swart, H. E. (2004). Non-linear channel-shoal dynamics in long tidal embayments. *Ocean Dynamics*, *54*(3–4), 399–407. https://doi.org/10.1007/S10236-003-0063-6/METRICS

Schuttelaars, H. M., & De Swart, H. E. (1999). Initial formation of channels and shoals in a short tidal embayment. *J. Fluid Mech*, *386*, 15–42. https://doi.org/10.1017/S0022112099004395

Schuurman, F., Shimizu, Y., Iwasaki, T., & Kleinhans, M. G. (2016). Dynamic meandering in response to upstream perturbations and floodplain formation. *Geomorphology*, *253*, 94–109. https://doi.org/10.1016/J.GEOMORPH.2015.05.039

Simmons, J. A., Splinter, K. D., Harley, M. D., & Turner, I. L. (2019). Calibration data requirements for modelling subaerial beach storm erosion. *Coastal Engineering*, *152*, 103507. https://doi.org/10.1016/J.COASTALENG.2019.103507

Small, C., & Nicholls, R. J. (2003). A Global Analysis of Human Settlement in Coastal Zones on JSTOR. *Journal of Coastal Research*, *19*(3), 584–599. http://www.jstor.org/stable/4299200

Smit, P. B., Stelling, G. S., Roelvink, D., Van Thiel de Vries, J., McCall, R., Van Dongeren, A., & Jacobs, R. (n.d.). *X-Beach: Non-*

hydrostatic model; Validation, verification and model description . https://oss.deltares.nl/documents/4142077/4199062/non-hydrostatic_report_draft.pdf/eadc1aff-6e19-6e82-2747-3c11c30457ee?t=1624871720408

Smit, P. B., Stelling, G. S., Roelvink, D., Van Thiel De Vries, J., Mccall, R., Van Dongeren, A., Zwinkels, C., & Jacobs, R. (2010). *XBeach: Non-hydrostatic model*.

Stefanon, L., Carniello, L., D'Alpaos, A., & Lanzoni, S. (2010). Experimental analysis of tidal network growth and development. *Continental Shelf Research*, *30*(8), 950–962. https://doi.org/10.1016/J.CSR.2009.08.018

Sutherland, J. (2016). COSMOS modelling and the development of model performance statistics. *Researchgate*. https://www.researchgate.net/profile/James-Sutherland/publication/238661654_COSMOS_MODELLING_AND_THE_DEVELOPMENT_OF_MODEL_PERFORMANCE_STATISTICS/links/570f5adb08aee76b9dae0eb1/COSMOS-MODELLING-AND-THE-DEVELOPMENT-OF-MODEL-PERFORMANCE-STATISTICS.pdf

Sutherland, J., Peet, A. H., & Soulsby, R. L. (2004). Evaluating the performance of morphological models. *Coastal Engineering*, *51*(8–9), 917–939. https://doi.org/10.1016/j.coastaleng.2004.07.015

Talke, S. A., & de Swart, H. E. (2006). *Hydrodynamics and morphology in the Ems/Dollard estuary: review of models, measurements, scientific literature and the effects of changing conditions* (Vols. R06-01). UU PHYS IMAU Marine and Atmospheric Research. https://dspace.library.uu.nl/handle/1874/42826

Tambroni, N., Bolla Pittaluga, M., & Seminara, G. (2005). Laboratory observations of the morphodynamic evolution of tidal channels and tidal inlets. *Journal of Geophysical Research: Earth Surface*, *110*(F4), 4009. https://doi.org/10.1029/2004JF000243

The MathWorks Inc. (2023). *MATLAB version 9.14.0.2337262 (R2023a)* . Natick, Massachusetts: The MathWorks Inc. . https://www.mathworks.com

Thielicke, W. (2023). *PIVlab - particle image velocimetry (PIV) tool with GUI* (2.62). https://nl.mathworks.com/matlabcentral/fileexchange/27659-pivlab-particle-image-velocimetry-piv-tool-with-gui

Thielicke, W., & Stamhuis, E. J. (2014). PIVlab – Towards User-friendly, Affordable and Accurate Digital Particle Image Velocimetry in MATLAB. *Journal of Open Research Software*, *2*(1). https://doi.org/10.5334/JORS.BL

US EPA. (2023). *Basic Information about Estuaries*. United States Environmental Protection Agency. https://www.epa.gov/nep/basic-information-about-estuaries

Van Rijn, L. C. V., Ruessink, B. G., & Mulder, J. P. M. (2002). Coast3D-Egmond: The Behaviour of a Straight Sandy Coast on the Time Scale of Storms and Seasons: Process Knowledge and Guidelines for Coastal Management: End Document. *Aqua Publications*.

Van Rijn, L. C., Wasltra, D. J. R., Grasmeijer, B., Sutherland, J., Pan, S., & Sierra, J. P. (2003). The predictability of cross-shore bed evolution of sandy beaches at the time scale of storms and seasons using process-based Profile models. *Coastal Engineering*, *47*(3), 295–327. https://doi.org/10.1016/S0378-3839(02)00120-5

Van Veen, J. (1950). Ebb and Flood Channel Systems in the Netherlands Tidal Waters. *Journal of the Royal Dutch Geographical Society*, 303–325. https://www.vliz.be/imisdocs/publications/ocrd/114295.pdf

Vousdoukas, M. I., Almeida, L. P., & Ferreira, Ó. (2011). Modelling storm-induced beach morphological change in a meso-tidal, reflective beach using XBeach. *Journal of Coastal Research*, 1916–1920. https://www-jstor-org.proxy.library.uu.nl/stable/26482510?casa_token=EJsde-mI4HwAAAAA%3ANTSWNPIfxt6goeCL0t7-rf6AG53fFZFbxRovNWfIUZCaU3Q36c1IxRbQgfCJ7THGsuzuxLDJDZzUiiXK1VAilr8yy5ldaSpaQGnIZKpbKlgMUiV7Yg

Walstra, D. J. R., Roelvink, J. A., & Groeneweg, J. (2000). Calculation of Wave-Driven Currents in a 3D Mean Flow Model. *Coastal Engineering 2000 - Proceedings of the 27th International Conference on Coastal Engineering, ICCE 2000*, *276*, 1050–1063. https://doi.org/10.1061/40549(276)81

Warmink, J. J., Booij, M. J., Van Der Klis, H., & Hulscher, S. J. M. H. (2007). *Uncertainty in water level predictions due to various calibrations*. 1–18.

Warner, J. C., Geyer, W. R., & Lerczak, J. A. (2005). Numerical modeling of an estuary: A comprehensive skill assessment. *Journal of Geophysical Research: Oceans*, *110*(C5), 1–13. https://doi.org/10.1029/2004JC002691

Weisscher, S. A. H., Boechat-Albernaz, M., Leuven, J. R. F. W., Van Dijk, W. M., Shimizu, Y., & Kleinhans, M. G. (2020). Complementing scale experiments of rivers and estuaries with numerically modelled hydrodynamics. *Earth Surface Dynamics*, *8*(4), 955–972. https://doi.org/10.5194/ESURF-8-955-2020

Weisscher, S. A. H., Van den Hoven, K., Pierik, H. J., & Kleinhans, M. G. (2022). Building and Raising Land: Mud and Vegetation Effects in Infilling Estuaries. *Journal of Geophysical Research: Earth Surface*, *127*(1), e2021JF006298. https://doi.org/10.1029/2021JF006298

Wetz, M. S., & Yoskowitz, D. W. (2013). An 'extreme' future for estuaries? Effects of extreme climatic events on estuarine water quality and ecology. *Marine Pollution Bulletin*, *69*(1–2), 7–18. https://doi.org/10.1016/J.MARPOLBUL.2013.01.020

Appendix A | Metronome experiment logs

In the study data from metronome experiment 54 and 59 was used. Both experiments are designed to study the influence of different dike set-ups on the estuary.

Experiment 054

------ 16-05-2023 ------
Cleaned the river filters.
Shovelled the sand.
Filled the flume.
Did some initial smoothening.

------ 17-05-2023 ------
Did a lot of smoothening with Michelle, Nicole and Haiwei.
Turned off the lights.

------ 22-05-2023 ------
Finalized the smoothening.
Tested the PIV trigger with Marcel. It works!
The pump of the upstream weir it no longer attached to the weir. Marcel is going to look at it tomorrow.

Took a laser scan of the system at 00000 cycles: Exp054_00000.
Took photos with laser gantry camera of the dry system: Exp054_00000_dry.
Filled the flume.
Took photos with laser gantry camera of the wet system: Exp054_00000_wet.
Did some minor smoothening.
Took photos with the hand-held SLR camera.
Turned off the lights and put river at 300 L/h.

------ 23-05-2023 ------
Brechtje came by to try out some water level measurements.
We put the sensors at: y-locations 103 - 148 - 193 cm (hall side = 0); x-locations 19.50, 18.40, 14.50, 9.70, 5.60 m.
Still: 19.50, 18.40, 14.50, 9.70, 5.60 m
Still + Waves: 19.50, 18.40 m

Tried one cycle with a few plastic PIV grains to test if it works.

Started experiment 054 for 1 cycle with the following settings:

Tilt period: 40s
Tilt amplitude 1st: 75mm
Tilt amplitude 2nd: 15mm
Frequency multiplier: 2
Phase shift: 90 degrees
Wave elements: 100

Weir period: 40s
Weir amplitude 1st: 12mm
Weir amplitude 2nd: 2.4mm
Frequency multiplier: 2
Phase shift: 90 degrees
Offset: 67mm
Wave elements: 100

No sediment feed and river discharge of 500 l/h (in ebb phase). Waves on with 2 Hz in flood phase.

Accidently 300 l/h river discharge this cycle.
Also tested water level sensors at 19.50 m.
Everything seems to work fine.

------ 24-05-2023 ------
Tried the PIV for the first time with Brechtje, Maarten, Janneke, Lonneke and Sheng.
Filled the flume with plastic grains.
Did three cycles of minor symmetrical tilting with following different settings:
Tilt amplitude 1st: 30mm
Tilt amplitude 2nd: 0mm
Weir amplitude 1st: 10mm
Weir amplitude 2nd: 0mm

Continued experiment 054 for 10 cycles with the same settings the film and trigger on with 10 photos of 25 Hz triggers each 15 seconds: 00001-00011
It turns out that many sand grains clump together so Maarten worked with some pressure air to prevent that.

Continued experiment 054 for 11 cycles, with the first 4 cycles without trigger and the remaining 7 cycles with film and trigger.
There is still lot of clumping. So we're first going to check whether this works with the PIV software before further continuing the experiment.
Unfortunately and inexplicably the images were not stored this time for all cameras.
Did a laser scan of the wet system with plastic grains in it: Exp054_00022.
Took photos with laser gantry camera of the wet system: Exp054_00022_wet.
Took photos with the hand-held SLR camera.

Increased the sea level, put river on and put the flume on a small tilt to vacuum the plastic grains out of the flume.
Got practically all plastic grains out of the flume with Brechtje.

Did one cycle with a minor symmetrical tilting with following different settings:
Tilt amplitude 1st: 10mm
Tilt amplitude 2nd: 0mm
Weir amplitude 1st: 10mm
Weir amplitude 2nd: 0mm

Upper left and lower right computer don't connect with the RDL disc anymore.
Shut down all computers and started lower right first to see if the problem still occurs.
This solves the problem for lower right, but not for upper left.
Shut down all computers again and now started upper left first to see if the problem still occurs.
This didn't work as it says access is denied. Possibly my solis ID doesn't have the credentials for this computer.
Marcel fixed it.
Cleaned river filters.
Turned off the lights and put river at 300 L/h.

------ 25-05-2023 ------
Continued experiment 054 for 28 cycles with the same settings with normal trigger and did water level measurements:
Y-locations 103 - 148 - 193 cm (hall side = 0); x-locations 19.50, 18.40, 14.50, 9.70, 5.60 m.
19.50 m for the first 5 cycles from the start.
All other positions for 3 cycles.

Took photos with laser gantry camera of the wet system: Exp054_00050_wet.
Took photos with the hand-held SLR camera.
Took a laser scan of the system at 00050 cycles: Exp054_00050.
Took photos with laser gantry camera of the dry system: Exp054_00050_dry.
Turned off the lights and put river at 300 L/h.

------ 31-05-2023 ------
Found the metronome with the sea drained, but the river input on. At some point the electronics malfunctioned so that both sea pumps stopped working.
If the river remains on at 300 L/h, the water reaches to just before the delta, but not into the sea.
The sea drainage caused an erosion channel and delta at the wall side of the sea side. Took photos of this with the hand-held SLR camera.
Removed the drainage channel and minor delta and smoothened the bed to approximately the previous position. Took photos of this with the hand-held SLR camera and added to 00050.
Marcel looked at it. It turns out both sea pumps don't work anymore. We have to wait for new delivery of pumps.

------ 06-06-2023 ------
Pumps arrived and were installed. Also the pumps at the upstream weir were fixed.
Much water was drained so added 2 cups of dye.

Continued experiment 054 for 20 cycles with the same settings with imagery at 2 Hz throughout all the cycles.
The 2 Hz imagery was shot to have a background image for PIV measuring.
Students from Philosophy of Science were toured by Maarten.
Measured the elevation sensors at: y-locations 103 - 148 - 193 cm (hall side = 0); x-locations 10.50, 1.00 m.
Still: 1.00, 10.50 m
10.50 m is the suspected shortcut channel location.

Continued experiment 054 for 30 cycles with the same settings with original overhead imagery settings.
Measured the elevation sensors after 5 cycles at: y-locations 103 - 148 - 193 cm (hall side = 0); x-locations 10.50, 1.00 m.
Tilt: 10.50, 1.00 m

Took photos with laser gantry camera of the wet system: Exp054_00100_wet.
Took photos with the hand-held SLR camera.
Took a laser scan of the system at 00100 cycles: Exp054_00100.
Took photos with laser gantry camera of the dry system: Exp054_00100_dry.
Marcel finalized the wired of the new pumps and also replaced the river pump.
Filled the flume.
Decided to keep the upstream weir pump off, because I'm unsure if the drainage happens fast enough.
Continued the 54th experiment with another 900 cycles with the same settings.
Restarted the flume because of a program crash.
It turned out that the flume position was at 0.02 mm. Did one cycle with a tilt amplitude of 1 mm.
Reattempted the continuation of the 54th experiment with another 900 cycles with the same settings.

------ 07-06-2023 ------
Took photos with laser gantry camera of the wet system: Exp054_01000_wet.
Took photos with the hand-held SLR camera.
Drained the flume.
Took photos with laser gantry camera of the dry system: Exp054_01000_dry.
Took a laser scan of the dry system at 01000 cycles: Exp054_01000.
Cleaned the river filters.
Filled the flume.
Continued the 54th experiment with another 1500 cycles with the same settings.
Kept the pump of the upstream weir on.

------ 08-06-2023 ------
Took photos with laser gantry camera of the wet system: Exp054_02500_wet.
Took photos with the hand-held SLR camera.
Drained the flume.
Moved one dike enforcement to a weak spot.
Took photos with laser gantry camera of the dry system: Exp054_02500_dry.
Took a laser scan of the dry system at 02500 cycles: Exp054_02500.
Cleaned the river filters.
Filled the flume.
Continued the 54th experiment with another 1500 cycles with the same settings.

------ 08-06-2023 ------
Took photos with laser gantry camera of the wet system: Exp054_04000_wet.
Took photos with the hand-held SLR camera.
Drained the flume.
Sprayed some anti-algae spray.
Took photos with laser gantry camera of the dry system: Exp054_04000_dry.
Took a laser scan of the dry system at 04000 cycles: Exp054_04000.
Cleaned the river filters.
Filled a small hole behind the dike.
Filled the flume.
Continued the 54th experiment with another 1500 cycles with the same settings.

------ 12-06-2023 ------
Took photos with laser gantry camera of the wet system: Exp054_05500_wet.
Took photos with the hand-held SLR camera.
Drained the flume.
Took photos with laser gantry camera of the dry system: Exp054_05500_dry.
Took a laser scan of the dry system at 05500 cycles: Exp054_05500.
Cleaned the river filters.
Filled the flume.
Continued the 54th experiment with another 1500 cycles with the same settings.

------ 13-06-2023 ------
Took photos with laser gantry camera of the wet system: Exp054_07000_wet.
Took photos with the hand-held SLR camera.
Drained the flume.
Took photos with laser gantry camera of the dry system: Exp054_07000_dry.
Took a laser scan of the dry system at 07000 cycles: Exp054_07000.
Cleaned the river filters.
Filled the flume.
Continued the 54th experiment with another 1500 cycles with the same settings.
Group with prof. Poldergeist came to visit the metronome.

------ 14-06-2023 ------
Refilled some sand behind dikes.
Took photos with laser gantry camera of the wet system: Exp054_08500_wet.
Took photos with the hand-held SLR camera.
Drained the flume.
Took photos with laser gantry camera of the dry system: Exp054_08500_dry.
Took a laser scan of the dry system at 08500 cycles: Exp054_08500.
Cleaned the river filters.
Filled the flume.
Continued the 54th experiment with another 1500 cycles with the same settings.

------ 15-06-2023 ------
Took photos with laser gantry camera of the wet system: Exp054_10000_wet.
Took photos with the hand-held SLR camera.
Refilled some sand behind dikes and restored dike structure.
Drained the flume.
Took photos with laser gantry camera of the dry system: Exp054_10000_dry.
Took a laser scan of the dry system at 10000 cycles: Exp054_10000.
Cleaned the river filters.
Filled the flume.
Continued the 54th experiment with another 1000 cycles with the same settings.

------ 15-06-2023 ------
Refilled some sand behind dikes and restored dike structure.
Took photos with laser gantry camera of the wet system: Exp054_11000_wet.
Took photos with the hand-held SLR camera.
Drained the flume.
Took photos with laser gantry camera of the dry system: Exp054_11000_dry.
Took a laser scan of the dry system at 11000 cycles: Exp054_11000.
Cleaned the river filters.
Filled the flume.
Turned off lights and put river on at 300 l/h.

------ 20-06-2023 ------
Did PIV with Brechtje, Maarten, Menno, Silke and Ilaria.
Filled the flume with plastic grains.

Continued experiment 054 for 15 cycles, with the first 4 cycles with trigger at 22.5 s and the remaining 11 cycles

with film and trigger each 15 seconds (starting at 0): 11000-11015.
Continued experiment 054 for 15 cycles, with the first 5 cycles with trigger at 22.5 s and the remaining 11 cycles with film and trigger each 15 seconds (starting at 0): 11015-11030.

Increased the sea level, put river on and put the flume on a small tilt to vacuum the plastic grains out of the flume.
This didn't really work this time because hte grains were not clumping enough.
We fixed it by using small sieves under maximum sea level and filtering all grains out of the water.
Turned lights off and put river at 300 L/h.

------ 21-06-2023 ------
Continued experiment 054 for 10 cycles without particles, with the first 3 cycles with trigger at 22.5 s
and the remaining 7 cycles with film and trigger each 15 seconds (starting at 0): 11030-11040.
Restarted the flume because tilt didn't start.

Continued the 54th experiment with another 960 cycles with the same settings.
We put the sensors at: y-locations 103 - 148 - 193 cm (hall side = 0); x-locations:
Still: 19.50.
Tilting: each 0.50 m starting at 19.50 and ending at 1.00.
We started measuring after 6 cycles and each measurement took 3 cycles.

------ 22-06-2023 ------
Took photos with laser gantry camera of the wet system: Exp054_12000_wet.
Took photos with the hand-held SLR camera.
Drained the flume.
Took photos with laser gantry camera of the dry system: Exp054_12000_dry.
Took a laser scan of the dry system at 12000 cycles: Exp054_12000.
Cleaned the river filters.
Filled the flume.
Continued the 54th experiment with another 1000 cycles with the same settings.

------ 23-06-2023 ------
Took photos with laser gantry camera of the wet system: Exp054_13000_wet.
Took photos with the hand-held SLR camera.
Drained the flume.
Took photos with laser gantry camera of the dry system: Exp054_13000_dry.
Took a laser scan of the dry system at 13000 cycles: Exp054_13000.
Cleaned the river filters.
Filled the flume.
Continued the 54th experiment with another 1000 cycles with the same settings.

------ 26-06-2023 ------
Did some patching around the dikes.
Took photos with laser gantry camera of the wet system: Exp054_14000_wet.
Took photos with the hand-held SLR camera.
Drained the flume.
Took photos with laser gantry camera of the dry system: Exp054_14000_dry.
Took a laser scan of the dry system at 14000 cycles: Exp054_14000.
Cleaned the river filters.
Filled the flume.
Continued the 54th experiment with another 1000 cycles with the same settings.

------ 27-06-2023 ------
A huge ridge has formed between 8.40 and 10.80 metres.
Took photos with laser gantry camera of the wet system: Exp054_15000_wet.
Took photos with the hand-held SLR camera.
Drained the flume.
Took photos with laser gantry camera of the dry system: Exp054_15000_dry.
Took a laser scan of the dry system at 15000 cycles: Exp054_15000.
Took additional photos with the hand-held SLR camera of the ridge complex.
Cleaned the river filters.
Filled the flume.
Continued the 54th experiment with another 1000 cycles with the same settings.
Restarted flume because tilt didn't start.

------ 28-06-2023 ------
Some sand washed over the bars.
Took photos with laser gantry camera of the wet system: Exp054_16000_wet.
Took photos with the hand-held SLR camera.
Drained the flume.
Took photos with laser gantry camera of the dry system: Exp054_16000_dry.
Took a laser scan of the dry system at 16000 cycles: Exp054_16000.
Cleaned the river filters.
Moved one dike enforcement. Refilled some sand behind the dikes.
Filled the flume.
Continued the 54th experiment with another 1000 cycles with the same settings.
Two groups of a PhD summer school by Jaap Nienhuis came to visit.
A surprise visit of a group led by Kim Cohen also came to visit.

One group of employees of the UU came to visit with Stephan van Meulenbrouck

------ 29-06-2023 ------
Took photos with laser gantry camera of the wet system: Exp054_17000_wet.
Took photos with the hand-held SLR camera.
Drained the flume.
Took photos with laser gantry camera of the dry system: Exp054_17000_dry.
Took a laser scan of the dry system at 17000 cycles: Exp054_17000.
Cleaned the river filters.
Moved one dike enforcement. Refilled some sand behind the dikes.
Filled the flume.
Continued the 54th experiment with another 1000 cycles with the same settings.

------ 30-06-2023 ------
Took photos with laser gantry camera of the wet system: Exp054_18000_wet.
Took photos with the hand-held SLR camera.
Drained the flume.
Took photos with laser gantry camera of the dry system: Exp054_18000_dry.
Took a laser scan of the dry system at 18000 cycles: Exp054_18000.
Cleaned the river filters.
Refilled some sand behind the dikes.
Filled the flume.
Continued the 54th experiment with another 1000 cycles with the same settings.

------ 03-07-2023 ------
Applied anti-fungi spray.
Took photos with laser gantry camera of the wet system: Exp054_19000_wet.
Took photos with the hand-held SLR camera.
Drained the flume.
Took photos with laser gantry camera of the dry system: Exp054_19000_dry.
Took a laser scan of the dry system at 19000 cycles: Exp054_19000.
Cleaned the river filters.
Refilled some sand behind the dikes.
Filled the flume.
Continued the 54th experiment with another 1000 cycles with the same settings.

------ 04-07-2023 ------
Took photos with laser gantry camera of the wet system: Exp054_20000_wet.
Took photos with the hand-held SLR camera.
Cleaned the river filters.
Drained the flume.
Took photos with laser gantry camera of the dry system: Exp054_20000_dry.
Took a laser scan of the dry system at 20000 cycles: Exp054_20000.
Filled the flume.
Continued the 54th experiment with another 1000 cycles with the same settings.
Stephan van Meulenbrouck visited with Rob Ramaker (NOS) shortly to show the lab.

------ 05-07-2023 ------
Took photos with laser gantry camera of the wet system: Exp054_21000_wet.
Took photos with the hand-held SLR camera.
Cleaned the river filters.
Drained the flume.
Took photos with laser gantry camera of the dry system: Exp054_21000_dry.
Took a laser scan of the dry system at 21000 cycles: Exp054_21000.
Experiment is finished.
Turned off lights.

Experiment 059

------ 02-10-2023 ------
Drained the reservoir and area behind the pumps.
Power washed the inside of the reservoir and pumps as best as possible.

------ 03-10-2023 ------
Removed the upper layers of worst occurrences of fungi/algae/diatoms.
Levelled the whole bed with the bridge
Measured the width for the sea side opening which is 1.83m
Made lines with ropes from both sides of the river opening to the sea.
Put in the dikes as straight as possible.
Filled the reservoir and measured the taps discharge.
Started to dig the sand between the dikes out and level this part with the bridge.
Because the slider on the bridge used for the smoothening of the inner dike area is to wide, the narrow upstream part has to be done by hand.

------ 04-10-2023 ------
Continued smoothening the inner dike area by hand.
Cleaned up the sides manually.
Made a delta at the sea end
Vacuum cleaned the grass along the sides of the metronome, the bridge and at the delta area

Took photos with laser gantry camera of the dry system: Exp059_00000_dry.

Took a laser scan of the dry system at 00000 cycles: Exp059_00000.

------ 05-10-2023 ------
Did some trying with the elevation sensors.
Lowered/evened the river side a bit more, took a laser scan of the dry system at 00000 cycles: Exp059_00000_redo.
Did Exp058_exp4 (using different weir heights).

Measured the elevation sensors at: y-locations 103 - 148 - 193 cm (hall side = 0); x-locations 10.50, 1.00 m.
Still: 1.00, 10.50 m
For different levels of the weir.

------ 06-10-2023 ------
Took photos with laser gantry camera of the wet system: Exp059_00000_wet.

Took photos with the hand-held SLR camera.

Filled the flume.
Drained the flume

Started experiment 059 for 10 cycles with the following settings:

Tilt period: 40s
Tilt amplitude 1st: 75mm
Tilt amplitude 2nd: 15mm
Frequency multiplier: 2
Phase shift: 90 degrees
Wave elements: 100

Weir period: 40s
Weir amplitude 1st: 12mm
Weir amplitude 2nd: 2.4mm
Frequency multiplier: 2
Phase shift: 90 degrees
Offset: 67mm
Wave elements: 100

No sediment feed and river discharge of 500 l/h (in ebb phase). Waves on with 2 Hz in flood phase.

Conducted PIV measurements.
Filled the flume with plastic grains.

Continued experiment 059 for 10 cycles with the same settings the film and trigger on with 10 photos of 25 Hz triggers each 15 seconds: 00001-00010
The first 4 cycles were run with the trigger at 22.5 seconds and the remaining 6 cycles with film and trigger, starting at 0, then 15, then 30, then 5 s etc.
Removed the PIV particles from the water and the bed.

------ 09-10-2023 ------
Finished the PIV particle cleaning

Continued the 59th experiment with another 40 cycles with the same settings.
We put the sensors at: y-locations 103 - 148 - 193 cm (hall side = 0); x-locations:
Still: 19.50. Weir at 68.99 mm
Tilting: each 0.50 m starting at 19.50 and ending at 1.00.
We started measuring after 6 cycles and each measurement took 3 cycles.

There were some problems with the weir and the starting of the metronome (weir started but the tilting not). Marcel looked at it but didn't have a solution
Did some test cycles so continuing the water level measurements at cycle 55.
Found out in cycle 63 that the overhead recording wasn't started so started it from there.

Took photos with laser gantry camera of the wet system: Exp059_00100_wet.
Took photos with the hand-held SLR camera.
Drained the flume.

Took photos with laser gantry camera of the dry system: Exp059_00100_dry.
Took a laser scan of the dry system at 00100 cycles: Exp059_00100.
Filled the flume.

Continued the 59th experiment with another 100 cycles with the same settings.
Continuing the water level measurements
Took photos with laser gantry camera of the wet system: Exp059_00200_wet.
Took photos with the hand-held SLR camera.
Drained the flume.

Took photos with laser gantry camera of the dry system: Exp059_00200_dry.
Took a laser scan of the dry system at 00200 cycles: Exp059_00200.

Turned the lights of and river on at 300.

------ 10-10-2023 ------
Scooped some foam off the water.
Cleaned the river filters.

Continued the 59th experiment with another 100 cycles with the same settings.
Took photos with laser gantry camera of the wet system: Exp059_00300_wet.
Took photos with the hand-held SLR camera.
Drained the flume.

Took photos with laser gantry camera of the dry system: Exp059_00300_dry.
Took a laser scan of the dry system at 00300 cycles: Exp059_00300.
Filled the flume.
Continued the 59th experiment with another 200 cycles with the same settings.
Overhead cameras didn't shoot anything (probably human error).

Took photos with laser gantry camera of the wet system: Exp059_00500_wet.
Took photos with the hand-held SLR camera.

Took still water level measurements at 19.76 and above the weir (20.76)
Drained the flume

Took water level measurements above the weir during the movement of the weir (3 cycles) and 1 minute above the not moving weir at 69.00 mm
Took photos with laser gantry camera of the dry system: Exp059_00500_dry.
Took a laser scan of the dry system at 00500 cycles: Exp059_00500.
Filled the flume.

Continued the 59th experiment with another 15 cycles with the same settings. without waves
Took water level measurements above the weir and at 19.76 during 3 cycles each
Overhead cameras were once again not working (all settings were correct).

Turned the lights of and the river on at 300.

------ 11-10-2023 ------
Restarted the metronome which fixed the overhead cameras problems
Continued the 59th experiment with another 5 cycles with the same settings. To see if the overheads were working again which they did
Continued the 59th experiment with another 230 cycles with the same settings.

Took photos with laser gantry camera of the wet system: Exp059_007500_wet.
Took photos with the hand-held SLR camera.
Drained the flume.
Took photos with laser gantry camera of the dry system: Exp059_00750_dry.
Took a laser scan of the dry system at 00750 cycles: Exp059_00750.
Filled the flume.

Continued the 59th experiment with another 250 cycles with the same settings.

Took photos with laser gantry camera of the wet system: Exp059_01000_wet.
Took photos with the hand-held SLR camera.
Drained the flume.
Took photos with laser gantry camera of the dry system: Exp059_01000_dry.
Took a laser scan of the dry system at 01000 cycles: Exp059_01000.

Filled the flume.
Turned the lights off and left the river on at 300.

------ 12-10-2023 ------
Cleaned the river filters.
Continued the 59th experiment with another 250 cycles with the same settings.
Took photos with laser gantry camera of the wet system: Exp059_01250_wet.
Took photos with the hand-held SLR camera.
Drained the flume.
Took photos with laser gantry camera of the dry system: Exp059_01250_dry.
Took a laser scan of the dry system at 01250 cycles: Exp059_01250.
Filled the flume.

Continued the 59th experiment with another 250 cycles with the same settings.

Turned the lights off and left the river on at 300.

------ 13-10-2023 ------
Cleaned the river filters.
Took photos with the hand-held SLR camera.
Restarted the metronome, as the gantry camera did not connect.
Took photos with laser gantry camera of the wet system: Exp059_01500_wet.
Drained the flume.
Took photos with laser gantry camera of the dry system: Exp059_01500_dry.
Took a laser scan of the dry system at 01500 cycles: Exp059_01500.
Filled the flume.

Continued the 59th experiment with another 500 cycles with the same settings.
Took photos with the hand-held SLR camera.
Restarted the metronome, as the gantry camera did not connect.
Took photos with laser gantry camera of the wet system: Exp059_02000_wet.
Drained the flume.
Took photos with laser gantry camera of the dry system: Exp059_02000_dry.
Took a laser scan of the dry system at 02000 cycles: Exp059_02000.

Filled the flume.

Turned the lights off and left the river on at 300.

------ 16-10-2023 ------

Cleaned the river filters.
Continued the 59th experiment with another 500 cycles with the same settings.

Took photos with the hand-held SLR camera.
Took photos with laser gantry camera of the wet system: Exp059_02500_wet.
Drained the flume.
Took photos with laser gantry camera of the dry system: Exp059_02500_dry.
Took a laser scan of the dry system at 02500 cycles: Exp059_02500.
Fixed the area around collapsed dikes.

Filled the flume.
Continued the 59th experiment with another 500 cycles with the same settings.

------ 17-10-2023 ------

Took photos with the hand-held SLR camera.
Took photos with laser gantry camera of the wet system: Exp059_03000_wet.
Cleaned the river filters.
Took photos with laser gantry camera of the dry system: Exp059_03000_dry.
Restarted the metronome, as the laser turned off after 11 m.
Took a laser scan of the dry system at 03000 cycles: Exp059_03000.
Fixed the area around collapsed dikes.
Filled the flume.

Continued the 59th experiment with another 500 cycles with the same settings.

Took photos with the hand-held SLR camera.
Restarted the metronome to connect to the gantry camera (which it didn't).
Took photos with laser gantry camera of the wet system: Exp059_03500_wet.
Drained the flume.
Took photos with laser gantry camera of the dry system: Exp059_03500_dry.

------ 18-10-2023 ------

Took a laser scan of the dry system at 03500 cycles: Exp059_03500.
Fixed the dikes some more.
Filled the flume.
Continued the 59th experiment with another 500 cycles with the same settings.

Took photos with the hand-held SLR camera.
Took photos with laser gantry camera of the wet system: Exp059_04000_wet.
Drained the flume.
Took photos with laser gantry camera of the dry system: Exp059_04000_dry.
Took a laser scan of the dry system at 04000 cycles: Exp059_04000.
Fixed the dikes (again).

Continued the 59th experiment with another 500 cycles with the same settings.

------ 19-10-2023 ------

Took photos with the hand-held SLR camera.
Took photos with laser gantry camera of the wet system: Exp059_04500_wet.
Drained the flume.
Took photos with laser gantry camera of the dry system: Exp059_04500_dry.
Took a laser scan of the dry system at 04000 cycles: Exp059_04500.
Fixed the dikes (again).
Filled the flume.
Continued the 59th experiment with another 500 cycles with the same settings.

Took photos with the hand-held SLR camera.
Took photos with laser gantry camera of the wet system: Exp059_05000_wet.
Drained the flume.
Took photos with laser gantry camera of the dry system: Exp059_05000_dry.
Took a laser scan of the dry system at 05000 cycles: Exp059_05000.
Filled the flume.

Turned the lights off and left the river on at 300.

------ 20-10-2023 ------

Cleaned the river filters .
Continued the 59th experiment with another 1000 cycles with the same settings.

------ 23-10-2023 ------

Turned the river on and off for a bit at 300.
Took photos with the hand-held SLR camera.
Took photos with laser gantry camera of the wet system: Exp059_06000_wet.
Drained the flume.
Took photos with laser gantry camera of the dry system: Exp059_06000_dry.
Took a laser scan of the dry system at 06000 cycles: Exp059_06000.
Fixed the dikes.

Filled the flume.

Continued the 59th experiment with another 1000 cycles with the same settings.

------ 24-10-2023 ------
Turned the river on and off for a bit at 300.
Took photos with the hand-held SLR camera.
Took photos with laser gantry camera of the wet system: Exp059_07000_wet.
Drained the flume.
Cleaned the river filters.
Took photos with laser gantry camera of the dry system: Exp059_07000_dry.
Took a laser scan of the dry system at 07000 cycles: Exp059_07000.
Fixed the dikes.
Filled the flume.

Continued the 59th experiment with another 1000 cycles with the same settings.

------ 25-10-2023 ------
Turned the river on and off for a bit at 300.
Took photos with the hand-held SLR camera.
Took photos with laser gantry camera of the wet system: Exp059_08000_wet.
Drained the flume.
Took photos with laser gantry camera of the dry system: Exp059_08000_dry.
Took a laser scan of the dry system at 08000 cycles: Exp059_08000.
Fixed the dikes.
Filled the flume.

Continued the 59th experiment with another 500 cycles with the same settings.

Checked if the dikes were still oke
Continued the 59th experiment with another 500 cycles with the same settings.

------ 26-10-2023 -----
Took photos with the hand-held SLR camera.
Took photos with laser gantry camera of the wet system: Exp059_09000_wet.
Drained the flume.
Cleaned the river filters.
Took photos with laser gantry camera of the dry system: Exp059_09000_dry.
Took a laser scan of the dry system at 09000 cycles: Exp059_09000.
Filled the flume.

Continued the 59th experiment with another 1000 cycles with the same settings.

------ 27-10-2023 -----
Took photos with the hand-held SLR camera.
Took photos with laser gantry camera of the wet system: Exp059_10000_wet.
Drained the flume.
Took photos with laser gantry camera of the dry system: Exp059_10000_dry.
Took a laser scan of the dry system at 10000 cycles: Exp059_10000.
Fixed the dikes.
Filled the flume.

Turned the lights off and left the river on at 300.

------ 30-10-2023 -----
Continued the 59th experiment with another 160 cycles with the same settings.
We put the sensors at: y-locations 103 - 148 - 193 cm (hall side = 0); x-locations:
Still: 19.50. Weir at 69.15 mm
Tilting: each 0.50 m starting at 19.50 and ending at 1.00.
We started measuring after 6 cycles and each measurement took 3 cycles.

Took photos with the hand-held SLR camera.
Took photos with laser gantry camera of the wet system: Exp059_10160_wet.
Drained the flume.
Took photos with laser gantry camera of the dry system: Exp059_10160_dry.
Took a laser scan of the dry system at 10160 cycles: Exp059_10160.
Filled the flume.

Conducted PIV measurements.
Filled the flume with plastic grains.

Continued experiment 059 for 10 cycles with the same settings the film and trigger on with 10 photos of 25 Hz triggers each 15 seconds: 10160-10170
The first 4 cycles were run with the trigger at 22.5 seconds and the remaining 6 cycles with film and trigger, starting at 0, then 15, then 30, then 5 s etc.
Removed the PIV particles from the water and the bed.

Continued the 59th experiment with another 830 cycles with the same settings.

------ 31-10-2023 -----
Took photos with the hand-held SLR camera.
Took photos with laser gantry camera of the wet system: Exp059_11000_wet.
Drained the flume.
Took photos with laser gantry camera of the dry system: Exp059_11000_dry.
Took a laser scan of the dry system at 11000 cycles: Exp059_11000.

Filled the flume.

Continued the 59th experiment with another 1000 cycles with the same settings.

------ 01-11-2023 -----
Took photos with the hand-held SLR camera.
Took photos with laser gantry camera of the wet system: Exp059_12000_wet.
Cleaned the river filters.
Drained the flume.
Took photos with laser gantry camera of the wet system: Exp059_12000_dry.
Took a laser scan of the dry system at 12000 cycles: Exp059_12000.
Fixed the dikes.
Filled the flume.

Continued the 59th experiment with another 1000 cycles with the same settings.

------ 02-11-2023 -----
Took photos with the hand-held SLR camera.
Took photos with laser gantry camera of the wet system: Exp059_13000_wet.
Drained the flume.
Took photos with laser gantry camera of the wet system: Exp059_13000_dry.
Took a laser scan of the dry system at 13000 cycles: Exp059_13000.
Fixed the dikes.
Filled the flume.
Continued the 59th experiment with another 500 cycles with the same settings.

The delta reached under the wave maker so the experiment is over

Took photos with laser gantry camera of the wet system: Exp059_13500_wet.
Took photos with the hand-held SLR camera.
Drained the flume.
Took photos with laser gantry camera of the dry system: Exp059_13500_dry.
Took a laser scan of the dry system at 13500 cycles: Exp059_13500.

Turned the lights off

------ 03-11-2023 -----
Measured water levels in the reservoir.
Removed the bio/uv unit out of the reservoir to prevent it from drowning
Filled the reservoir until it is almost full
Measured the water levels in the reservoir again.
Raised the weir until the whole bed was flooded.
Closed of the return valves under the metronome.
Filled the basins at river and sea side. The parts behind the weir.
Measured the water levels in a few of the reservoir compartments.
Positioned the water level sensors at x = 10.
Measured the water levels with the flooded bed for 1 minute.
Plugged the pumps back in while starting the water level sensor measurements again.
The sensors have a minimum measurement distance of 10 cm so we keep filling the metronome to roughly a cm under that.
Turned off the pumps and water level measurement and measure water levels in reservoir again.
Drained the flume
Pumped out some of the water in the reservoir so the bio/uv unit can be placed back
Measured the water levels in the reservoir again to estimate the volume for dye application later

Appendix B | X-Beach Runs

In the process of getting the hydrodynamics right, several things were tested. These variables and code changes are described here and in **table B**. In this table, all runs can be found with a short description of the parameters tested/changed in that run and the results which came out. Important to not here is that the conversion from surface velocity to average depth velocity was done later. Best runs run conditions in this overview are not always true due to this later insight of the necessary conversion. In preparation of this thesis, Eise Nota did some tests with the initial model to get it running. This was a version of X-Beach in which the metronome tilt was added. These adaptations were made by Prof. Dano Roelvink. The end result of this pre-testing process is the initial test run, here referred to as run 000. From these tests it appeared that the tilt was not yet correctly incorporated in the model. Furthermore, the results showed large scale floods. These floods first occur after 20 seconds in the first cycle, when the first flood phase begins. After this, water flows back and forth over the sides where there should not be any water.

Initial tests (Run 001-005)

To start the testing phase, a few smaller parameters were tested. First of all, the possibility was tested whether the floods could be caused because of some instability of the model related to the time steps. Therefore, the Courant-Friedrichs-Lewy parameter was lowered. This however did not change anything. Together with this, the 'tstart' parameter was added to see if the floods were also occurring later in time, which indeed was the case. Additionally, a test was done with the bed roughness. The model was using a manning value of 0.02 for the bed roughness. The real roughness of the metronome is unknown but is estimated at a Chézy value of 15 $m^{1/2}/s$. By changing the bed roughness, the water flowed slightly slower but the floods are still present. Lastly a small test was done with the flow boundary condition. Thus far the condition abs_1d was used. With this condition, the flow should be able to go in and out freely. This was changed to the wall condition, in which the water is confined to the basin and cannot flow out. The results showed no big changes between the two conditions.

Tide input (Run 006-015)

The next series of runs focuses on the tide input. In this stage, the movement of the seaside weir was used as tide input as this weir controls the water level in the metronome. Different combinations of weir movement and correction for the tilt of the metronome were tried in combination with the wall or abs_1d flow boundary condition. In all cases, the floods still occurred. When the correction for the tilt is turned off, the extent of the floods during ebb is smaller. When this tilt correction is included, the floods are the same as in earlier runs.

Wall building & excluding tilt (Run 016-024)

Because there is too much water flowing into the domain, the bed level file was adapted. In the file, a 2 metre high wall was built at the seaside. In theory, this should prevent water from getting in. However, the basin still flooded. To check whether the river was not causing the floods, a run without any river discharge was also performed. This gave the same result, showing that the river discharge is not the cause of the floods. Therefore, the wall was moved towards the coast. When the wall is made thicker and placed in the mouth of the channel at x = 17.5 m, without a direct connection to the sea, the flooding situation is looking slightly better. Now there are only some small parts of the areas behind the dikes on which a thin layer of water moves back and forth. Next to this, a situation without tilting was tested. First the tilt and tides were both turned off. This resulted in a stationary water level, as expected. In the next run, the tides were turned on while the tilt was still turned off, and the floods were back. Again, it appeared that the tide is probably the main problem causing the floods.

Measured water levels (Run 025-026)

Until this point, the movement of the seaside weir was used as tidal input as the weir controls the water level in the metronome. However, the water levels in the model outputs are way too high, so too much water is coming from the seaside. Therefore, additional water level measurements were done as far in the sea as possible at x = 19.76 m right next to the wavemaker. The wave maker was turned off during these measurements. These values were then used as tidal input for the model. This lead to no big changes in the flooding pattern in the basin. The X-Beach outputs are still too high compared to these measured values, even while forcing these values to the corners of the seaside.

Varying bed friction (Run 027-030)

To prevent too much water from coming in, an attempt was made with varying bed frictions. To do so, a bed friction grid was created. In this grid the 5 most seaside columns were given a much higher roughness than the rest of the grid. This way, it should slow down water entering the domain, making less water flow in. Different values and extents for the friction were tried, all resulting in the floods seen before. From this, it appeared that the friction cannot fix the flooding problem. However, it can probably be used to finetune the model when the flooding problem is solved.

Tideloc (Run 031-037)

The tideloc parameter defines where which water levels are forced. Three options were tried: tideloc 0, 1 and 2. Tideloc 0 takes a constant level as initial water depth. This approach also causes floods. However, the flooding pattern looks more like the situation in the runs where the tide file is not corrected for the metronome tilt. With tideloc = 1, a water level time series is forced to the two corner cells in at the seaside. This option was already used with the measured values as tidal input. However, now a time series with a constant water level during high water was tested. This run did not show any floods, but the water level was much too low, causing parts of the estuary to fall dry periodically. The third option is tideloc = 2. With this, two water level time series are used, one is forced to the corner cells of the seaside and the other one is forced to the corner cells of the riverside. For this last time series, measured water levels from x = 1 m were used, as this is the location closest to river where measurements are possible. The runs with tideloc = 2 showed a new flooding pattern. Instead of floods at the start of the flood phase from the seaside, the floods now also came from the riverside.

Changing tilt & raising diked area (Run 038-045)

Earlier on, a run without tilt was performed in which the tide file was still including a tilting correction. With the tide file with the measured values now available, this was done again. This time, the tilting correction was not included, so only the real measured values were used as a tidal input. For both tideloc 1 and 2, this gave no floods for the non-tilting basin. The water only goes up and down throughout the basin, no tidal wave is visible. After this, the tilt was included again, but some different amplitudes were tested. When a first amplitude of 0.015 m and a second amplitude of 0.003 m was used, the point was reached where the basin started to flood. For the smaller amplitudes of 0.010 m and 0.002 m, there are no floods. The water levels are similar to the measured water levels, although the behaviour is not. There is a small tidal wave visible, but its timing is not the same as in the measured values. In addition to changing the tides, the bed level grid was adapted again. The area behind the dikes was raised so it cannot flood. In these runs, the diked area stays dry as intended. However, the water levels in the channel are still way to high compared to the measured values.

Shifting the tide file (Run 046-048)

From previous runs it appeared that the tidal input was not behaving as expected. The values at the sea (and river with tideloc = 2) are way too high, compared to the measured values. Therefore, the tidal input file was adapted. The curve which describes the motion of the weir was fitted through the measured water level values. Then this curve was shifted down and the amplitude was decreased, both by 1 centimetre. This shifted curve was then taken as tidal input. This resulted in runs where the basin still flooded, even though the peak water level during high tide at the seaside was now the same height as the measured water level.

Updated model (Run 049-055)

While all these model runs were executed, Department of Physical Geography programmer Dr. Saeb Faraji Gargari worked on improvement of the X-Beach source code. This involved implementing the right tilting function for the metronome, which was not right in the first version of the model. The tilting function now includes the right phase shifts and periods for the two parts of the function. It is also shifted slightly up, to make the tilt start at 0. additionally, variables were included to put certain elements of the code on or off; the most important, which were tested in these runs, are the water level updating and the continuity. In the original model, the water levels are updated with the bed level change at the end of the code calculating the hydrodynamics. However, this can be interpreted as including the bed level change twice, as it should also be accounted for in the continuity equations, which calculate how high the water levels are based on the bed level. In the new code, this updating can be turned on or off. In the continuity, the bed level is accounted for, however the change of bed level is excluded. In the normal X-Beach model, this term is neglected, as over one time step the changes are very small for the large scale environments. However, in the metronome the bed level changes are significantly larger because the whole bed is tilting. Therefore, this term was included again, with an option to turn it on or off. Different combinations of activating and deactivating these two elements showed a new flooding pattern. In the runs where both were turned off or tuned on, the water flows back and forth more, letting one part of the metronome fall dry each time. This falling dry is even more present when only the continuity element is turned on. In the period between peak ebb and peak flood, the water stays mostly in the channel, with fewer floods on the sides than before.

Sea discharge (Run 056-062)

Instead of getting the desired water levels by forcing these water levels on the boundaries, a test was done by getting these water levels by letting a certain discharge go into the basin. This was done by adapting the discharge file and defining a new discharge inlet at the seaside boundary. Discharge values were gathered in the metronome based on water level measurements. The discharge time series was put in the discharge file of the model. In the first run, the tidal input was also still on. However, this did not lead to more floods than before. It was therefore unclear whether the new discharge file was working properly. Therefore, several tests were performed, with higher and negative discharges in combination with low sea levels. From this it appeared that the discharge file was indeed working as supposed. However, the discharges are apparently too low to clearly see the effects in the model.

Runs without tidal input (Run 063-070)

In this set of runs, the tidal input was excluded and an initial constant sea level was used, corresponding with the tideloc = 0 condition. This resulted in unexpected good results. Water levels and flow velocities are both following the measured values rather well. Some tests were done with changing the bed friction, to make the modelled velocities match better with the measured ones. This resulted in runs where the velocities match considerably better.

Final model (Run 071-079)

In this set of runs, the new boundary condition was implemented, making it possible to force a water level time series to the riverside and seaside boundary. With this new possibility, the modelled water levels on those sides are matching exactly with the measured ones. Again, some tests were performed with changing bed frictions to get the modelled flow velocities to match the measured ones better. Best results with this were obtained with a Chézy of 20 $m^{1/2}/s$. Additionally, an attempt was made to get rid of the small patches of water in the area behind the dikes. This was done by raising the dikes and the area behind them. This did not have the desired result. Therefore, the model was updated again with the introduction of the num_boundary_water_level statement. This makes the water on the sides almost disappear. However, it increases the water levels in the channel, a unwanted result.

Final model (Run 080-095)

In the final runs different bed frictions were tried. This to improve the modelled velocities which were too low for the earlier used Chézy value of 15 $m^{1/2}/s$. In steps of 5 $m^{1/2}/s$ different values were used. This was done for both the first version of the new boundary condition as well as for the updated version of the new boundary condition. In between a run was done to take a look at how the model was performing with a developed bed instead of the flat channel which is used thus far. Also some last test were performed to try and improve the new boundary condition.

Run	What was done?	Results?
000	Initial test run by Eise Nota.	Too much water in the basin.
	CFL/tstart	
001	Changing CFL parameter from 0.9 to to 0.1 to check stability model.	Basin is still flooding. Checked u and v ranges but these are still the same as for run 000.
002	Adding tstart = 200 in params.txt.	Basin is still flooding. Checked u and v ranges but these are still the same.
	Bed roughness	
003	Changing bed roughness to Chézy with a value of 15 $m^{1/2}/s$. CFL to 0.9 again, no tstart.	Basin is still flooding. Looked the same as before, water flows a bit slower than before.
004	Changing bed roughness to Chézy with a value of 55 $m^{1/2}/s$. CFL to 0.9 again, no tstart.	Chézy 55 $m^{1/2}/s$ is the standard value of Delft 3D. This causes the basin to empty in the first eb stage and the flood. The water flows quicker back and forth.
	Front flow boundary condition	
005	Changed front parameter to wall instead of abs_1d.	The basin is still flooding. Hardly any difference between abs_1d and wall parameters.
	Tide	
006	Run with front parameter wall without tide.	The basin is not flooding anymore, however there are a lot of dry places in the channel.
007	Run with tide but with other tide.txt file found in another folder.	Smaller flood extent but during ebb stages.
008	Run without changing weir, with tilt component weir, abs_1d.	Similar flooding pattern as previous tests. Whole bed floods after first ebb.
009	Run with changing weir, without tilt component weir, abs_1d.	Smaller flood extent but during ebb stages.
010	Run with changing weir, with tilt component weir, abs_1d.	Similar flooding pattern as previous test. Whole bed floods after first ebb. Less flooding without tilt component in the weir but water level to high during ebb.
011	Run without changing weir, with tilt component weir, wall.	Similar flooding pattern as previous tests. Whole bed floods after first ebb.
012	Run with changing weir, without tilt component weir, wall.	Smaller flood extent during ebb stages.
013	Run with changing weir, with tilt component weir, wall.	Similar flooding pattern as previous test. Whole bed floods after first ebb. Front wall does not have a big impact.
014	Run without changing weir, without tilt component weir, wall.	Smaller flood extent but during ebb stages. Still floods without doing anything with the weir.
015	Run with inversed motion weir.	Flooding extent in between 012 and 013. Flooding now between ebb and flood.
	Wall building	
016	Run with adapted depth file: wall of 2 meter in the sea.	Still floods like before.
017	Run with 0 river discharge without wall.	Does not really change a lot. The bed dries up a bit quicker during the first ebb stage. River does not cause the floods.

018	Run with 2 meter wall, 0 river discharge.	Still floods like before.
019	Moved wall 25 cm landwards. No discharge.	Still floods like before.
020	Wall moved to x=17.5 m in the channel now.	The channel is still flooding somehow although the access to sea is completely closed off. Maybe the water goes through the pores in the sand? Try thicker wall.
021	Made the wall thicker so no water can go through.	Channel is still flooding. Try without the tides.
022	Run with 2 meter wall, 0 river discharge and constant sea level no tides.	Almost no flooding. However, the water levels are still not similar to the measured values.
	Excluding metronome tilt	
023	No tilting metronome, constant sea level from weir.	Stationary water as expected.
024	No tilting metronome, moving sea level by weir.	Big floods. Tide file with tilt correction was used.
	Measured water levels as tide	
025	Run with measured water levels + tilt according to MATLAB script as tide input.	Same flood pattern as before.
026	Run with measured water levels without tilt correction.	Same flood pattern as before. Something probably going wrong with the tides in the model.
	Varying bed friction	
027	Run with varying bed friction. Chézy = 0.01 $m^{1/2}/s$ at 5 seaside columns.	Still floods. Hardly any change.
028	Run with varying bed friction. Chézy = 0.0000000001 $m^{1/2}/s$ at 10 seaside columns.	Border between frictions is visible in u plots. Still floods.
029	Run with friction everywhere at 0.0000000001 $m^{1/2}/s$.	Still floods.
030	Friction from run 028 with tide.txt from run 026.	Still floods. Looks the same as Run 026. A wrong friction is not the cause of the floods.
	Tideloc	
031	Tideloc = 0 with zs0 = 0.069 and no tilting.	Still water level at 0.069 as expected.
032	Tideloc = 0 with zs0 = 0.0652 (mean measured value) with tilting.	Floods similar to situation with tide file without bed correction.
033	Tideloc = 1 with measured values, corrected for tilt during ebb and constant at 5.9 cm during flood.	Does not flood in earlier cycles, channel is even falling dry. Later the old floods return.
034	Tideloc = 2 with measured values in tide.txt from 19.75 and 1 m corrected for tilt.	New flooding pattern. Floods from both sides but smaller extent.
035	Same as 034 but with tidetype = hybrid.	Made no changes. Might be useful when morphology is turned on.
036	Same as 034 but with Chézy = 55 $m^{1/2}/s$.	Water flows faster than 034 and still floods.
037	Same as 034 but with Chézy = 0.001 $m^{1/2}/s$.	Water flows slower than 034 and still floods.
	Changing metronome tilt	
038	Run without metronome tilt, with tide file based on measured water levels.	No floods. Water goes slowly up and down.

039	Run without metronome tilt, with tideloc = 2.	No floods. Water goes slowly up and down. A bit more variation because of the tideloc 2.
040	Metronome amp1=0.010, amp 2 = 0.002, tideloc 2 with measured values.	X-Beach values have a similar range as the measured values. Also sort of a small flood roller is visible however, wrong timing.
041	Metronome amp1=0.020, amp 2 = 0.004, tideloc 2 with measured values	Floods start to happen. Smaller than normal but same timing and behaviour
042	Metronome amp1=0.015, amp 2 = 0.003, tideloc 2 with measured values.	Floods start to happen. Smaller than normal but same timing and behaviour.
	Channelizing dikes	
043	Run 003 but with higher dikes. Entire area behind dikes at 2m.	Water stays withing the channel but water levels are way too high.
044	Run 043 but with abs_2d.	Exactly the same as run 043 with abs_1d.
045	Run 043 with tideloc 2.	Similar to 043. Still way to high water levels. X-Beach is following neither of the tide files.
	Adapting tide file	
046	Adapting the weir function to match the measured values, then shifting it 1 cm down and decrease amplitude 1 cm.	X-Beach maximum water levels same height as measured values but it still floods. Floods have a smaller extent than before.
047	Same as 046 but now with new model version.	Still flooding. Water on left or right side. Sea level exactly follows the tide file.
048	Same as 47, adapted tide file based on weir motion.	Still floods at riverside. Water on left or right. Sea level exactly follows the tide file.
	New model version	
049	New model again. Tilt 0. countinuty_with_Dzb_activation = 1, zs_updating_with_zb_activation = 1.	Water levels are very close to measured values, velocity almost 0 -> no tilting so no flow caused by the tilting.
050	zs_updating_with_zb_activation = 1, countinuty_with_Dzb_activation = 0 (only zs_up, Dano's model).	The normal floods as expected. New options all turned off. Seaside much higher than tide.
051	zs_updating_with_zb_activation = 0, countinuty_with_Dzb_activation = 0 (neither).	Floods only at 1 side of the basin at the time. Large floods during flood, small ones during ebb. In between most water in channel, looks quite decent. Seaside follows tide very good.
052	zs_updating_with_zb_activation = 1, countinuty_with_Dzb_activation = 1 (both zs_up and Dzb cont).	Exactly the same as 051.
053	zs_updating_with_zb_activation = 0, countinuty_with_Dzb_activation = 1 (only Dzb cont).	Larger floods than in 051/052. Largest difference in between ebb and flood. Much more water on sides. Seaside lower than tide.
	New cos function with 0.015 shift	
054	Run 052 with tide file with corrected function zb (tideloc = 1).	No big changes compared to old tide file. Slightly bigger floods as water level was raised by 0.015.

055	Run 052 with tide file with corrected function zb (tideloc = 2).	Bigger floods. Almost all the time, the basin is flooded.
	Sea discharge	
056	Run 052 but with adapted hydro file based on measured values.	No big changes in the flooding pattern.
057	Run 057 but with tideloc=0, zs0 = 0.0001 (to really see the discharges).	Much less water in there. Not sure if the hydrofile is working as supposed as no river input is noticeable. The sea is sometimes empty.
058	Run with original hydrograph file with tideloc = 0 zs0 = 0.0001 to check if there is river input now.	Still no river output visible.
059	Run with new hydro file with 0.11 m3/s discharge in river. No tilt.	Hydro file is working right for river.
060	Run like 059 but with 0.001 discharge at river and sea discharge with river time series at 0.1.	Water is coming from the sea so that works. Negative discharge needs still to be checked.
061	Run with negative values at seaside of -0.01 m3/s.	Water is flowing out but large discharges are needed. So new hydrofile should work.
062	Run of 4000 long to see if the floods stabilizes.	Model stops after 1060 modelled seconds. Results show stabilization after ~600 seconds.
	Updated model	
063	Trying the updated model.	The previous model is used. Need to install it again.
064	New model is working now. Without tide file tideloc=0, zs0 = 0.06.	Best run so far. No big floods on the sides. Water levels and velocities are similar to measured values.
065	Same run as 064 but with zb_updating_activation = 0.	Big floods again, water and floods going back and forth.
066	Same run as 064 but with tideloc = 1.	Enormous floods.
067	Run with zs0 = 0.06.	No floods
068	Run at meeting with Dano, manning of 0.01 was used instead of 0.02.	Velocity values much closer to PIV values
069	Run with new model with water_depth_sea = 0.06 water_depth_river = 0.01.	No floods, Water levels close to measured values PIV not quit right yet
070	Same run as 069 but Chézy 25 $m^{1/2}/s$.	Some floods at the river side
	Final model	
071	Run with the new boundary conditions.	Sea and river side exactly follow measured values. In the middle it looks quite good, at sides some weird dips. Velocity much to low.
072	Run like 071 but with grid of exp 059 and not 054.	No floods with this other gridfile. Also this run has strange deviations at sea and riverside next to the forced values. Velocity again too low.
073	Run like 071 but with Chézy = 30 $m^{1/2}/s$ instead of 15 $m^{1/2}/s$.	Velocity values much better. Water levels still not quite like the measured ones especially at the river and sea ends.
074	Run with new dep file with area behind dikes at 0.07 m and dikes at 0.09 m.	Only a bit of water on the sides.
075	Try with erodible layer and morphology.	Nice channel pattern develops but much too quickly.

076	Run 074 with thicker dikes.	Looks the same as with the thinner dikes.
077	Run like 071 but with Chézy 40 = $m^{1/2}/s$ instead of 15 $m^{1/2}/s$.	Velocities even closer.
078	Run with updated model version: num_boundary_layer_water_level = 1 and thicker dikes grid and Neumann boundary at lateral sides.	Water on the areas behind dikes almost all gone. However, water levels in channel a bit too high.
079	Run with lateral no_advec boundaries.	Very similar to the Neumann boundaries. Still too high water levels.
	Bed roughness testing	
080	Run like 072 with Chézy = 40 $m^{1/2}/s$.	PIV measurements match much better. Water levels a bit more off.
081	Run like 072 with Chézy = 20 $m^{1/2}/s$.	Water levels getting worse with higher Chézy. Velocities improving.
082	Run like 072 with Chézy = 25 $m^{1/2}/s$.	Water levels getting worse with higher Chézy. Velocities improving.
083	Run like 072 with Chézy = 35 $m^{1/2}/s$.	Best results for velocities.
084	Run like 072 with Chézy = 45 $m^{1/2}/s$.	Water levels getting worse with higher Chézy. Velocities getting worse again.
085	Run like 072 with Chézy = 50 $m^{1/2}/s$.	Water levels getting worse with higher Chézy. Velocities getting worse again.
086	Run like 072 with Chézy = 30 $m^{1/2}/s$.	Water levels getting worse with higher Chézy. Velocities improving.
087	Run like 083 but with developed bed.	Model crashes. Probably has to do with something in the grid file although the values look to be fine. It is only one row of cells larger.
088	Run like 078 but with Chézy = 35 $m^{1/2}/s$.	Water levels still too high. Velocity also slightly too high.
089	Run like 078 but with Chézy = 25 $m^{1/2}/s$.	Water levels still not good. Velocity better.
090	Run like 078 but with Chézy = 20 $m^{1/2}/s$.	Water levels still not good. Velocities worse than 089.
091	Run like 078 but with Chézy = 30 $m^{1/2}/s$.	Water levels still not good. Velocities worse than 089.
092	Run like 089 but with improved model with impicit_iteration_threshold = 2.	Water levels still a bit to high. Modelled velocity a bit out of phase.
093	Run like 092 with Chézy 15.	Water levels still a bit to high. Modelled velocity a bit out of phase.
094	Run like 093 with num_boundary_layer_water_level = 3.	Water levels still a bit to high. Modelled velocity a bit out of phase.
095	Run like 072 with bed of exp 054 instead of 059.	Water levels and velocities almost the same.

Appendix C | PIV Measurements experiment 059

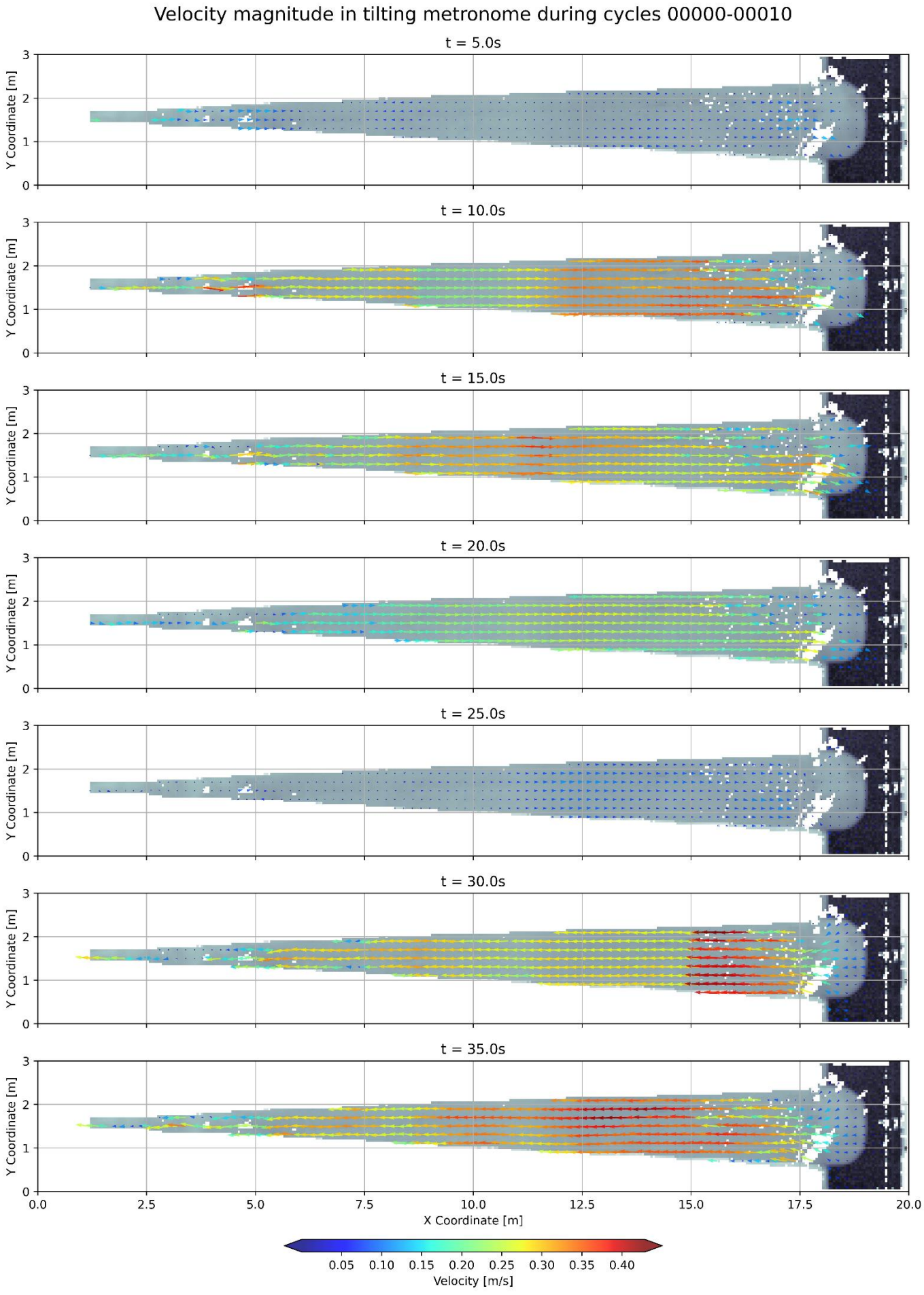

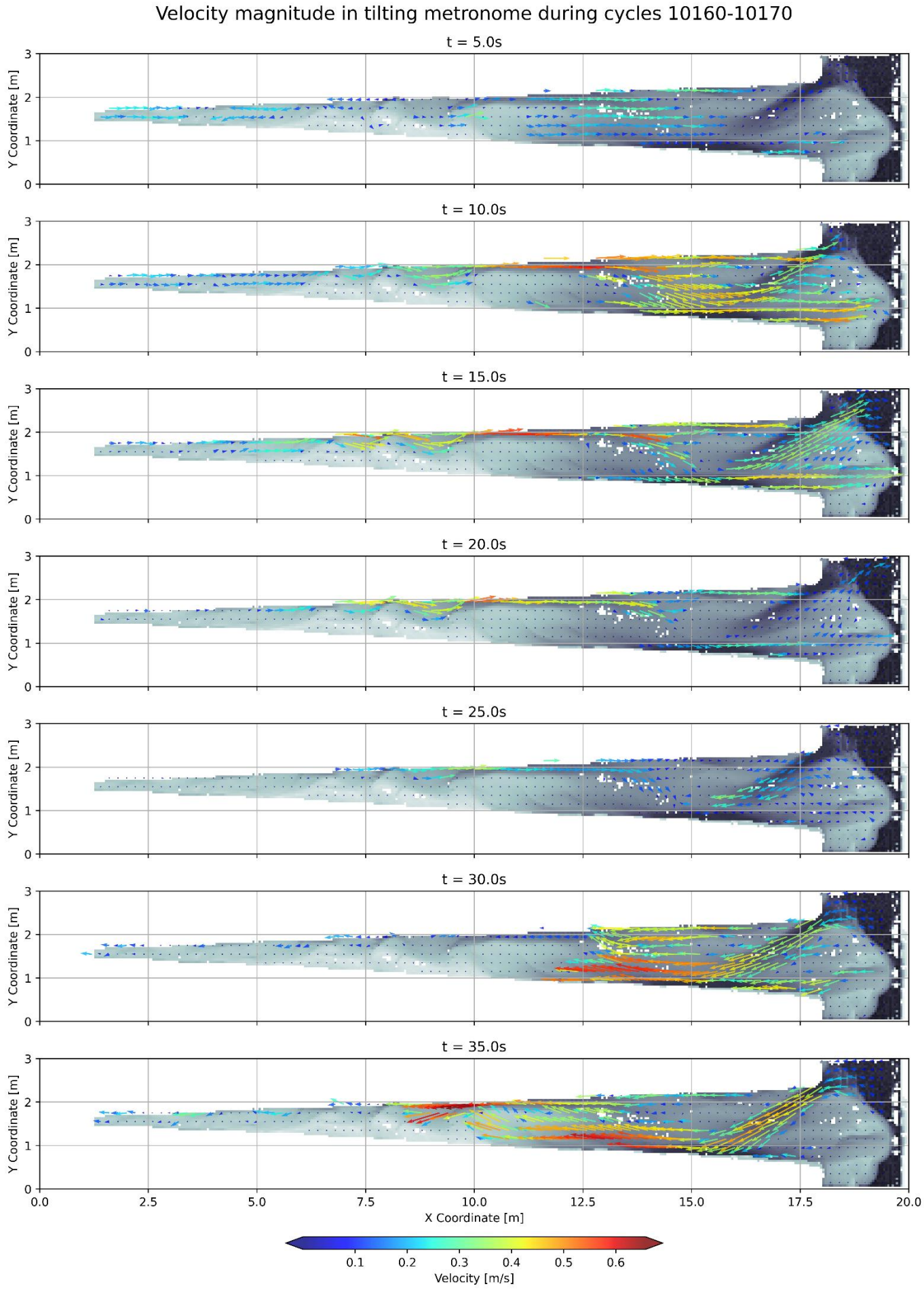
Velocity magnitude in tilting metronome during cycles 10160-10170
t = 5.0s
t = 10.0s
t = 15.0s
t = 20.0s
t = 25.0s
t = 30.0s
t = 35.0s
Y Coordinate [m]
X Coordinate [m]
0.0
2.5
5.0
7.5
10.0
12.5
15.0
17.5
20.0
0.1
0.2
0.3
0.4
0.5
0.6
Velocity [m/s]